

Comprehensive Model-Based Design and Analysis  
Approach for Thermal Management  
Systems in Hybridized Vehicles

by

Joshua Kurtis Carroll

A Thesis Presented in Partial Fulfillment  
of the Requirements for the Degree  
Master of Science

Approved April 2017 by the  
Graduate Supervisory Committee:

Abdel Ra'ouf Mayyas - Chair  
Jeffrey Wishart  
James Contes

ARIZONA STATE UNIVERSITY  
May 2017

## ABSTRACT

This research effort focuses on thermal management system (TMS) design for a high-performance, Plug-in Hybrid Electric Vehicle (PHEV). The thermal performance for various components in an electrified powertrain is investigated using a 3D finite difference model for a complete vehicle system, including inherently temperature-sensitive components. The components include the electric motor (EM), power electronics, Energy Storage System (ESS), and Internal Combustion Engine (ICE).

A model-based design approach is utilized, where a combination of experimental work and simulation are integrated. After defining heat sources and heat sinks within the power train system, temporal and spatial boundary conditions were extracted experimentally to facilitate the 3D simulation under different road-load scenarios. Material properties, surface conditions, and environmental factors were defined for the geometrical surface mesh representation of the system. Meanwhile the finite differencing code handles the heat transfer phenomena via conduction and radiation, all convective heat transfer mode within the powertrain are defined using fluid nodes and fluid streams within the powertrain.

Conclusions are drawn through correlating experimental results to the outcome from the thermal model. The outcome from this research effort is a 3D thermal performance predictive tool that can be utilized in order to evaluate the design of advanced thermal management systems (TMSs) for alternative powertrains in early design/concept stages of the development process.

For future work, it is recommended that a full validation of the 3D thermal model be completed. Subsequently, design improvements can be made to the TMS. Some

possible improvements include analysis and evaluation of shielding of the catalytic converter, exhaust manifold, and power electronics, as well as substituting for material with better thermal performance in other temperature-sensitive components, where applicable. The result of this improvement in design would be achieving an effective TMS for a high-performance PHEV.

## ACKNOWLEDGMENTS

This research was funded by Argonne National Laboratory, General Motors, and the US Department of Energy. Without programs such as EcoCAR 3, the opportunity to conduct this research may never have occurred otherwise. I'd like to thank my committee Dr. Abdel Ra'ouf Mayyas, Dr. Jeffrey Wishart, and Professor James Contes for pushing me to do more and believing I could succeed.

For those who helped me in the late sleepless and tireless nights, Josh Rosenberg and Hayden Hostetler. Without them I wouldn't have had such an amazing CAD mesh and high fidelity model. To Corey Page and Zachary Yeskey working day in and day out on increasing the numerical model fidelity. To my fiancé, Afifeh Khatabi, the love of my life and the reason I work so hard to make a life for us.

# TABLE OF CONTENTS

	Page
LIST OF TABLES .....	vii
LIST OF FIGURES .....	viii
ABBREVIATIONS .....	xii
INTRODUCTION .....	1
Background and Motivation.....	2
Problem Statement .....	5
Approach .....	7
LITERATURE REVIEW .....	9
METHODOLOGY .....	21
Simens NX - CAD and Meshing.....	21
3D CAD Model Construction.....	21
Meshing .....	28
MATLAB Simulink - Numerical Simulation.....	39
Numerical Methodology.....	39
Assumptions .....	43
Driver Graphical User Interface .....	44
Driver Model .....	45

	Page
Vehicle Model .....	45
ICE Propulsion .....	47
Traction Battery System .....	48
Intake & Exhaust Flow Rates .....	55
TAITherm – Thermal Analysis .....	57
Parts Editor Tab .....	57
Fluids .....	61
Fluid Streams .....	63
Curves .....	67
Weather .....	73
Scenario .....	78
RESULTS .....	82
Numerical Simulation .....	82
Combined Methodology .....	86
Inverter & EM .....	88
ESS .....	90
Heat Exchangers – Inverter & EM 1 & 2, ICE, and ESS .....	92
ICE & Exhaust Manifold .....	95
Temperature Curve Results .....	97

	Page
CONCLUSION & FUTURE WORK.....	102
REFERENCES .....	104
APPENDIX	
A – PARTS TAB FUCNTION, EXPLAINATION, AND VALUES.....	108
B – FLUID EDITOR FUNCTION, EXPLAINATION, AND VALUES.....	112
C – FLUID STREAMS FUNCTION, EXPLAINATION, AND VALUES .....	115
D – DATA COLLECTED JANUARY-MARCH 2017 .....	118
E – DATA COLLECTED JANUARY-MARCH 2017.....	151

## LIST OF TABLES

Table	Page
1: Major Powertrain Component List .....	22
2: Low-Voltage Harness Power Losses due to Resistance and Temperature .....	53
3: Commonly Used Part Tab Selections .....	61
4: Fluid Stream Node Biasing Editor .....	65
5: Fluid Stream Boundaries Editor .....	67
6: Historic Weather Data Excerpt 07/15/2016.....	74
7: Scenario Editor Tab .....	80
8. Tabulated Results.....	86
9: Final, Average, & Maximum Temperatures .....	97
10: Component Hot Spot Max Thermal Temperature .....	98



## LIST OF FIGURES

Figure	Page
1: Chevrolet Volt Coolant Loops .....	5
2: Proposed Vehicle Architecture and Components Diagram .....	9
3: Series Cooling Case [8] .....	11
4: Parallel Cooling Case [8] .....	12
5: Thermal Effects on Capacity Storage Over Time [16] .....	14
6: Thermal Effects on Power Storage Over Time [16] .....	15
7: Common AC Configuration [20] .....	16
8: Typical ICE Configuration [10] .....	17
9: Typical Exhaust System Configuration .....	19
10: IGBT Cooling Process [29] .....	20
11: Full Vehicle CAD Model .....	22
12: Powertrain .....	23
13: Transmission, Drive Shaft, and Differential .....	24
14: Electric Powertrain .....	25
15: ESS .....	25
16: Updated Low-Temperature Heat Exchanger Model .....	26
17: Updated High-Temperature Heat Exchanger Model .....	27
18: Free Edge Correction .....	29
19: Element Aspect Ratio Correction .....	29
20: Friction Brake Mesh .....	31

Figure	Page
21: TAITherm Brake Thermal Links [4] .....	32
22: Preliminary Engine Mesh .....	33
25: LEA Engine Intake and Exhaust Manifolds Into Cylinders .....	35
26: LEA Engine .....	36
27: Interior Mesh.....	37
28: Drivetrain Mesh .....	38
29: ESS Mesh.....	39
30: TMS Design Approach.....	40
31: US06 Input Drive Cycle .....	42
32: Driver GUI.....	45
33: Full Vehicle Model .....	46
34: Electric Plant Model .....	48
35: Vehicle Current Usage and Regenerative Braking.....	49
36: Battery Model .....	52
37: Total Resistance with Temperature Change .....	54
38: Total Power Loss with Temperature Change .....	55
39: Parts Editor Tab – Front.....	58
40: Parts Editor Tab - Back.....	59
41: Fluid Editor .....	62
42: Fluid Stream Editor.....	63
43: Fluid Stream Node Biasing.....	64
44: Fluid Stream Boundaries Editor .....	66

Figure	Page
45: Battery Heat Rate Curve .....	68
46: Engine Heat Rate Curve .....	68
47: Inverter Heat Rate Curve .....	69
48: EM Heat Rate Curve.....	69
49: Transmission Heat Rate Curve .....	70
50: Total Intake Air.....	71
51: One Cylinder Intake Flow.....	71
52: One Cylinder Manifold Exhaust Flow .....	72
53: Total Exhaust Flow .....	73
54: Environment.....	75
55: Background Conditions .....	76
56: Wind Conditions.....	77
57: Sky Conditions.....	78
58: Scenario Tab .....	79
59: Average Heat Generation vs. Time.....	83
60: No Coolant minus Standard Coolant Loop.....	84
61. Standard Coolant Loop minus Controlled Coolant.....	85
62: Initial TAItherm Mesh.....	87
63: Inverter & EM Temperature Curve .....	89
64: Inverter & EM Conduction Net Heat Rate .....	89
65: Inverter & EM Convection Net Heat Rate.....	89
66: Inverter & EM Radiation Net Heat Rate .....	90

Figure	Page
67: ESS Temperature Curve .....	91
68: ESS Conduction Net Heat Rate .....	91
69: ESS Convection Net Heat Rate .....	92
70: ESS Radiation Net Heat Rate .....	92
71: Heat Exchangers Temperature Curve .....	93
72: Heat Exchangers Conduction Net Heat Rate .....	94
73: Heat Exchangers Convection Net Heat Rate .....	94
74: Heat Exchangers Radiation Net Heat Rate .....	94
75: ICE & Exhaust Manifold Temperature Curve .....	95
76: ICE & Exhaust Manifold Conduction Net Heat Rate .....	96
77: ICE & Exhaust Convection Net Heat Rate .....	96
78: ICE & Exhaust Radiation Net Heat Rate .....	96
79: Inverter & EM TAItherm Mesh at 400 s .....	99
80: ESS TAItherm Mesh at 400 s .....	99
81: Heat Exchangers TAItherm Mesh at 400 s .....	100
82: ICE & Exhaust TAItherm Mesh at 400 s .....	100

## ABBREVIATIONS

GHG	Greenhouse Gas
CAFÉ	Corporate Average Fuel Economy
HEV	Hybrid Electric Vehicle
PHEV	Plug-in Hybrid Electric Vehicle
FCV	Fuel Cell Vehicle
EV	Electric Vehicle
ESS	Energy Storage System
EM	Electric Motor
TMS	Thermal Management System
AC	Air Conditioning
MBD	Model-Based Design
CAD	Computer Aided Drafting
CAE	Computer Aided Engineering
GM	General Motors
SOH	State of Health
WTW	Well-to-Wheel
CAC	Criteria-Air Constraints

AF	Air-to-Fuel
IGBT	Insulated Gate Bi-Polar Transistor
FEA	Finite Element Analysis
EGR	Exhaust Gas Recirculation
EPA	Environmental Protection Agency
GUI	Graphical User Interface
HTC	Human Thermal Comfort
CS	Charge Sustaining
CD	Charge Depleting

## INTRODUCTION

The United States only consumes a significant amount of the total oil produced globally. Local, state, federal, and global restrictions are being placed on the greenhouse gas (GHG) emissions generated by the combustion of fossil fuels in vehicles. Vehicles account for the vast amount of harmful emissions that are generated each year, and the United States is the second-leading producer of harmful GHG emissions. In light of the federal emissions regulations and rising Corporate Average Fuel Economy (CAFE) standards, companies in the marketplace have been incentivized to develop alternative powertrains to reduce emissions and increase fuel economy.

These alternative powertrains seek to reduce the GHG production of vehicles through the utilization of alternative power sources. Currently, various manufacturers have already started production of electrified vehicles with alternative powertrains. These include Hybrid Electric Vehicles (HEVs), Plug-in Hybrid Electric Vehicles (PHEVs), Fuel Cell Vehicles (FCVs), and Electric Vehicles (EVs). These vehicles suffer a lack of robustness in the thermal management system (TMS) to support the inconsistent temperature envelope of onboard electronic modules, such as the inverter, energy storage system (ESS), and electric motors (EMs), that are inherently sensitive to high temperatures from one side and the high temperature ICE power source. Also, because the ICE in electrified powertrains is either often turned off during deceleration and idling periods or not present at all in the powertrain, air conditioning (AC) systems become a significant load in such powertrains. Hence, a robust TMS and an optimized human thermal comfort system become a necessity to increase the energy efficiency and extend the range for these electrified vehicles.

Although, numerical simulations are an efficient tool to devise discrete thermal control in vehicles powertrains; they are not capable of capturing all heat transfer with high fidelity especially in radiation. To account for all modes of heat transfer, a 3D representation is critical in order to account for the viewing factor and multi-bouncing radiation between visible surfaces. On the other hand, developing 3D models to predict the thermal performance of complex hybrid powertrains is a challenging task due to an inclusion of temperature-sensitive powertrain modules.

Moreover, electrochemical energy storage devices used in electrified powertrain are prone to drastically lower performance at both high and low temperatures. Resulting in a decrease in reliability and reduction in the calendar life of these specific types of vehicles.

## Background and Motivation

When compared to costly and time consuming physical prototypes, using a Model-Based Design (MBD) approach has proven to be a cost- as well as a time-effective approach to assess the thermal performance of alternative powertrains. This method employs the use of modeling and simulation software programs to evaluate a system or part quickly. The use of the MBD has grown significantly, in recent years, due to the reduced cost and development time. The MBD approach employs mathematical models to determine an output of a system of equations. One of the most powerful modeling and simulation tools is MATLAB from MathWorks Incorporated [1]. In the automotive industry, use of MATLAB and other, similar programs has become a quick and reliable way to help design the most cost-effective thermal management designs. Further, using



these software programs reduces the costly necessity of physically building multiple prototypes as most design iterations are completed virtually.

Analyzed separately, discrete component models do not capture the complex physics of heat transfer phenomena that takes place throughout the complex alternative powertrain. Numerical analysis programs combine the separate equations to determine the outcome of a total vehicle model. However, it is cumbersome to develop a robust discrete TMS in coordination with creating high-fidelity numerical models. Adding discrete thermal analysis to these models increases computational demand and, therefore, is not appropriate for the development of real-time thermal control.

Ongoing analysis of thermal computational models can be facilitated using computer-aided design and engineering (CAD/CAE). Programs such as Siemens NX allow for three-dimensional object creation in a virtual environment for analysis before the building of such components [2]. This 3D CAD representation allows for, at a finite level, an analysis of the heat transfer interaction between components with different temperature ranges in a heterogeneous environment.

Programs such as TAItherm by ThermoAnalytics (used in this research) assist in the utilization of cross-platform simulation, combining the fidelity of both types of modeling, for the purpose of heat transfer analysis [3]. TAItherm represents a powerful program with cross-functional areas of analysis in both steady-state and transient heat distribution over complex surface meshes of a component system. It allows for full 3D models to become analytical tools for conduction, convection, and multi-bounce radiation [4]. Multi-bounce radiation is used for complex radiation boundaries specifically where windows are present. When a surface is defined with an emissivity less than 0.7 percent,

diffusion by numerical approximations can no longer be used [5]. The output of TAItherm shows a complex temperature map of the heat boundaries produced by the model both by individual pieces and the entire model.

TAItherm combines the strength of both: CAD/CAE and numerical-based simulation software, and allows for both discrete and steady-state thermal analysis between two variant programs. TAItherm offers an attractive nature as discrete models require significantly less computational time than the numerical models with higher fidelity in the CAD/CAE programs. Thermal management is often measured late in the creative process of creating a vehicle, using thermocouples and thermal cameras [6, 7]. This research proposes the use of high-fidelity modeling techniques, both numerical and 3D geometrical meshes, must be considered when implementing a TMS during the design phase. With HEVs and PHEVs entering the market and thus the introduction of highly temperature-sensitive components to a vehicle, there is a need for multiple coolant loops; thermal management strategies must be robust.

The various optimum temperature requirements in the Chevrolet Volt lead General Motors to develop the heat exchanger and coolant loops shown in Figure 1. Four separate operational cooling loops are utilized within the powertrain system of the Chevrolet Volt. The power electronics and battery system are thermally managed with a split-core heat exchanger with two separate cooling loops after which the AC condenser is prioritized in the second slot. The prioritization of the loops, which is seen in the physical arrangement of the heat exchangers, shows the effort given by General Motors (GM) in the thermal modeling process. By doing so, the battery life and thermal efficiency of each component can be increased, thereby reducing the life cost of the vehicle.

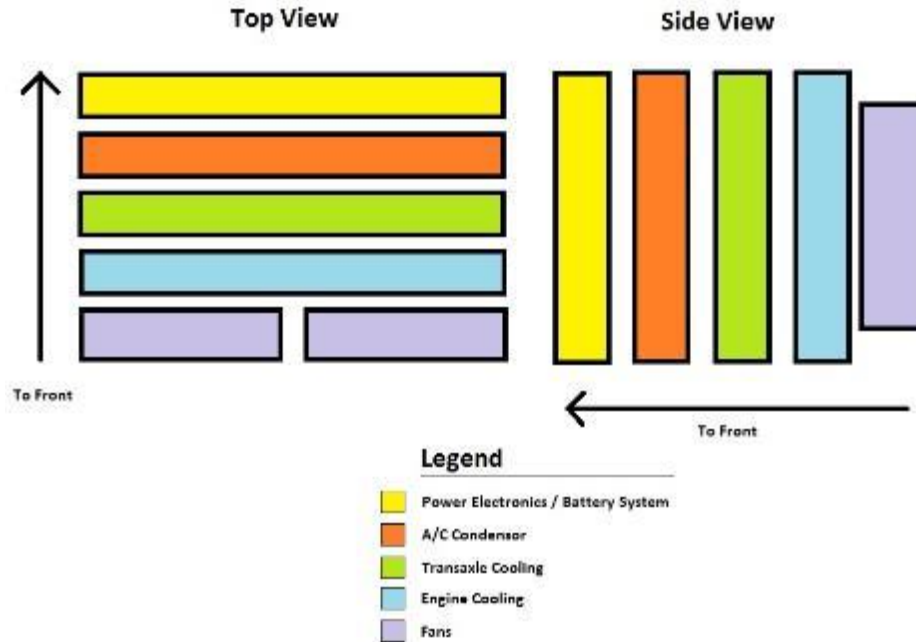


**Figure 1: Chevrolet Volt Coolant Loops**

### Problem Statement

Current, in-production Plug-in Electric Vehicles (PEVs, a classification that includes EVs and PHEVs) still suffer a lack of robust thermal management design. The problem is exhibited in thermal management of power electronics and the high-voltage batteries. These components are inherently temperature sensitive, and variance in temperatures can cause significant changes in the behavior of the components. When kept at high temperatures, battery chemistries exhibit larger current flows. These higher current flows cause degradation in the State of Health (SOH) of the ESS. This causes problems in the long-term durability of the ESS, reducing the overall capacity and cycle use.

On the other hand; cold starts highly affect the GHG emissions of ICE due to high fuel/air ratio entering the combustion chamber during the warm up phase. Hence, robust thermal management to warm up engine block in short period of time is critical to reduce

the GHG emissions. Yet, preventing the ICE from reaching high temps is important to protect the underhood electronic components. . As such, power electronics and battery systems are also highly affected by the same issue. The variance caused by the cold in battery systems and its power electronics limit the amount of current that can be provided by the electric traction system. Additionally, there is a decrease in performance seen as power electronics when the temperatures rise to high. The power electronics enter become de-rated and enter a period of limited functionality when hot spots exist. Therefore, under-hood hotspots are an area of concern and are critical to identify in order to optimize the component location through robust thermal packaging and shielding to create a robust TMS.

Additionally, the thermal management design complexity is compounded further as volumetric constraints limit the area in which components may be located. A robust thermal analysis accounts for volumetric constraints while identifying potential improvements. The improvements may include heat shields, rerouting of temperature sensitive coolant lines, and even relocation of components. In order to cope with these complexities, 3D thermal management design tool that considers the interaction via conduction, convection and more important by radiation between tightly packed powertrain components in PHEVs is required. Radiant heat transfer is most dominant mode of heat transfer for these types of vehicles as high temperature components may be tightly packaged next to a low temperature component. The heat from, for example, an exhaust manifold would radiate large amounts of heat into power electronics causing limited to no functionality of the component. Careful consideration to packaging and heat shielding must be shown in order to properly control these modes of heat transfer.

In summary, the lack of 3D representation of the system under consideration and the existing low-fidelity discrete models requires additional tools for devising an optimal TMS and thermal control strategy. In fact, these discrete models do not account for the interactions due to radiation and hence result in an overdesigned thermal strategy, producing non-optimal energy consumption. Radiation is inherently difficult to model using discrete models. This is due to the lack of physical 3D awareness in the program. In order to adequately compensate, the component is overdesigned from a lack of fidelity in all modes of heat transfer. Therefore, the company must overdesign the component rather than risk an under designed component.

#### Approach

This research employs a model based design approach using 3D CAE finite differencing code with a complex heat transfer solver and coupled with a numerical simulation to facilitate the deployment of boundary conditions and also integrated with experimental work for further validation. Both heat sources and heat sinks are defined, allowing for temporal and spatial boundary conditions to be explored numerically under various loading scenarios. Material properties and environmental factors are defined for the geometrical surface mesh representation of the system, allowing for convective, conductive, radiative, and evaporative heat transfer modes to be analyzed within the vehicle.

The 2016 Chevrolet Camaro V6 2LT has been transformed into a parallel pre-transmission (P2) PHEV for the EcoCAR 3 competition. This high-performance platform is targeted in this study due to its complexity when it comes to thermal packaging and space claim constrains. However, there are several P2 vehicles currently on the market,

such as the Porche Panamera, Volkswagen Touareg, Porche Cayenne, and Chevrolet Malibu, to name a few. The choice to build a parallel pre-transmission hybrid was made due to high-performance capabilities while maintaining high energy efficiency. Multiple powertrains were studied for a year prior to this research in order to decide upon the best possible architecture. The PX notation is defined by the placement of the EM in the hybrid architecture. A P0 configuration is a start/stop assist in which the EM is used to start the engine in place of a starter motor, thereby lowering power consumption during the start of an engine. In a P1 configuration, the EM is positioned between the ICE and clutch that connects to the transmission. This allows the ICE-EM combination to be decoupled from the powertrain. A P2 configuration is similar as the EM is before the transmission, but it is downstream of the clutch such that only the ICE can be decoupled. A P3 configuration has the EM after the transmission but before the rear differential. Finally, in a P4, the EM is located between the rear differential and the wheels; it should be noted that the ICE and EM may power different wheelsets, and in this case, the configuration is known as a “through-the-road” parallel architecture.

The P2-PHEV Chevrolet Camaro architecture of the ASU EcoCAR 3 team can be seen in Figure 2. The Camaro utilizes a 4-cylinder GM LEA engine for fuel efficiency with an engine displacement of 2.4 liters. Many PHEVs found on the market today are front-wheel drive economy cars rather than high-performance rear-wheel drive vehicles. The ICE utilizes E85 for fuel with a 140 kW EM placed between the engine and transmission. A clutch is used to engage the ICE and may be disengaged to decouple the ICE and lower fuel consumption. E85 was chosen as the preferred fuel type because of its low well-to-wheel (WTW) emissions.

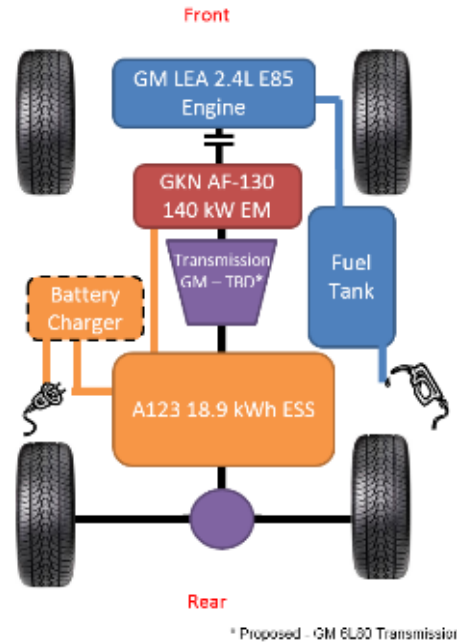


**Figure 2: Proposed Vehicle Architecture and Components Diagram**

The traction battery system consists of a GKN AF130-4 and a powerful 18.9-kilowatt hour ESS produced by A123. The ESS is similar in energy capacity to that of the Chevrolet Volt. The heat generated by the vehicle model was extracted from a numerical model designed in MATLAB. The MATLAB numbers generated and imported are explained in Section 0. The numbers generated were imported into TAITherm rather than experimentally extracted numbers. The vehicle mesh is imported from Siemens NX. The mesh allows the numerical simulation to be applied to a geometrical representation of the P2-PHEV Camaro.

## LITERATURE REVIEW

The increased demand on the market for more efficient vehicles has increased the attractiveness of PEVs. Yet, battery technology and demand have been limiting factors in the past for automotive companies to produce these vehicles. With a call for GHG

reduction requirements coming from both federal and state regulations, vehicle makers no longer can ignore the attractiveness of bringing electricified vehicles to the market.

Battery performance, life expectancy, and cost have caused for slow market penetration of HEVs and PEVs. High temperatures have a huge effect on the life expectancy of the batteries [8]. Robust thermal management for batteries becomes a crucial key [9]. On the other hand, thermal management in a conventional internal combustion engine, ICE, powertrains require different cooling schemes and is set to a specific flow rate and acted only as a mechanical and most recently as electrical auxiliary system. These systems introduce a simple TMS that causes increased disparity within large coolant loops especially in complex alternative power trains.

Also, with the addition of traction battery systems to vehicle's power train, new problems are introduced. The fact that ICE is routinely being turned off and on, in HEVs and PHEVs, requires different solutions to many common components that must be found. For instance, the air conditioning (AC) system must move from the mechanical engine to the electrical system, whether low voltage or high voltage. This creates an additional load on the LV or HV system, but usually the HV ESS accommodates this load. Also, a DC/DC step down converter may be required to keep the LV system operating in the absence of an alternator.

The most significant change is in volumetric requirements necessary for robust thermal packaging. Each component may not have similar operating temperatures and frequently may have drastic differences between them. This variation requires additional heat exchangers, heat shields, coolant pumps, and coolant lines that are required to be



sent to various portions of the vehicle. Depending upon the complexity of the powertrain, this can be challenging. Additional issues arise with the addition of such components, such as increasing the overall weight of the vehicle. The industry practice is that components that operate at similar temperatures can be use a serial connection coolant loop [6, 7]. In large serial coolant loops, the pressure and mass flow at which the pump should flow is compounded. This issue may be mitigated by use of push and pull coolant pump systems in long cooling loops.

An example of a challenge for a robust TMS is that frequently, the ESS is located near the rear of the vehicle while the heat exchanger is in the front. This creates a problem of running extended coolant lines from the front to the rear of the vehicle. A system with extended coolant lines may make use of multiple coolant pumps that pump the same volume of fluid to keep the entire system moving. This can cause major disparities between temperature-sensitive components. A comparison between a series coolant loop, Figure 3, and a parallel loop, Figure 4 is shown below.

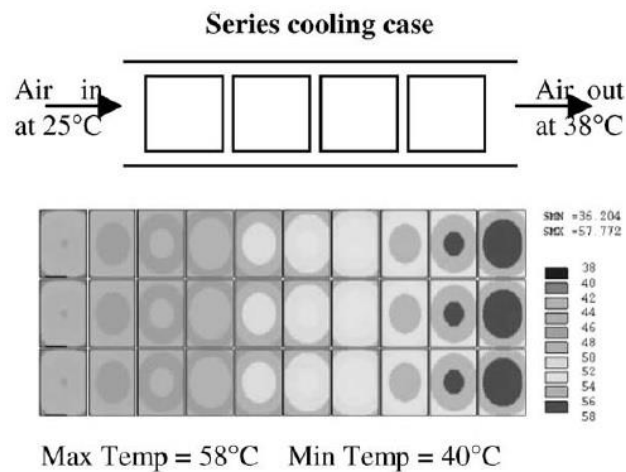


**Figure 3: Series Cooling Case [10]**

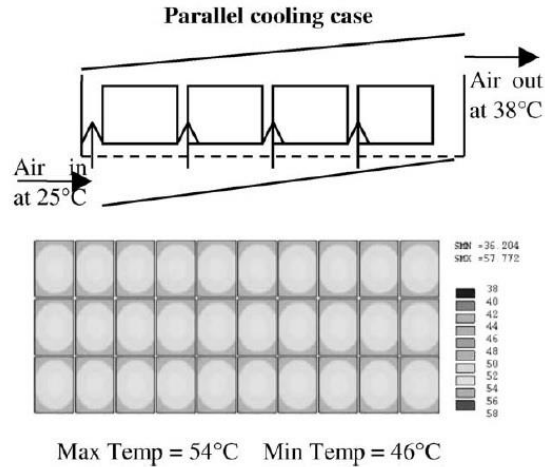


**Figure 4: Parallel Cooling Case [10]**

In a series coolant loop the output of one system becomes the input to the next. This causes a large heat disparity from the beginning to the end of the loop. In a parallel loop, the input to the system for modules is shared causing less heat disparity in the entire system. In Figure 3, the difference between the minimum and maximum temperature is 18 °C. In contrast, Figure 4 the difference between the minimum and maximum temperature is 8 °C. The major difference is the ability to maintain the temperature within a window which the parallel loop is able to maintain a smaller temperature differential.

A robust TMS becomes critical in optimizing the maximum performance output of the vehicle [11, 12, 13]. With the introduction of faster supervisory controllers, microcontrollers, and additional sensors, thermal management is becoming less of a burden [11, 12]. The burden is lessened with better coolant chemistries, pumps, electronically actuated valves, etc.

For any HEV or PEV, the ESS is the most temperature-sensitive component. Without a fully functioning ESS, the powertrain cannot fully function. Each battery chemistry

should ideally operate within a desired temperature range that coincides with actual operating temperatures, that will achieve optimal performance and maintain long shelf life [14]. By decreasing the loss of SOH over the period of operation for the ESS, the overall system cost is reduced over the lifetime of the vehicle. Improving ESS performance and cost will increase market demand for the purchase of HEVs and PEVs.

Each battery manufacturer has proprietary blends of each electrochemistry. However, it is in the best interest of the manufacturer to market the optimum temperature range of the battery system. The problem increases with slight variations of the battery chemistry between manufactured cells [15]. These slight variations cause uneven heat generation of each battery, and a TMS should be able to adapt to such situations [11].

Many factors can cause the module disparities. These include the number of cells in the pack, the geometry of the cell configuration, geometry of the cooling plate, the thermal conductivity of the case, cell interconnects, and variation in current density [11]. The temperature disparity created by these factors cause non-uniform heat generation within each of the modules [11, 16].

Other problems arise from the difference in operating temperature range and optimal temperature range [8]. The optimal range is located within a larger operating domain for battery use. When using a battery in this range, damage within the chemistry may occur, which reduces the overall SOH and, thus, the lifespan of the battery, thereby increasing lifetime cost [9, 10].

Two major factors affect the overall performance of the battery system. High ambient temperatures cause battery capacity to degrade; this process is called aging. The thermal

stress and temperature increase due to charging also heavily affects a battery system. These thermal effects degrade the performance of the battery and lower the output of the system as seen in Figure 5 and Figure 6 over time. The other major contributing factor is a low temperature that highly affects the way a battery performs [17, 18]. At low temperatures, the performance of the pack decreases however, this loss is temporary as the cell temperature increase with use.

Figure 5 shows the de-rating of the capacity of a battery system when the batteries are stored at an elevated temperature. As the temperature is lowered, the effect is lessened. Figure 6 shows similar de-rating as a function of power over time. The output is drastically reduced as temperature is increased. Inversely, as the batteries are held at stable temperatures the overall loss is mitigated. Thus, showing the need for the ESS to be held within the operating range.

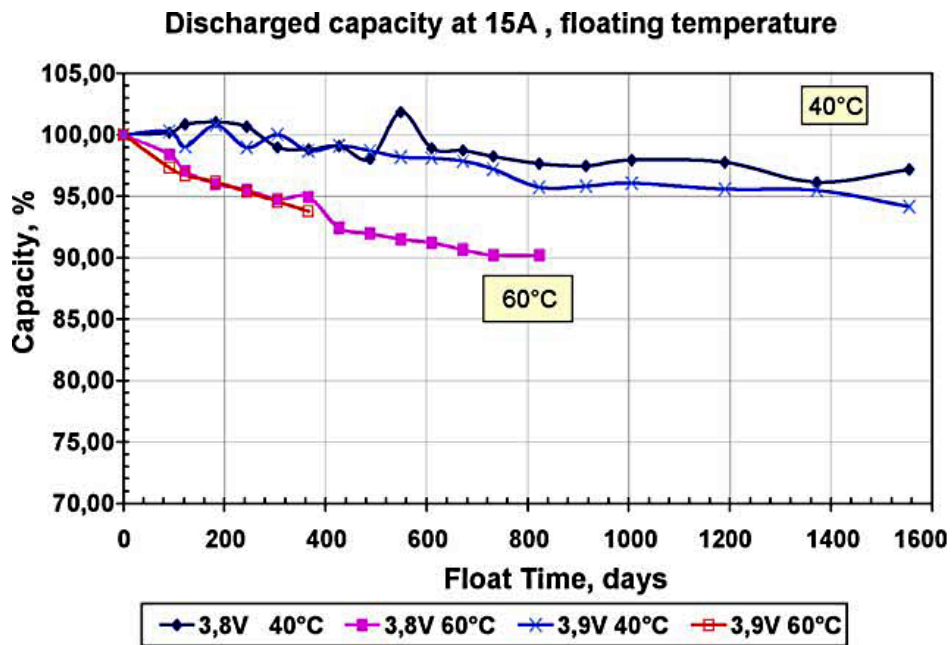
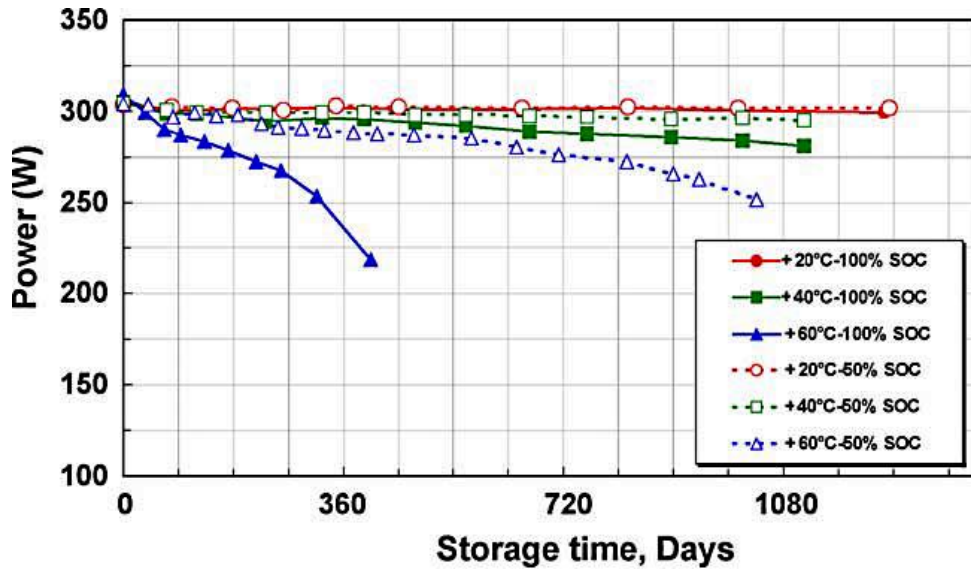


Figure 5: Thermal Effects on Capacity Storage Over Time [18]



**Figure 6: Thermal Effects on Power Storage Over Time [18]**

By operating the batteries in the optimal temperatures range, thermal stress on the electrochemistry of the pack will have less impact on the system [19]. These issues should be addressed to form an optimal thermal control strategy within HEVs and PEVs. Today's vehicles may see a rise in TMSs that can overcome many different obstacles such as those found in conventional vehicles with ICEs [8].

The AC system presents a significant portion, of energy consumption in a vehicle [20]. On a typical ICE vehicle, the increase in fuel consumption can be as high as 12 to 17 percent in the compact to mid-size vehicles [21]. Significant research has been conducted in the reduction of such loads [20, 21]. Improvements in AC systems not only increase the comfort level within the cabin of the vehicle but can heavily affect the fuel consumption. As such, careful analysis should be placed on the cabin air conditioning system.

In an HEV, PHEV, or ICE vehicle the AC system is commonly setup as seen in Figure 7. An AC system works quite simply: the compressor increase the refrigerant pressure, causing the refrigerant to become a gas. The gas is then sent through the evaporator where the refrigerant absorbs the surrounding heat from the surrounding air that is supplied by the blower motor. As the refrigerant is heated, the expansion valve opens and sends the refrigerant into the condenser to be cooled. As the expansion valve is opened, a pressure drop is created within the loop, and the condenser again creates a high-pressure system to repeat the cycle [22, 23]. The process of compression of the refrigerant in an AC system from low to high pressure is defined as adiabatic compression [23]. The AC system controls the Human Thermal Comfort (HTC). Simply put this is the comfort level of a human inside the cabin environment of the vehicle. The AC system is what cools the cabin climate when applied.

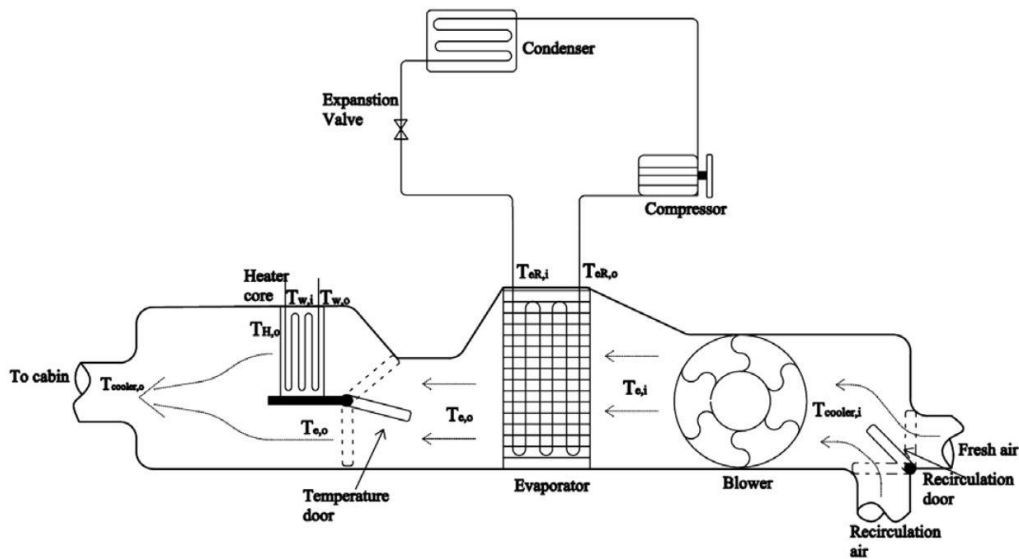
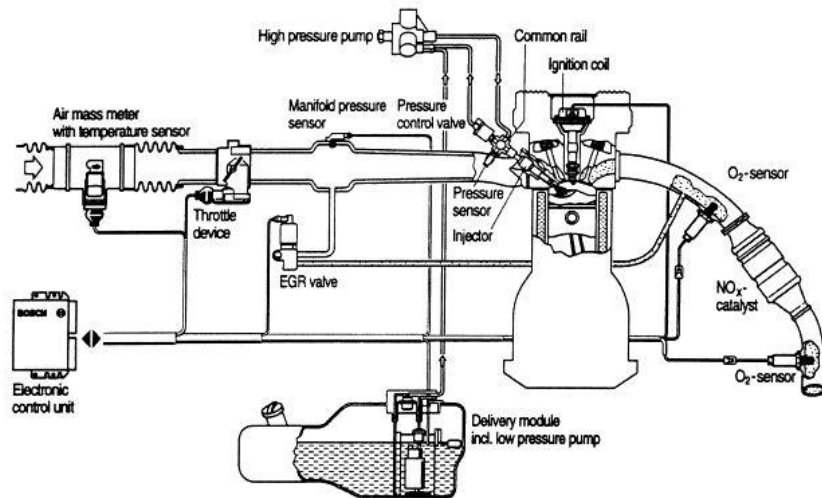


Figure 7: Common AC Configuration [22]

Within the ICE, attention must be paid to the overall system temperature. The ICE runs at a temperature range that exceeds all other temperature-sensitive components. Simply put, the ICE operates by the ebb and flow of air through a cylinder by use of valves [24, 25]. When the combustion process occurs, exhaust gas temperatures may reach more than 600 °C. A typical ICE configuration is seen in Figure 8. This is due to the combustion chamber temperature rise as the process occurs. This process is ignited by the spark plugs and fuel is introduced by use of a fuel injector. The heat caused by the combustion process expands the air and exits through the use of valves through the exhaust manifold. The EGR valve recirculates a small amount of air back into the chamber to increase efficiency of the burn during the combustion process. The temperatures described are mostly seen in the combustion chamber, cylinder head, and exhaust manifold.



**Figure 8: Typical ICE Configuration [12]**

At lower engine temperatures, the ICE is less efficient, causing an increase in criteria-air contaminants (CACs) and GHG emissions [26]. Lower temperatures cause an increase in emissions due to the severe increase of engine rotation, fuel vaporization dynamics, and deviations of cylinder intakes [75]. This causes disproportionate amounts of fuel to be injected, highly affecting the air-to-fuel (AF) ratio [27]. At warm temperatures, accurate measurement of fuel injectors, valve timing, air compression, load and spark timings at steady-state is achieved in the ICE [25]. If an ICE cylinder temperature of approximately 120 °C is maintained, the efficiency of the engine can be maximized for a start/stop operation [27, 28].

The exhaust often poses the most significant threat to powertrain electronics. Depending on the application, exhaust temperatures can reach upwards of 400 °C or more. Power electronics typically require an operating temperature range of 50 to 100 °C. Battery systems typically require no more than 30 °C. Attention, in HEV and PEV applications, must be shown to the routing of the exhaust to provide a significant reduction of harmful effects it may produce in the electric drive portion of the vehicle.

Exhaust systems have been optimized for ICE vehicles to adequately control phenomena seen in the combustion process [29]. However, for accurate thermal analysis, the combustion air must be properly simulated to produce real-time results for the system [30]. An example of the exhaust process is shown in Figure 9. While the exhaust manifold is heated increased GHG is seen when the catalytic converter is cold. Thus, potential heat shields for temperature sensitive components may be in this area. Exhaust tail pipes may see temperatures as high as 100 °C and may have an impact on the ESS.





**Figure 9: Typical Exhaust System Configuration**

Typically, EMs and inverters are analyzed in pairs [31]. This analysis may include voltage, current, and torque output. This is because inverters control the EM, determining its operating parameters and torque output [31]. The inverter must be able to provide and receive the voltage and current provided by the EM in both scenarios. Failure to choose pairs that operate within the same voltage and current ratings may result in a catastrophic failure for the inverter.

Inverters operate using Insulated Gate Bi-Polar Transistors (IGBTs). These IGBTs represent the bulk of the loss within the inverter, and that loss is mostly translated into thermal losses [31]. When a transistor becomes heated, the operation of the inverter will decrease. Therefore, by adequately supplying cooling to the IGBTs, the degradation due to thermal conditions may be mitigated. An application of thermal mitigation used in inverters today may be seen in Figure 10 [31]. Complex serial and parallel coolant loops may be used as seen in Figure 9.a. By controlling the inverter and EM temperatures, the efficiency output of the system can be increased by as much as 15 percent [31, 32].

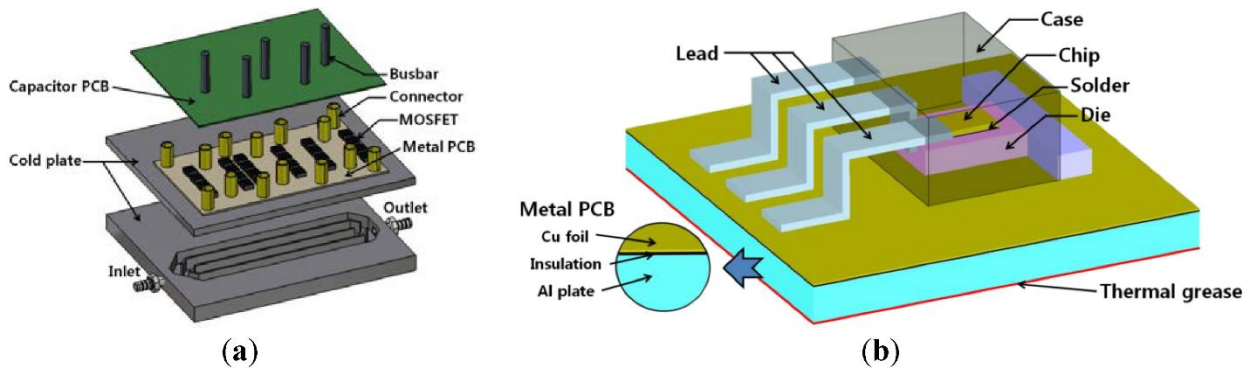


**Figure 10: IGBT Cooling Process [29]**

Over the course of time, there has been extensive research and development into various TMSs [9, 10, 11]. However, topics typically include individual systems for analysis. Many different methods have been used to provide analysis of the system including finite element thermal analysis, heat transfer and thermal imaging techniques, fluid flow analysis, and various thermal simulation programs [8, 16, 33].

This paper discusses the basic requirements of a total vehicle TMS. It will review some of the complex tradeoffs automobile manufacturers make when designing a thermal system [20, 34]. The focus of this research is on creating an optimized thermal solution for the ASU EcoCAR 3 vehicle and to emphasize the necessity for vehicle designers to use simulation software to mitigate thermal concerns before building a prototype.

## METHODOLOGY

### Siemens NX - CAD and Meshing

As mentioned earlier, Siemens NX was the primary software used for 3D modeling to verify packaging and assembly of the PHEV during the design phase. GM provided the CAD model for the 2LT Chevrolet Camaro, 2.4-liter LEA engine from the Chevrolet Equinox, and all associated hardware as a basis for the P2 hybridization. The main vehicle assembly was then heavily modified to accommodate the upgraded hybrid powertrain and ESS. Once the design was validated, the finalized CAD assembly could then be exported as an idealized part file (ipart) and meshed in Nastran, an NX plugin, for finite element analysis.

### 3D CAD Model Construction

Before any meshing for a thermal model can begin, there must be a base CAD model for the system being analyzed. As mentioned previously, GM provided the Chevrolet V6 Camaro 2LT model, which was used as a starting point when modeling the hybrid powertrain. The design of the hybrid powertrain was based on many factors that are beyond the scope of thermal considerations, such as packaging of all components, structural analysis, and electrical routings. The completed vehicle model is shown below in Figure 11.

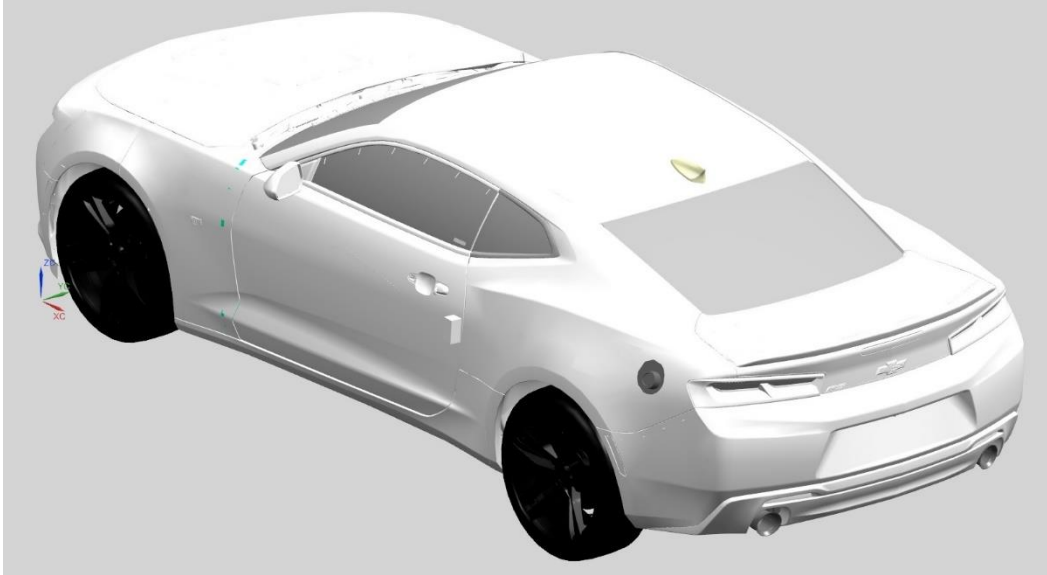


**Figure 11: Full Vehicle CAD Model**

*Powertrain Modifications*

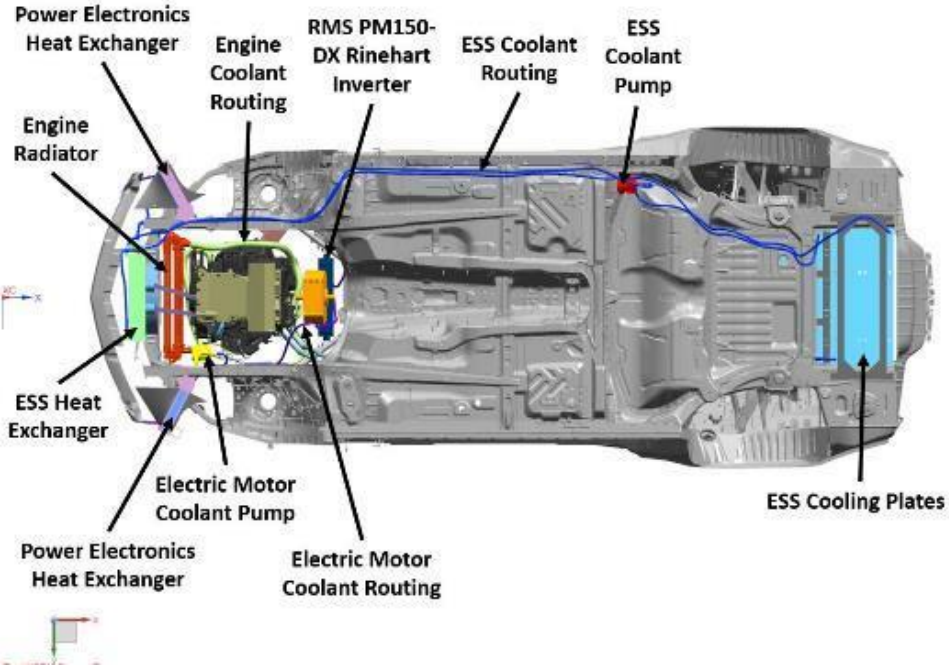
The major powertrain components that have been added to the vehicle to transform the Chevrolet Camaro into a PHEV are listed in Table 1.

Table 1: Major Powertrain Component List

<b>Component</b>	<b>Model</b>
Engine	GM 2.4 L LEA E85
Electric Motor	GKN AF-130 [35]
Inverter	Rinehart PM150-DX [36]
Battery	A123 18.9 kWh 7-Module 15s3p [37]
Transmission	GM 8L90 8-Speed Automatic
ESS Coolant Plates	Custom Solution
Coolant Pump	Meziere WP336S [38]
Clutch Actuator	FTE Automotive CPx-Unit [35]

Component	Model
Coolant Routing	AN#10 SS Braided Line

The packaging of all the main components was a challenge task. Many auxiliary components were required to be relocated as the new components were added. Many constraints existed in the development of the vehicle. For example, in a typical vehicle, a pull-style fan is utilized to pull the ambient air through the heat exchanger. In this vehicle, the fan required placement in front of the heat exchanger in a pull configuration due to the length of the powertrain. The major powertrain components and the respective placement is shown in Figure 12 and Figure 13.



**Figure 12: Powertrain**

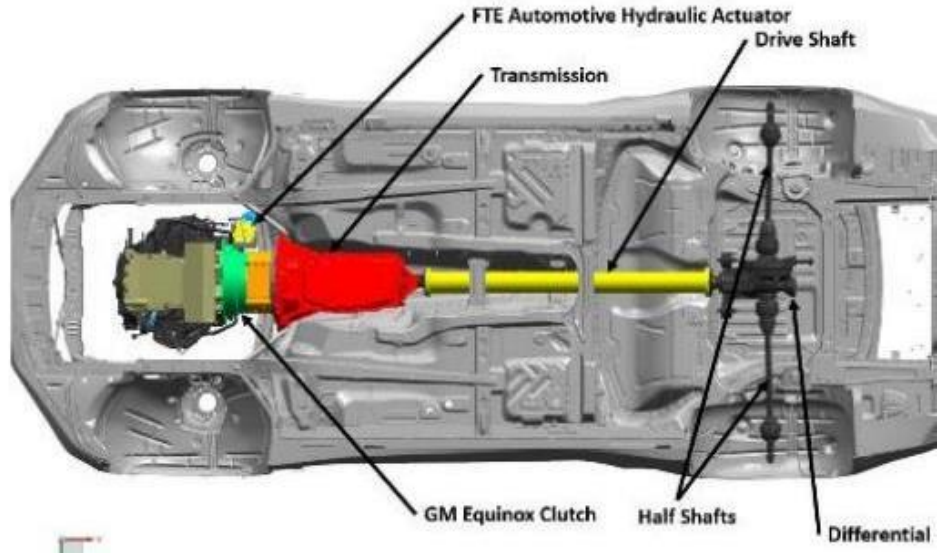


**Figure 13: Transmission, Drive Shaft, and Differential**

The electric drivetrain is configured as a P2 architecture for hybrid vehicles. This means that the EM is never disengaged from the transmission. Due to ambient noise created by the DC- to-AC conversion ESS power, these power lines were considered a priority to be as short as possible. Thus, the inverter is positioned above the EM, as shown in Figure 14.

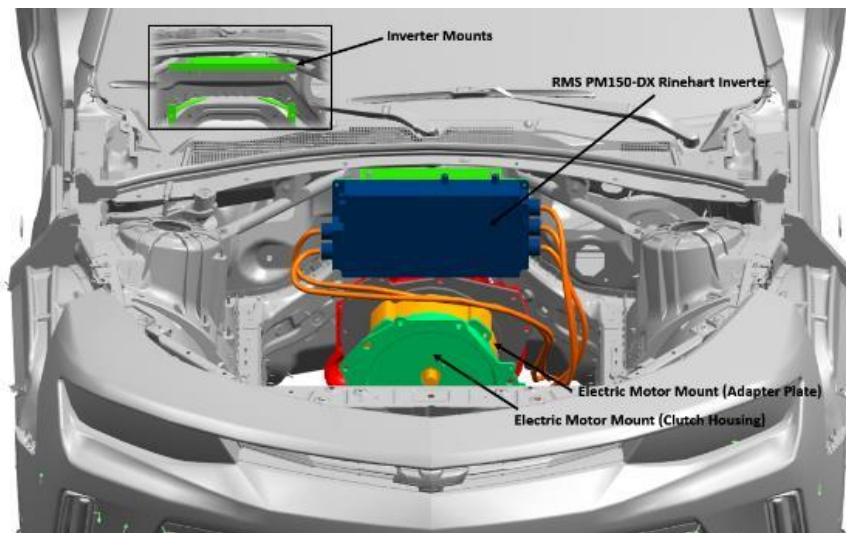


### Figure 14: Electric Powertrain

The large 7-module A123 ESS is in the rear of the vehicle inside the trunk. A major constraint was to not change the five-passenger occupancy of the vehicle. Therefore, because of the large size of the ESS, a trade-off was made to reduce space claim in the trunk to allow for the ESS to be integrated. The ESS is shown in Figure 15.

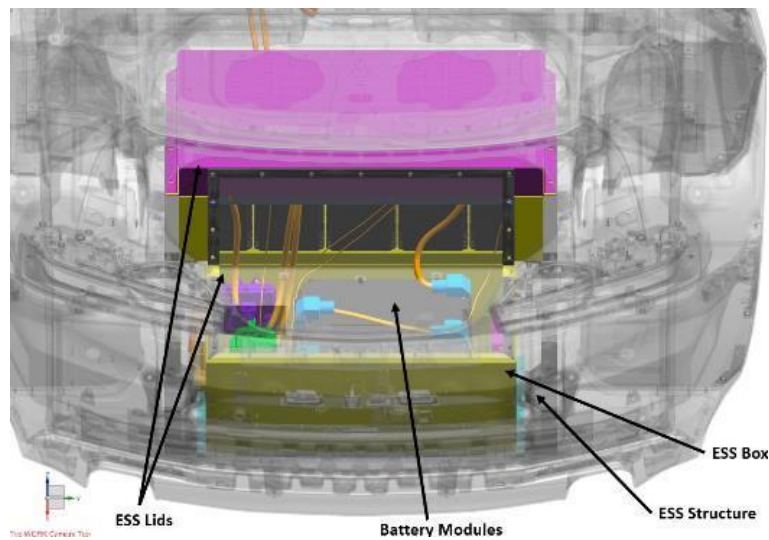
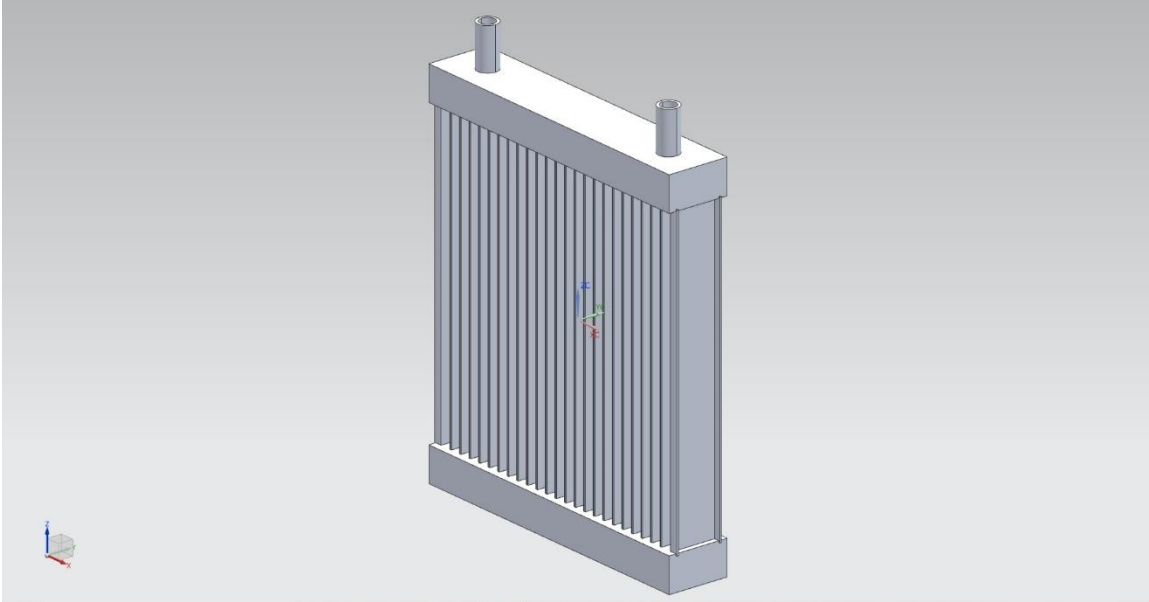


Figure 15: ESS

### *Heat Exchanger Optimization*

TAItherm requires dedicated parts for each fluid passage to define a fluid stream. Consequently, the simplified heat exchangers in the initial powertrain model needed to be updated with individual radiator cores to increase the fidelity of the low-temperature GKN and Rinehart serial cooling loop. The heat exchangers in the vehicle are stock to the Chevrolet Camaro SS and have been repurposed for this application. The 23 core, dual-row heat exchangers were measured and modeled, as seen in Figure 16. The fins were left

out of the models to reduce complexity in the meshing process, and the associated convection coefficient was calculated and assigned in TAITherm as if the fins were visible.



**Figure 16: Updated Low-Temperature Heat Exchanger Model**

The supplied CAD model of the high-temperature radiator for the LEA engine was also optimized for the thermal model. The CAD file for this heat exchanger contained a solid block for the cores just like the low-temperature heat exchangers, and had to be improved. Therefore, the 96 individual cores in the radiator were modeled and implemented to increase the fidelity, as seen in Figure 17.



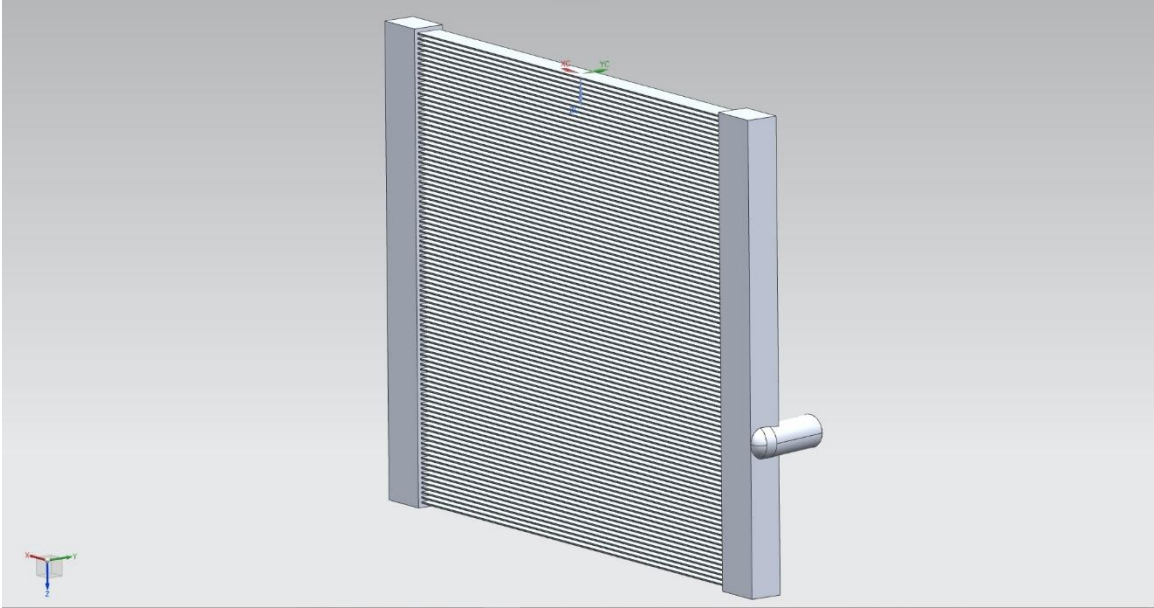


**Figure 17: Updated High-Temperature Heat Exchanger Model**

Now that the CAD model is completed, several steps are taken to create a simplified thermal model for initial testing. Considerations were made to remove all unnecessary components from the CAD file. The LEA engine, Rinehart, GKN EM, body panels, ESS, and drivetrain were deemed most pertinent to the TAITherm model and were recreated in a simplified form. The drivetrain includes adapter plates, clutch housing, transmission, driveshaft, differential, and half-shafts. By utilizing the Polygon Geometry tools problematic or skewed faces, edges and full parts could be modified or simplified to prepare each part for meshing. Every effort was made to reduce the amount of simplification made to the model to keep the high-fidelity nature of the CAD model. At the same time, clearing unnecessary parts

## Meshing

For a virtual thermal analysis to be performed in TAITherm, the faces of each component in the CAD assembly must be broken up into triangles or quadrilaterals known as elements. The accumulation of elements make up the mesh that is a necessity for all Finite Element Analysis (FEA) software. TAITherm is no different from other CAE software and runs computations on an element-to-element basis, thus simplifying calculations and shortening simulation run times. Meshing was performed using Siemens NX Nastran. The process begins with parts of the CAD model being converted to an ipart which is then imported into a FEA file. To decrease mesh computation time, the CAD model was broken into subsystems that were meshed individually. Each subsystem mesh was exported from NX Nastran as an NAS file and imported into TAITherm. The subsystems included friction brakes, ICE, cabin, exterior, powertrain, as defined above, and ESS.

Before the meshes were exported, mesh quality was evaluated for each subsystem. In order to create an accurate thermal model, an accurate mesh is crucial. Mesh quality for each subsystem was ensured through the elimination of free edges and misshaped elements. Free edges occur when two meshes meet but the nodes do not line up. This prevents conduction between the elements, which creates model inaccuracy. Free edges are eliminated by stitching edges. Figure 18 shows a comparison between a free edge (left picture) and an attached edge (right picture). Eliminating misshaped elements is just as important as these elements can create model inaccuracies. Misshaped elements can skew heat transfer values from and to the element. Figure 19 shows a comparison between a misshaped element (top picture) and the ideally shaped element

(bottom picture). Once the fixes were applied to each mesh, the meshes were imported into TAITherm.

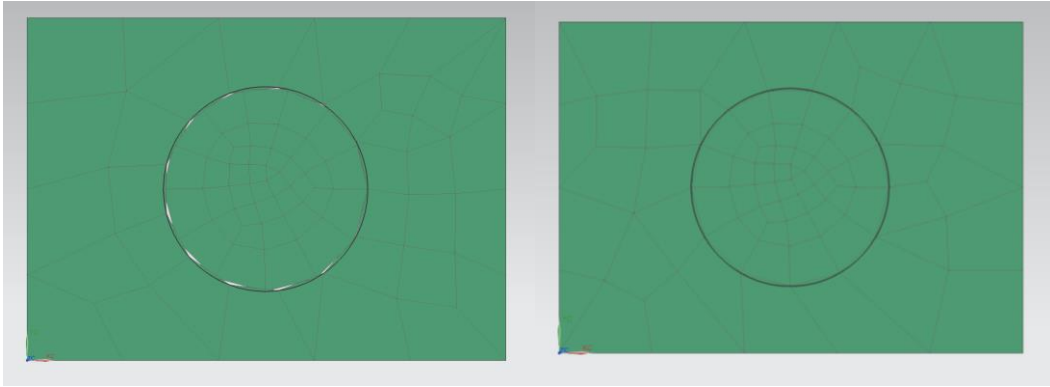


**Figure 18: Free Edge Correction**

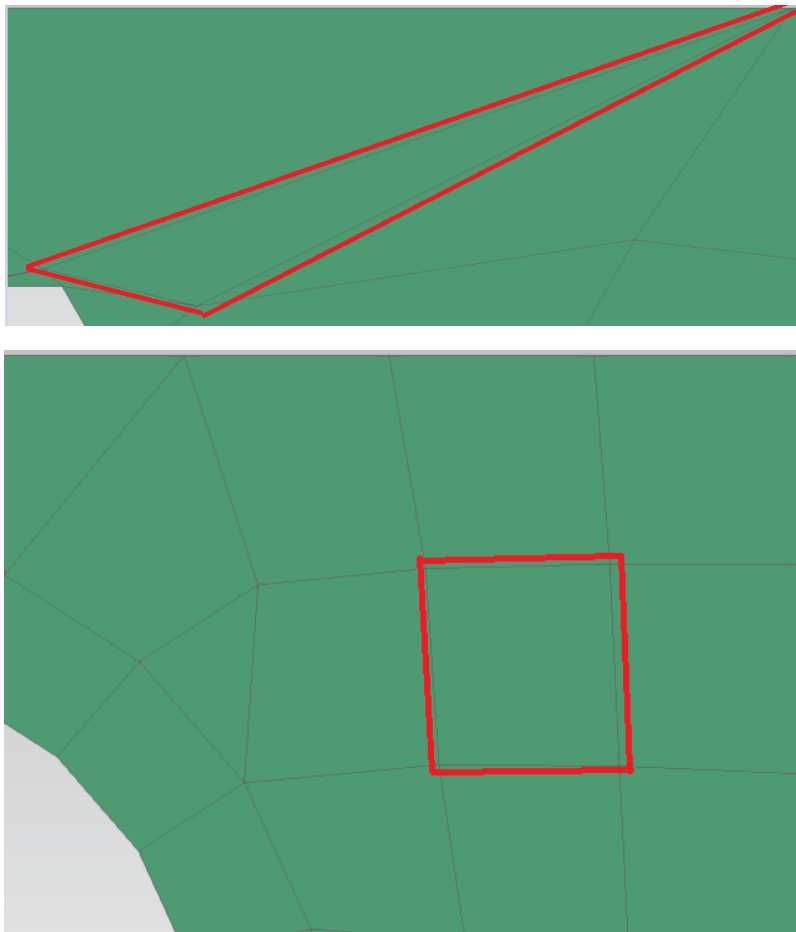


**Figure 19: Element Aspect Ratio Correction**

### *Friction Brakes*

Friction brakes in every automobile have one function: to convert kinetic energy into thermal energy and dissipate it to the surroundings to reduce vehicle speed. Yet, in hybrid electric power train, friction brake engagement is delayed whenever regenerative braking is engaged. Yet, braking systems are one of the most critical components to monitor in a thermal analysis, especially when considering that brake cooling capacity had to be increased due to the added mass in the PHEV Camaro. The supplied Camaro CAD model came with four stock 2LT caliper brakes, which were used for the thermal model. When the brakes were being meshed using the same procedure detailed above, certain faces and contact patches needed to be included as specified by the TAITherm user manual. The additional meshes are critical for TAITherm to simulate a rotating object.

Due to the complex surfaces that make up braking systems in the CAD environment, numerous faces were merged or split to allow the software to successfully generate a mesh. Surface meshes of the brake calipers, pistons, reservoirs, pads, backing plates, and rotors were created by utilizing the 2D mesh function in Nastran, shown in Figure 20. Afterward, the contact patches where the rotors touch the pads, or where the piston in the caliper touches the backing plate needed to be included. These contact patches are two-dimensional surface meshes that often overlap the full surface mesh of each component. However, TAITherm requires these duplicates to determine which elements are experiencing friction or pressure at any point in time. Finally, a volumetric 3D mesh of the brake rotor and pad were generated from the 2D surfaces to accurately analyze dissipation as the rotors spin.

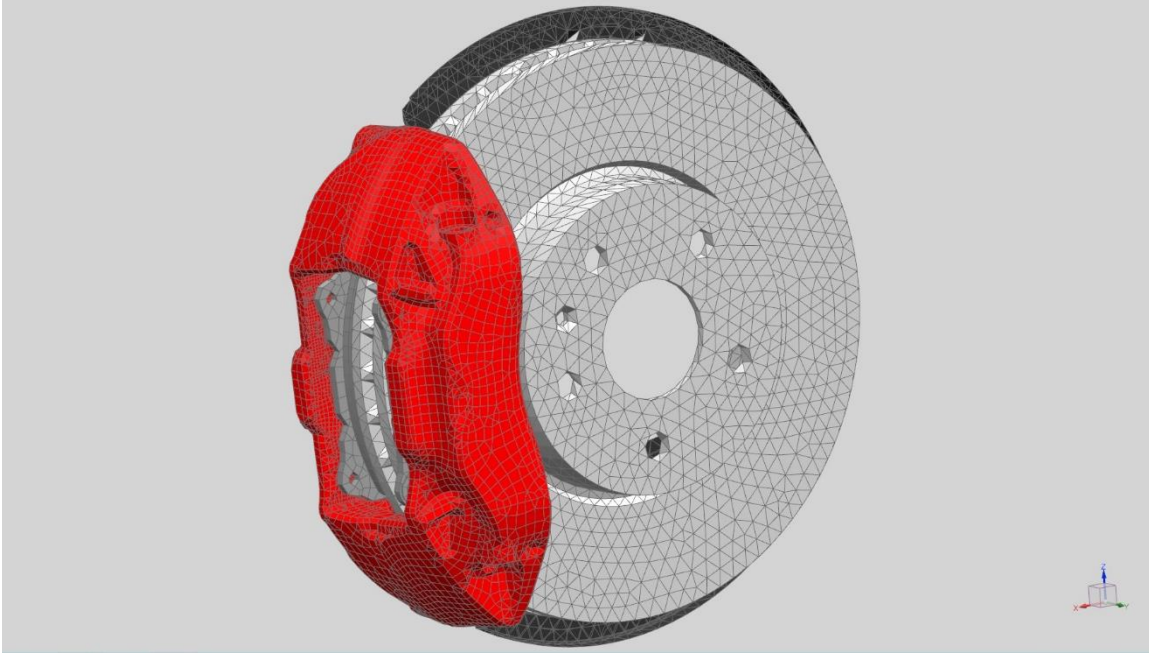


**Figure 20: Friction Brake Mesh**

The completed brake mesh was then exported from Nastran to TAITherm. Once in TAITherm, thermal links were created between the inboard and outboard rotor-to-pad contact surfaces, as shown in Figure 21. These links specify which contact patches are touching each other whenever the brakes are applied. Mathworks' MATLAB software was used to generate the associated heat rate, and contact curves across the US06 drive cycle. This was done by multiplying the percentage of braking input (0:1) by the convection value recommended in TAITherm's user manual of  $50 \text{ W/M}^2\text{-K}$  for the rotor, and  $30 \text{ W/M}^2\text{-K}$  for the caliper and pad [4]. The process was then reiterated with the suggested heat rate value of 30,000 W per rotor side [4]. These values are unknown for the Chevrolet Camaro and potential future work may include finding the actual values for this system.

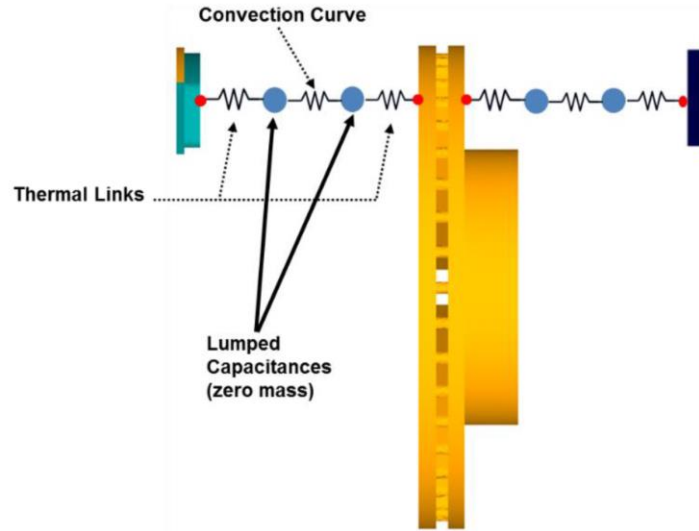


**Figure 21: TAItherm Brake Thermal Links [4]**

### *Engine*

The preliminary engine model in TAItherm consisted of a basic quadrilateral block and head combination with no internal mapping of the fluid jackets, as shown in Figure 22. This is very low fidelity considering most heat rejection in an engine is aided by water flow through the water jackets, and oil flow through the head. Due to the low fidelity, basic cylinders were implemented to simulate the combustion chamber and outer water jackets in the engine block. After some consideration, it was decided to improve the fidelity even further by meshing the entirety of the LEA Ecotec engine.

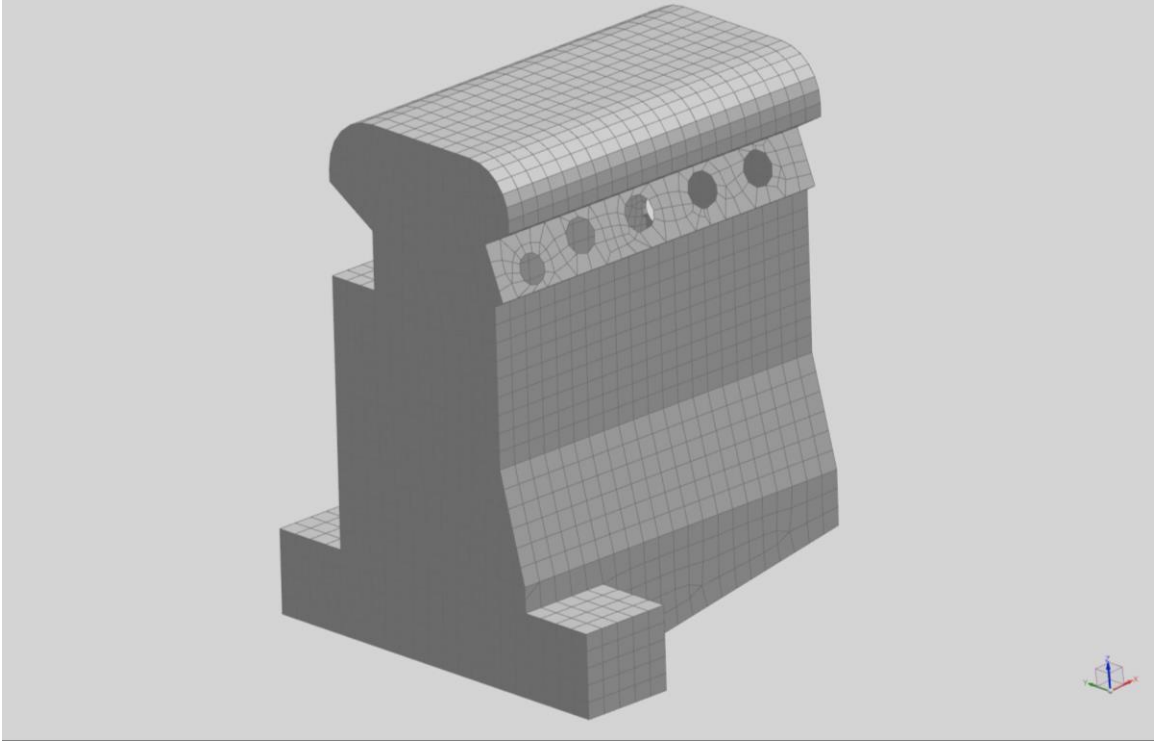


**Figure 22: Preliminary Engine Mesh**

To specify a fluid passage in TAITherm, individual meshes of each passage needed to be generated. Therefore, the improved engine mesh began with meshing the most significant cooling passages in an engine: the water jackets. Due to the supplied model not containing any specifications, diagrams, or additional information regarding the design, the CAD model was deconstructed virtually. After hiding a considerable amount of faces, the water jacket was exposed and each face and surface meshed. Water enters through the water inlet in the head and splits off around each cylinder simultaneously. After circulating the head, the water flows down into the block around each cylinder through a total of 19 drain holes. The result is not shown due to a non-disclosure agreement.

Moving forward with the engine meshing, the next passage to mesh was the oil jacket. In the LEA engine, oil is pumped from the bottom of the oil pan up into the head. The oil is then circulated in the head through a series of channels and openings to lubricate the cams and rockers. For the thermal analysis, it was assumed there would be minimal oil leakage through the cam and rocker lubrication holes and were thus sealed off for meshing. The complexity of the mesh to include potential loss was unavailable and not provided by the manufacturer. This assumption was made to reduce overall calculation time. This created a closed path for the oil to circulate in with one inlet and outlet. The combined oil jacket and water jacket are not shown due to a non-disclosure agreement.

The final internal components for the engine mesh were the cylinders, along with the intake and exhaust manifolds, as shown in Figure 23. The intake manifolds (blue) begin as one opening and split into two passages for each valve in the combustion chamber. The combustion chambers (orange) were sealed off on the bottom to create a closed cylinder for combustion to take place in the thermal model. Exhaust manifolds (red) are very similar compared to the intake manifolds. However, the Exhaust Gas Recirculation (EGR) passages were sealed off to decrease computation time in the thermal model. All valve holes that went through the top of the intake and exhaust manifolds were sealed considering there is no way to open the valves in the thermal model.



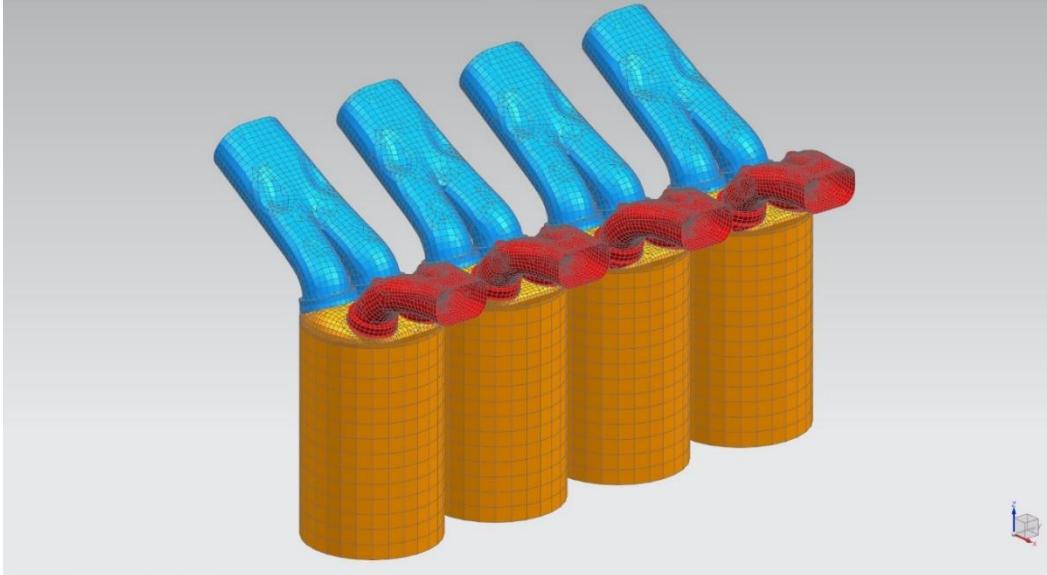


**Figure 23: LEA Engine Intake and Exhaust Manifolds Into Cylinders**

The final piece to the detailed engine mesh was to create a closed mesh of the engine block, head, and valve cover. The thickness of each component can be defined in TAITherm, so none of the structures inside of the engine were meshed. Some assumptions made in this mesh included the lack of oil filter and the numerous bolt holes used for mounting were sealed. A picture of the entire LEA engine mesh can be seen in Figure 24. This assumption was made as adding bolts adds complexity and calculation time. The oil filter affects the flow rate of the oil stream minimally.

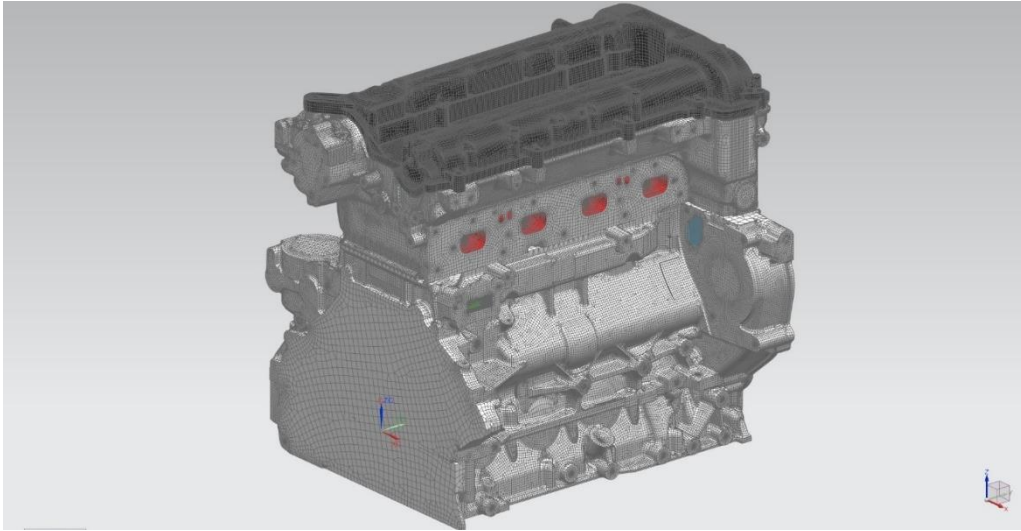


**Figure 24: LEA Engine**

### *Cabin*

In the supplied CAD model from GM, the interior was extremely detailed, and consequently, several part bodies were hidden before beginning the interior mesh as they would not affect the thermal analysis. The group of hidden parts included the shift lever, buttons, entertainment system, and door handles. The entertainment system was not included for heat rates as sufficient numbers could not be adequately determined. After the unnecessary parts had been hidden, the interior was meshed using a single 2D mesh for the dashboard and steering wheel. Afterward, the seat mesh was generated by individually selecting each face and stitching the numerous meshes together. The result can be seen below in Figure 25.

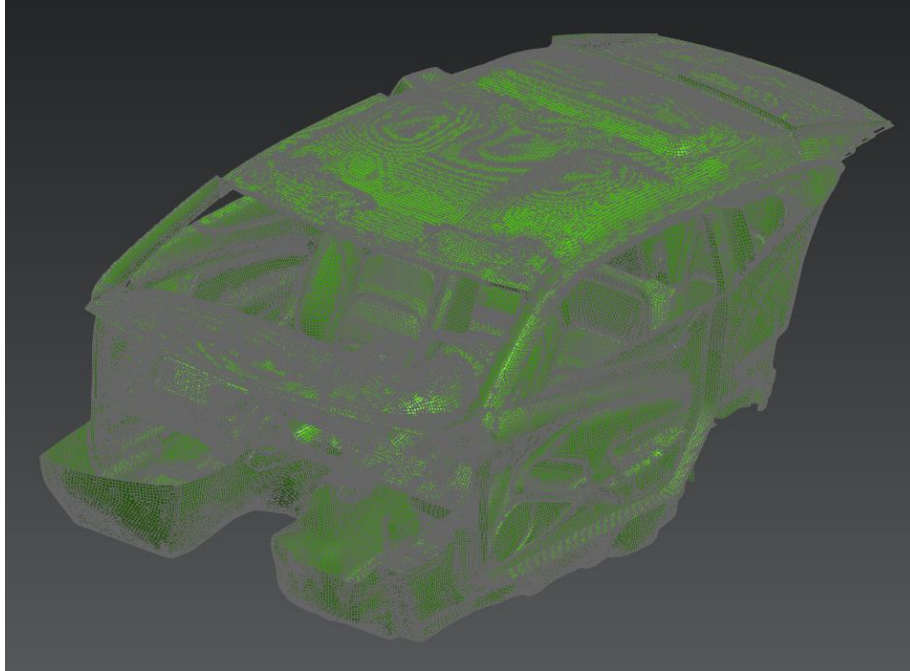


**Figure 25: Interior Mesh**

### *Exterior*

The exterior serves mainly as a visual design to influence consumer appeal; however, it is crucial when thermally analyzing a vehicle. This is due to the heat rejection it allows for the cabin and the passages it creates for air flows to and through heat exchangers. The exterior is also one of the more complex parts of the model. The Camaro body contains many fillets, blends, and holes that are not necessary for an accurate thermal model. In fact, all they do is complicate the mesh, creating longer model run times with no significant effect on model fidelity. Since this is the case, the exterior was simplified for meshing purposes. In order to optimize these parts, the team first needed to take out parts of the body that were unnecessary, such as internal door parts and latches. After this was complete, an idealized part file was created. This is where all the unnecessary holes and blends were deleted. After body panels and parts of the body were

optimized, a “10mm 2D CQUAD4” mesh was applied. The result can be seen below in Figure 26.

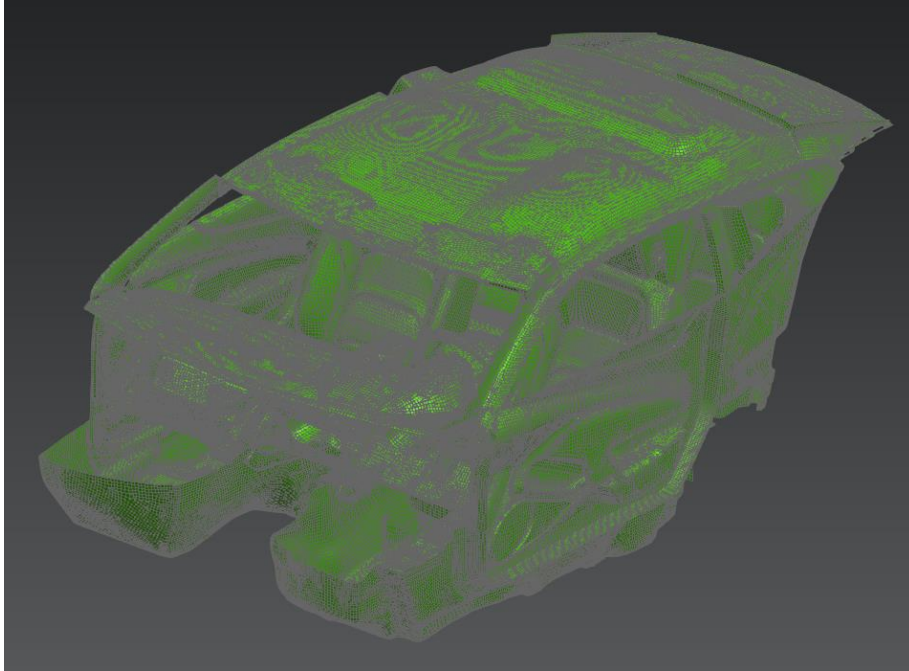


**Figure 26: Drivetrain Mesh**

### *ESS*

The ESS was based on a custom CAD model developed by ASU’s EcoCAR 3 team. The ESS model included the ESS itself, cooling plates, underside heat exchanger, reservoir, and pump. A 2D mesh was applied to all exterior faces of the model as well as every coolant passage in the model, including the coolant passages in the cooling plates so fluid nodes could be created in TAITherm. The ESS mesh is detailed below in Figure 27.

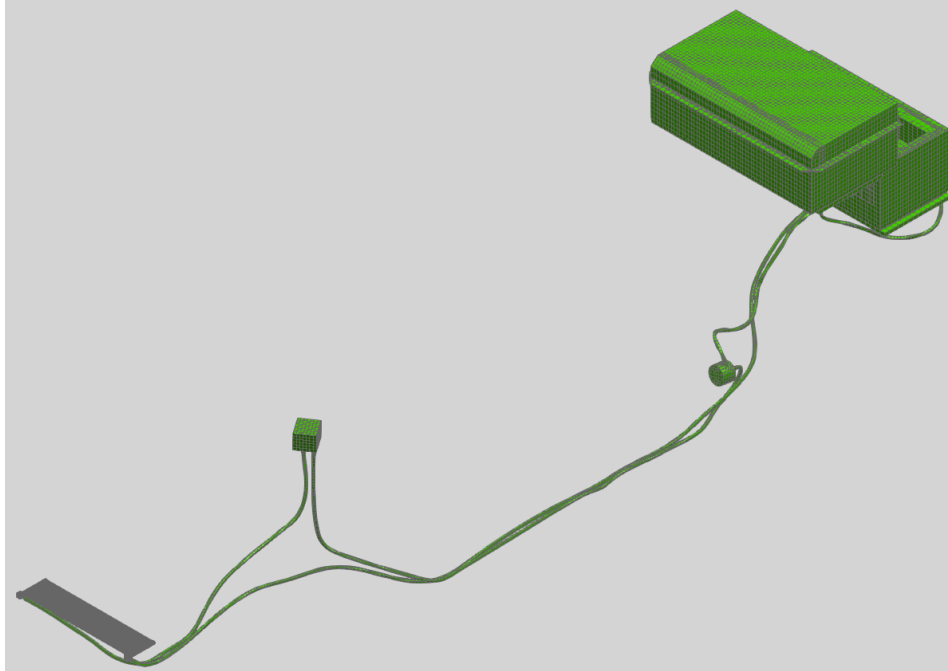


**Figure 27: ESS Mesh**

MATLAB Simulink - Numerical Simulation

Numerical Methodology

The design intent of the research was to develop a high-fidelity model with thermal analysis. PHEVs use large ESSs to store and provide significant amounts of electrical energy. Therefore, PHEVs generate large thermal load. The model is built in the MATLAB, Simulink, and SimScape modeling environment. The approach made towards building a TMS followed the listed approach below that was developed in references [11] and [6]. An illustrated flow diagram of the approach is shown in Figure 28.

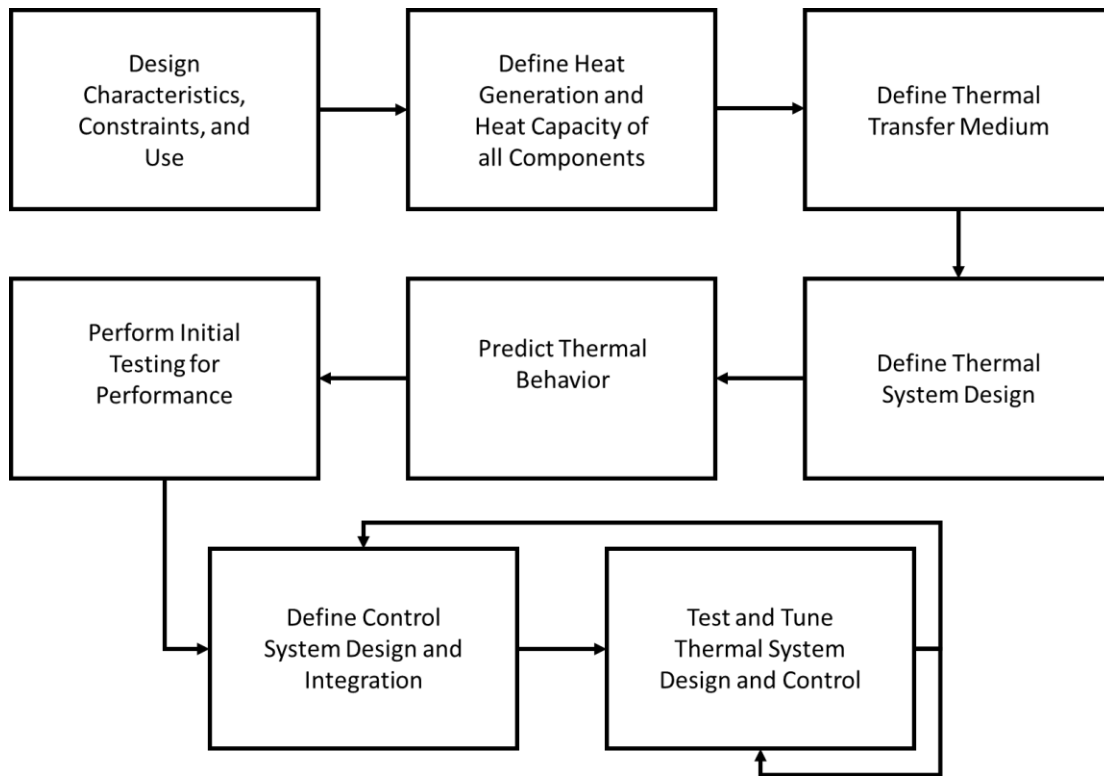


**Figure 28: TMS Design Approach**

The design components include the ICE, EM, ancillary equipment, transmission, inverter, high voltage battery, and AC compressor. The thermal characteristics of these components are crucial in the TMS design. Some constraints that must be included are the fact the ICE will require a standard radiator design as seen in most standard ICE production vehicles. The hybrid powertrain will create constraints upon the ESS for maximum voltage and current output. The inverter of a system may become a limitation if not properly sized. This highly affects the TMS as these systems create the most heat in the hybrid system while being some highly temperature-sensitive components.

Seven A123 18.9 Ah 15s3p modules were used to model the ESS. These batteries are used in various industries due to the high durability and performance. Information

regarding the impedance, voltage and current could be obtained from the manufacturer. The goal is to devise new thermal control strategies for these temperature-sensitive systems.

From this information, an estimate of the vehicle powertrain modules' thermal conductivity could be performed using a standard drive cycle. MATLAB software does incorporate convection and radiation blocks however, the use of such blocks significantly increases the calculation time. The blocks also require extensive knowledge of the physical system in order to accurately model these modes of heat transfer. The US06 drive cycle was chosen for the initial testing. Of the federal Environmental Protection Agency (EPA) drive cycles, the US06 is the most aggressive drive cycle used for testing and determining fuel economy. This is seen in Figure 29.

The aggressiveness of the drive cycle dictates a high demand for power and thus increases the intensity in which the ESS, EM, and ICE are used [16]. By producing increased thermal load, the control system could be tested to find the ability to mitigate the thermal stress on the entire powertrain. Standard thermal modeling blocks were used to predict the ICE, EM, and ESS behavior during the drive cycles.

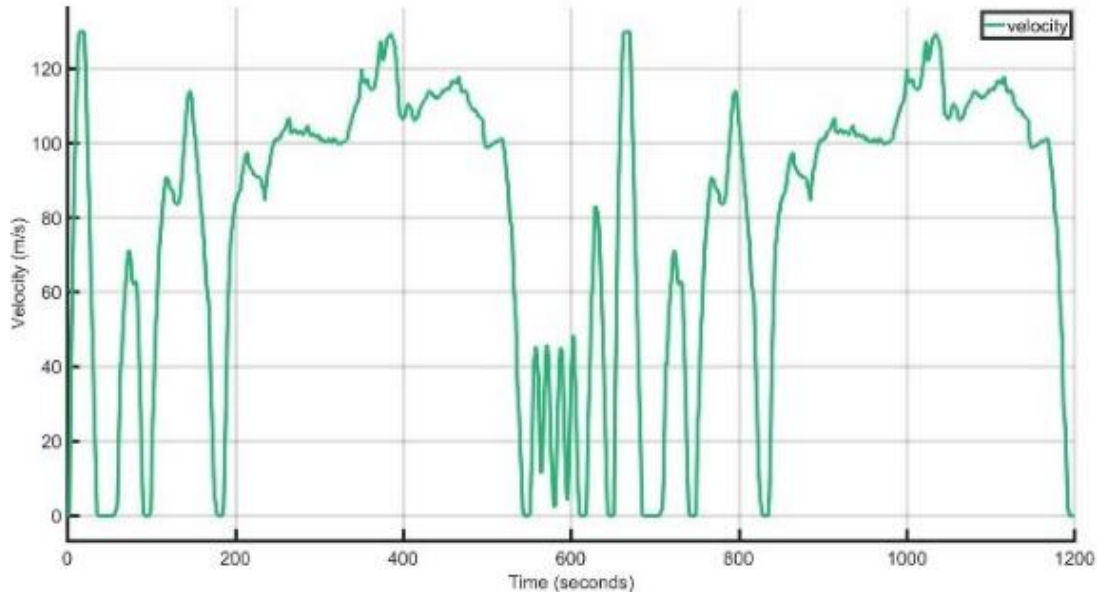


**Figure 29: US06 Input Drive Cycle**

Thermal load due to the execution of the entire vehicle model running the drive cycles is analyzed to predict the sizing required for the heat exchangers and liquid coolant system pump for temperature-sensitive powertrain modules. Current flow and power consumption from the ESS are logged and plotted in the simulation over the course of the drive cycle. The results of this analysis are given in Section 0.

The analysis performed will be conducted during Charge Sustaining (CS) mode. During CS mode, the ICE is frequently turned on for extended periods of time. It is important to analyze the overall system performance of under-hood power electronics and the resulting temperatures that are created. This allows for a robust TMS to be created for the under-hood electronics. CD mode does increase the overall thermal stress in the ESS with limited use the ICE. The use of CD mode reduces or potentially eliminates GHG emissions.



## Assumptions

There were some assumptions made during the numerical analysis. Many of the assumptions were made due to the complexity of the issue or lack of information provided by GM. All effort to reduce the impact of these assumptions and verification of the fidelity of the model have been made.

The internal transmission moment of inertia was used as the 8L90 weights were not provided. Also as the transmission fluid changes temperature, the shift pattern may also change. This information was not provided. Therefore, ideal situations of no changes were modeled.

The model also does not consider the road grade of the terrain. While significant changes can occur during these periods of time; a typical use of the US06 drive cycle is done with no road grade. ESSs are inherently temperature sensitive components, but as the batteries are liquid cooled, the ideal temperature range is assumed to be maintained. The optimal range for the A123 battery cells is between the temperature of 20 to 30 °C. It is assumed that the liquid cooling of the vehicle will keep the ESS within the optimal range. This assumption was made to simplify the model as coupling MATLAB with TAItherm is not yet possible. If the thermal system validation fails the system will be re-evaluated. However, results can be seen in Section 4.2.2.

The GKN AF130-4 EM does not have thermal efficiency ranges provided by the manufacturer. It was assumed that thermal efficiency would not cause a major discrepancy in the fidelity of the model. The EM is liquid cooled and assumed to be maintained at or within its operating temperature range. Similar to the ESS system, if

validation within the models fail the system will be re-evaluated. The results are shown in Section 4.2.1.

The ICE plays a major role in the vehicle fuel economy. When a typical ICE is at operating temperature, the fuel economy is changed. This is due to the warm-up period of the engine and the catalytic converter. While these changes are significant, the vehicle model assumes the engine is always in a warm state.

Disc brakes play a major role in changing how the vehicle stops. The information required to make high-fidelity disc brakes is also difficult to obtain. Therefore, to simplify the brakes, drum brakes were utilized. There is no thermal mitigation or effects given to the brakes, and assumptions were made on the surface area and friction coefficient based upon General Motors provided information.

Powertrain losses are typically dependent upon the angular speed. However, this dependency is not strong, and it was therefore assumed that is a constant percentage loss for each of the components [39, 40, 41]. This was true for every powertrain component except for the EM and the ICE. The ICE efficiency is based upon torque, speed, and fuel usage using information provided by General Motors. The EM efficiency maps were provided by Rinehart Motion Systems, LLC.

#### Driver Graphical User Interface

The driver graphical user interface (GUI), shown in Figure 30, was made to give a real-time assessment of the status of the vehicle at any given moment. The gauges show the vehicle speed, ICE angular speed, EM angular speed, ICE torque, EM torque, and total torque. The graph will show how well the vehicle is matching the drive cycle, which

is the US06, as previously mentioned.

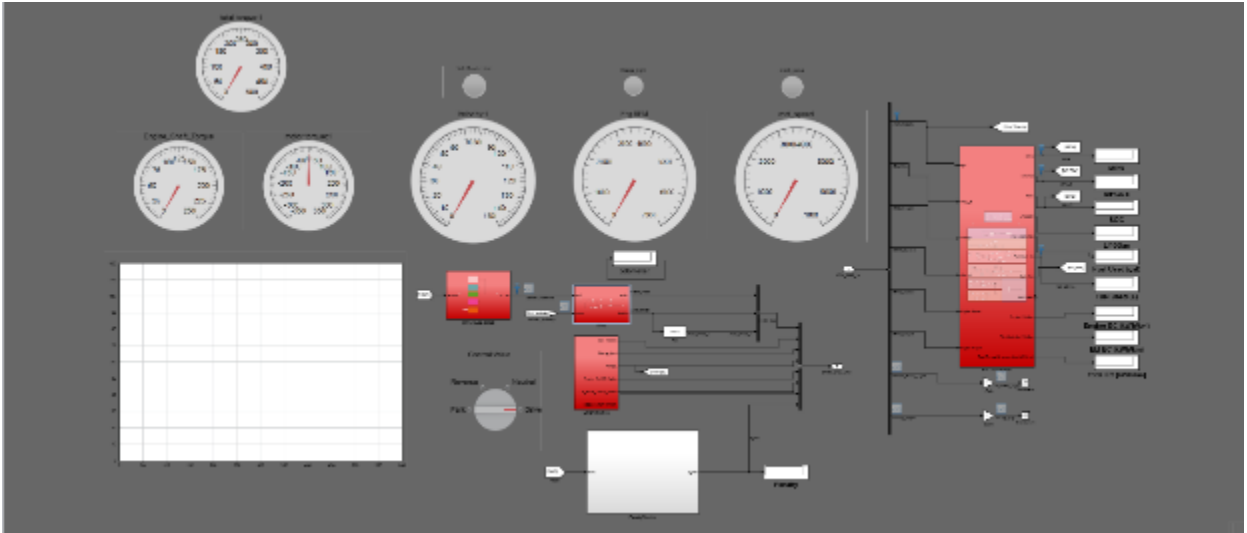


**Figure 30: Driver GUI**

### Driver Model

The driver model is meant to simulate driver input for the vehicle. A PID controller is used to create the signals for accelerator and brake. The US06 drive cycle is utilized for the set point for the PID and velocity is the variable. The set point consists of a repeating sequence block; the block will output a velocity corresponding to the given time step in the sequence. This value is compared to the velocity of the vehicle is sent into the PID, and the corresponding accelerator and brake pedal values are output.

### Vehicle Model

The vehicle model is used in a simulation with GM-provided and calculated variables to predict the behavior of the vehicle. The purpose of this model is to validate the hybrid supervisory controller code developed by the ASU EcoCAR 3 team in a safe, repeatable environment. During a simulation, the vehicle can follow standard drive cycles

and output information such as energy consumption, efficiency, torque provided, and vital signals required to run the supervisory controller. Each subsystem in the vehicle model has a plant model and a soft ECU. The plant models represent the function of the powertrain components and the vehicle body. The soft ECUs associated with each plant model represent the stock vehicle controllers with which the hybrid supervisory controller must communicate. The soft ECUs contain functions such as startup sequences and keep-alive counters. The model also incorporates full vehicle dynamics to test overall system performance. The full high-level system model can be seen in **Error! Reference source not found.** In the figure, the green color represents the torque producing components (i.e., ICE and EM), orange the electrical components (i.e., ESS), and turquoise is the torque multiplying and translational forces (i.e., torque converter, transmission, and wheels).

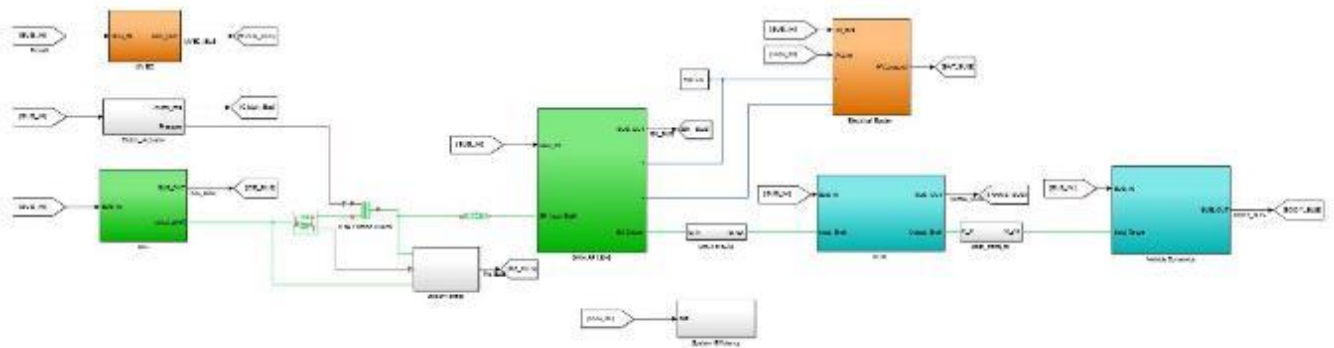


**Figure 31: Full Vehicle Model**

## ICE Propulsion

### *ICE Plant Model*

The ICE model used in the system consists of a Simscape generic engine block parameterized with torque, speed and inertia vectors associated with a GM 2.4L LEA ICE. The engine subsystem also contains a starter motor and a soft ECU to simulate the function of the actual ICE control module.

$$ICE\ Power\ Out\ (kW) = \omega * t * \frac{1}{1000} \quad (1)$$

where  $\omega$  is the rotational velocity of the output shaft (in rad/s), and  $t$  is the torque on the output shaft (in N·m).

### *Fuel System*

The fuel consumption of the ICE is calculated using data provided by GM. The data consists of torque and speed vectors, and a map for fuel flow in grams per second. This information is placed into a 2-D lookup table to be used in the dynamic simulation. The 7.96 kWh/kg is the lower heating value of E85.

$$fuel\ energy(kW) = \dot{m} * \frac{1}{1000} * 7.96 \frac{kWh}{kg} * 3.6e^6 * \frac{1}{1000} \quad (2)$$

$$\dot{m} = \text{mass flow of fuel in } \frac{\text{grams}}{\text{second}}$$

Engine Efficiency:

$$\frac{ICE\ Power\ Out(kWh)}{fuel\ energy(kWh)} \quad (4)$$

## Traction Battery System

### *Electric Plant Model*

The plant uses a full Battery Management System integration. **Error! Reference source not found.** shows a block diagram of the plant model. The plant allows controlling electrical contactors, EM, torque converters, resistances, and the vehicle differential. A SimScape electric servo motor was used as the torque-producing component. The SOC, voltage and current output are monitored carefully as these significantly affect the performance of the vehicle.

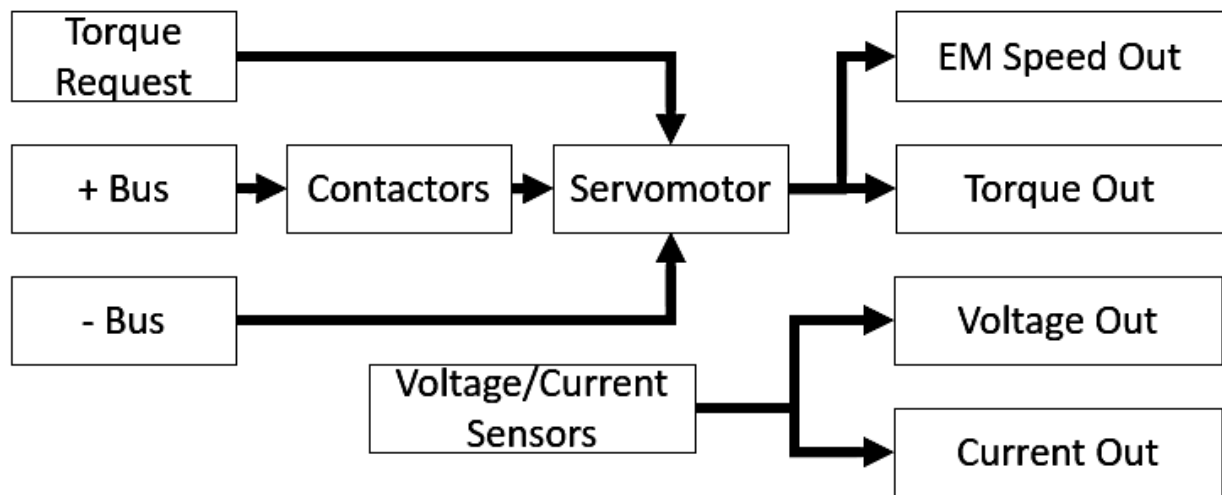


**Figure 32: Electric Plant Model**

EM Power Out:

$$EM\ Power\ Out\ (kWh) = \omega * t * \frac{1}{1000} \quad (5)$$

EM Efficiency:

$$\frac{EM\ Power\ Out(kWh)}{Electrical\ energy(kWh)} \quad (6)$$

The thermal load caused by regenerative braking may not be neglected in the simulation or physical systems. Regenerative braking is included in the model and reflected in the battery current as shown in Figure 33. Regenerative braking increases the thermal load of the battery system as current is sent back into the battery. The amount of recaptured energy is sent to the battery as determined by the information given by the manufacturer.

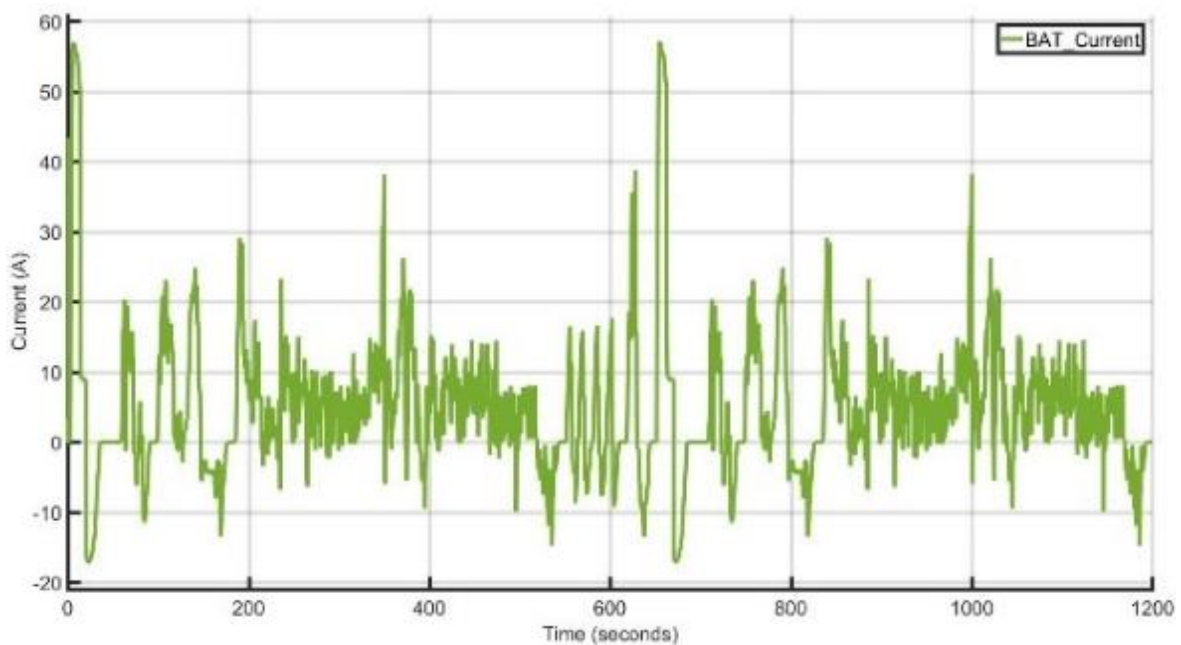


**Figure 33: Vehicle Current Usage and Regenerative Braking**

### ***ESS MODEL***

The ESS model simulates the power flow within each battery cell. The ESS is designed as an 18.9 kilowatt-hours ESS. Each battery cell impedance is calculated and then tabulated using a look-up table. The look-up table is then used to derive to the full

impedance of the module. The decision not to implement a parallel connection was done to simplify the coolant loops and follow the A123 recommendations.

A random Gaussian noise that has a normal distribution with a mean of zero is added to model dynamic change of the impedance in the battery cells. The calculated impedance is fed to a variable resistor to calculate the current loss of the system through a current sensor. Both current and impedance are sent to the thermal model to calculate power loss. The thermal mass of the system was calculated by using the mass of each battery cell multiplied by the cells within the module.

Similarly, the Open Circuit Voltage, OCV, of the system is calculated through a look-up table. The output of the lookup is multiplied by the number of cells of each module. The output then becomes the input to an ideal voltage source to model the steady-state voltage output of the module.

The system calculates the voltage and current out of the ESS at each time step thereby knowing the full energy consumption of the vehicle. This is accomplished by a current and voltage sensor. The total energy that is consumed in the vehicle is calculated using the equation below.

$$Total\ Energy\ Consumed = \sum Voltage_{in} * Current_{in} * \Delta t \quad (7)$$

The impedance information extracted from the datasheet is also utilized to calculate the SOC of the vehicle battery system [44]. SOC is calculated using the Coulomb Counting Method. The Coulombic Counting Method equation is shown below.

$$SOC = SOC(t - 1) + \frac{I(t)}{Q_n} \Delta t \quad (8)$$



where  $Q_n$  is battery capacity in Coulombs,  $I(t)$  is current in amps any the time step and  $\Delta t$  is the time step.

Total energy consumed, or power lost over time when multiplied by the impedance allows for the calculation of energy lost to thermal load. As the First Law of Thermodynamics states, energy can be neither created nor destroyed but must be transformed. The power lost is formulated using the equation below.

$$P_{lost} = I_{out}^2 * R_{ESS} \quad (9)$$

The power lost becomes important towards the thermal modeling as the heat produced from the flow of energy. Two specific areas of interest are the flows from ESS to the EM and vice versa, in the case of regenerative braking. The model accounts for both charge and discharge characteristics of the ESS.

The ESS thermal model provides an input to the overall thermal system model. **Error! Reference source not found.** illustrates the flow of information to produce each output of the ESS model, including the thermal information.  $R_0$  represents the value in which the resistance is at a specific SOC.

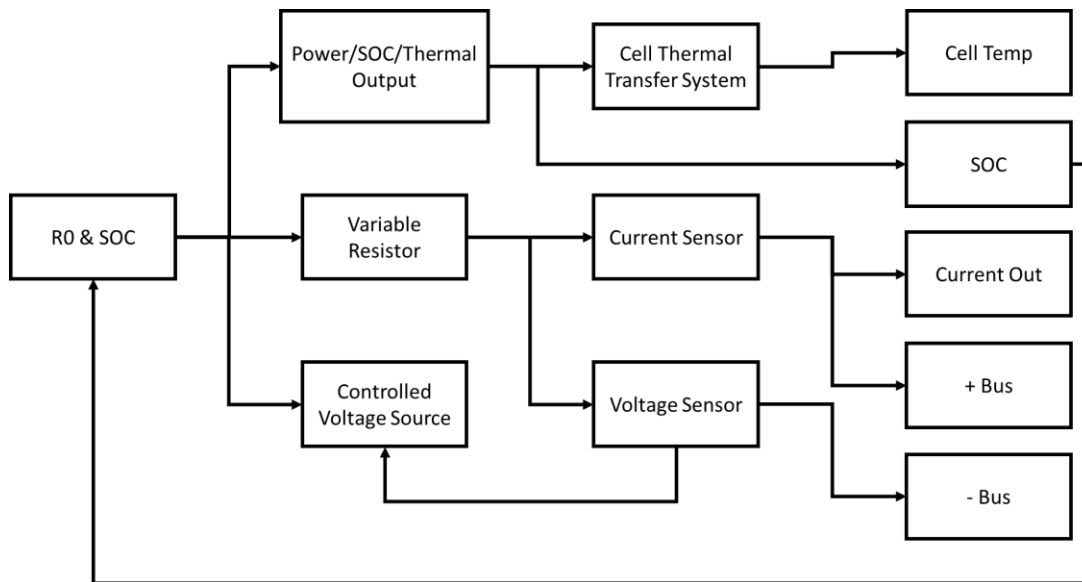


**Figure 34: Battery Model**

### *Electrical Losses*

The power loss analysis from the various electrical powertrain components was conducted using real-world data from the vehicle. The wire length and size of the electrical lines in question were determined using both CAD and in-vehicle measurements. The calculations were made to exhibit real-world power loss through the wire harness. These measurements were then added to the numerical model to integrate into the complete vehicle model. The resistivity of the lines was taken from the manufacturer's data sheets. A sample of the resistivity values is given in **Error! Reference source not found.** Values found between the numbers listed are interpolated. The value is then applied to a variable resistance in line to create a voltage drop in the system. The high-voltage harness is done in similar fashion using data from the respective datasheets [43].

**Table 2: Low-Voltage Harness Power Losses due to Resistance and Temperature**

Ambient Temperature (C)	Change in Resistance	Total Resistance with Temperature Change	Total Power Loss with Temperature Change
10	0.000515	0.013610	27.55998
20	0.001029	0.014125	28.60213
30	0.001544	0.014464	29.64428
40	0.002059	0.015154	30.68643
50	0.002573	0.015668	31.72858
60	0.003088	0.016183	32.77074
70	0.003602	0.016698	33.81289
80	0.004117	0.017212	34.85504
90	0.004632	0.017727	35.89719
100	0.005146	0.018242	36.93934
110	0.005661	0.018756	37.98149
120	0.006176	0.019271	39.02364

Equation 10 below shows the table used to determine the resistivity of the lines.

Additionally, the equation utilized to calculate the resistivity at given temperatures are shown below the equation below.

$$\Omega = \frac{(\rho * L)}{A} \quad (10)$$

$\Omega = \text{Total Resistance of the Wire}$

$\rho = \text{Resistivity of Copper}$

$L = \text{Length of the Wire}$

$A = \text{Cross Sectional Area of the Wire}$

By utilizing Equation 10 in conjunction with temperature curves from the data sheets, the power loss could be calculated in the low- and high-voltage electrical systems. This allowed for a more accurate estimation of the power curves and a better estimation of the vehicle technical specifications (VTSs) for refinements. As power is lost due to resistivity, the overall range and fuel economy and decreased.

As the temperature of the wires increases, the resistance of the lines increases, proportionally. An example of this relationship between resistance and temperature is shown in **Error! Reference source not found.**. Increasing model fidelity within the high-voltage electrical system is possible by utilizing the resistance curves generated.

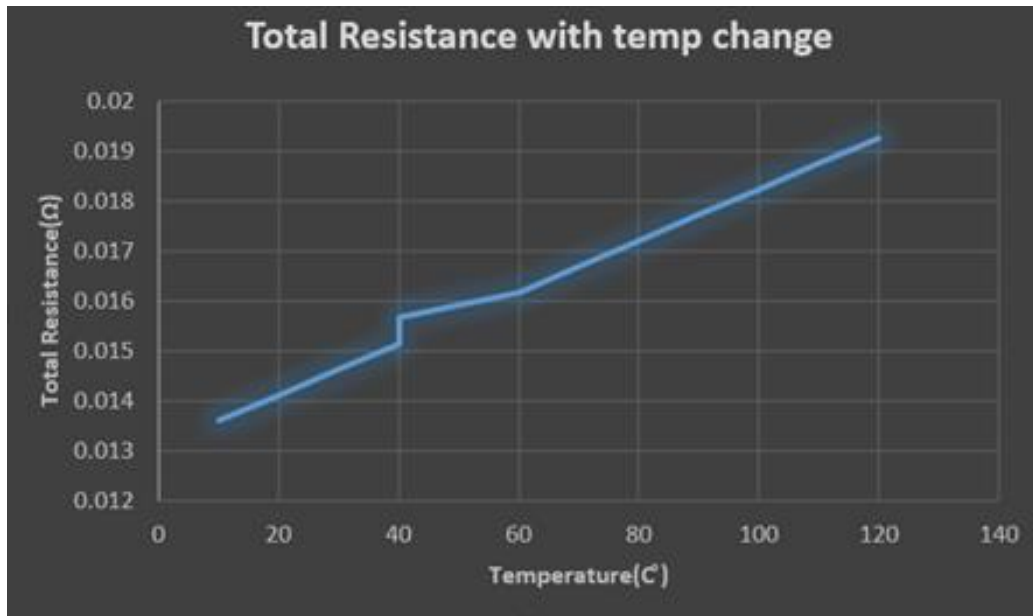


**Figure 35: Total Resistance with Temperature Change**

The total power lost due to the temperature change can also be estimated to increase model fidelity further. A sample of such a curve is shown in **Error! Reference source not found.** below. The higher power loss increases the output of the ESS, and these numbers allow for better numerical values to be generated to predict the thermal loss of the vehicle. This method gives good insight to understanding the transient power loss of the vehicle and enables planning for these changes during the ESS thermal mitigation strategy development.

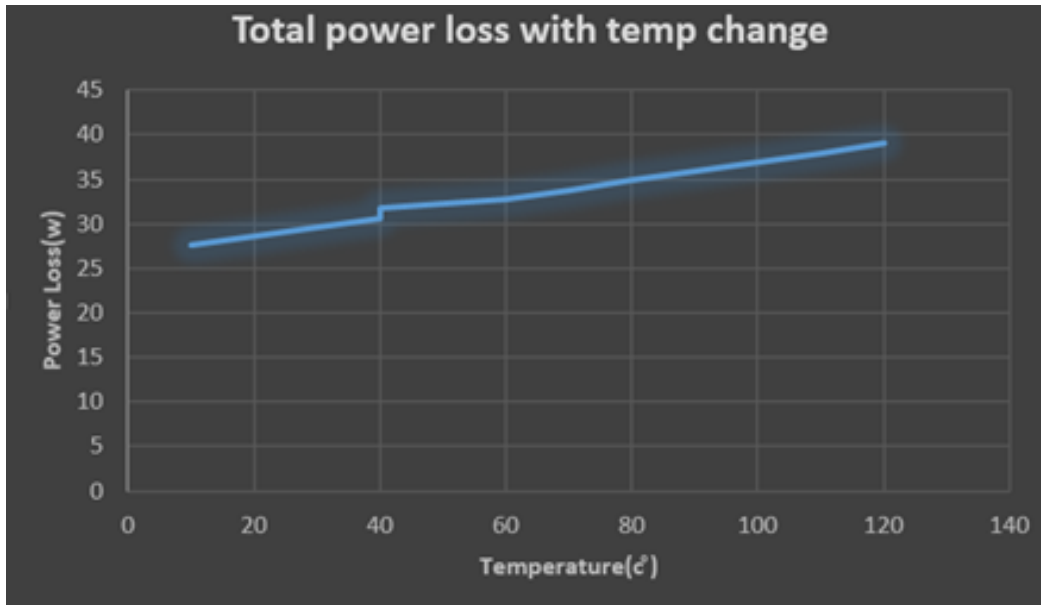


**Figure 36: Total Power Loss with Temperature Change**

#### Intake & Exhaust Flow Rates

The overall intake and exhaust air flow were modeled using standard calculations. The method involves determining the intake flow rate during the US06 drive cycle based on angular velocity from the MATLAB and Simulink model, and using this value along with the fuel mass to calculate the exhaust gas flow rate. This calculation assumes stoichiometric air-to-fuel ratio, and generates the exhaust flow rate curve. The equations used are detailed below:

$$Vd = \frac{D}{\# \text{ of } \textit{Cylinders}} \quad (11)$$

where  $D$  is the displacement.

$$Vc = \frac{D}{1-CR} \quad (12)$$

Where CR is the compression ratio.

$$V1 = Vc + Vd \quad (13)$$

$$V1 = Vc + Vd \quad (14)$$

$$M_m = \frac{P1 * V1}{R * T1} \quad (15)$$

where P1 is intake pressure, R is the atmospheric gas constant of air, and T1 is the intake temperature or temperature of the cylinder.

$$P2 = P1 * CR^k \quad (16)$$

where K is the specific heat capacity.

$$T2 = T1 * CR^{k-1} \quad (17)$$

$$V2 = M_m * \left(\frac{T2}{P2}\right) \quad (18)$$

$$M_{air} = (1 - AF) * (1 - E_{res}) * M_m \quad (19)$$

where AF is the air fuel ratio or stoichiometric of 14.7:1 and Eres is the Exhaust Residual of four percent.

$$M_{fuel} = \left(\frac{1}{AF}\right) * (1 - E_{res}) * M_m \quad (29)$$

$$M_{exhaust} = M_{fuel} + M_{mass} \quad (30)$$

This calculation provides the mass of the exhaust at any point in the angular velocity range. If the angular velocity curve is divided by two, this provides the number of exhaust strokes at that given point in time. The angular velocity curve is divided by two as at any given combustion cycle the system only uses two cylinders. By multiplying

the amount of exhaust strokes by the mass of the exhaust, the exhaust mass flow rate curve can be generated.

$$\dot{M} = \frac{RPM}{2} * M_{exhaust} \quad (31)$$

Since the angular velocity of the ICE is occasionally faster than the one-second iterations of the model, the flows were simplified to examine the constant circulation of the air from intake to exhaust. The simplification was needed as the model cannot keep up with the higher angular velocities. The cylinders of the ICE were exported from the mesh, and a constant rate inflow variable to angular velocity and fuel usage was created. The flow rate of the ICE based on the displacement of 2.4 liters was calculated and then split among the four separate cylinders.

Due to the heat generated during combustion, the air volume is expanded. Therefore, the intake air is coupled to a fluid node at the base of the cylinder and, with the use of advection links, coupled to each exhaust port. This method allows for a steady stream of intake air and the calculated output of combustion to be combined through the exhaust manifold and into the exhaust piping.

TAITherm – Thermal Analysis

Parts Editor Tab

The parts tab front menu of TAITherm is shown in **Error! Reference source not found.** and the back menu is shown in **Error! Reference source not found.**. These menus allow the part to be defined with various selections. A description of the critical

selections is contained in Appendix B. A brief explanation of each feature and option is also provided within the table in the Appendix.



**Figure 37: Parts Editor Tab – Front**

The back of the component menu is shown in **Error! Reference source not found.** While not quite as extensive as the front, this allows for the merger of dissimilar materials on each side. The “Middle” tab has an added benefit as additional layers could



be implemented to the mesh. This could be used, for example, in areas such as floorboards. This methodology could allow for differences in material properties such as carpet, multilayer floorboards, or firewalls.

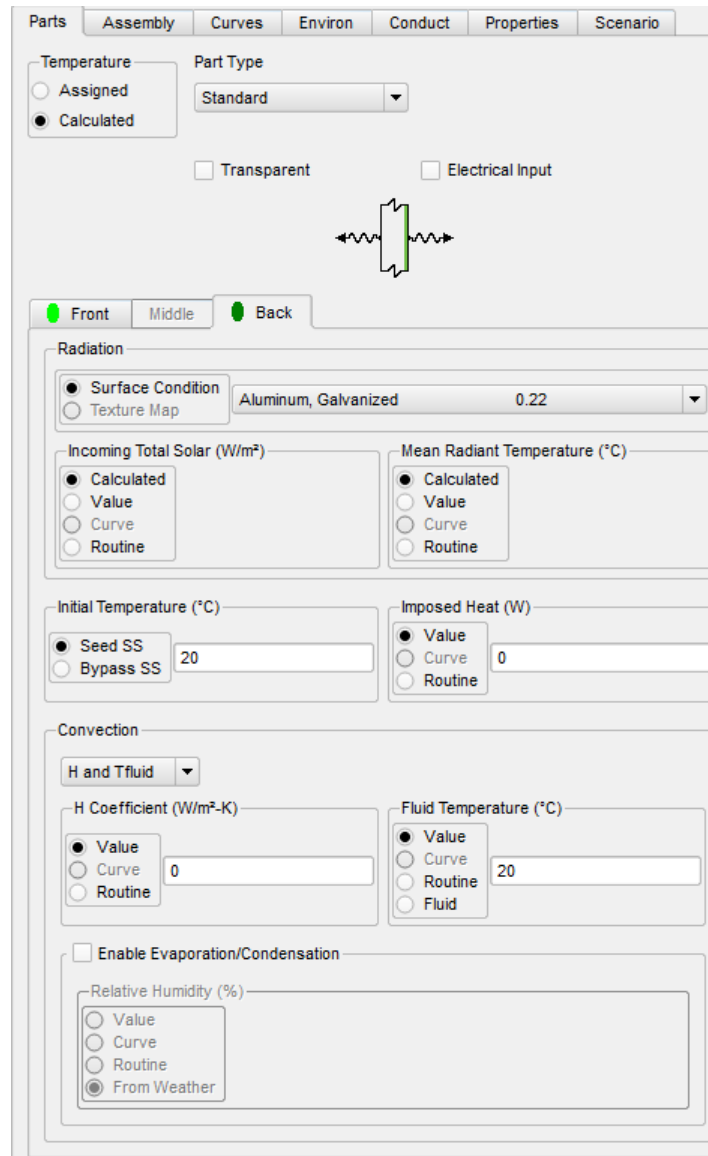


**Figure 38: Parts Editor Tab - Back**

Appendix B **Error! Reference source not found.** shows the most commonly used selections within the Part Tab. The temperature is continuously calculated as each part

involves the full conduction, convection, and radiation of the heat sources. The part type is only changed for highly conductive parts and is typically kept on the standard selection. The material and thickness vary due to the variance in some areas within the vehicle. However, typical values are aluminum and steel for powertrain and body parts. The incoming total solar and mean radiant temperatures are calculated using the weather file. If using a bounded box environment with what TAITherm calls a “defined solar lamp” fluid node, using the calculated option would be acceptable. The initial temperature is set to “Bypass SS” at 20 °C. The temperature was utilized as this is the set temperature within the lab space. The simulation is meant to be a realistic test as if the vehicle was sent from the lab to conduct a drive cycle outside.

The convection being set to “H and T Fluids” is one of the most important settings as it defines how the geometrical mesh interacts with the surrounds fluids. This is used as the fluid temperature, and can be set to a fluid or fluid stream to determine the value of the fluid surrounding the part. The H coefficient is utilized for the heat transfer between the solid and the liquid, and evaporation and condensation rates are based on the humidity of the area in which the vehicle is being simulated, which in turn is extracted from the weather file. Both evaporation and condensation are only used on the outside of the parts and not the inside of the meshes, as the heat generated would make these latter values negligible.

**Table 3: Commonly Used Part Tab Selections**

Parts Editor Utilized Values	
Category	Selections
Temperature	Calculated
Part Type	Standard
Material	Varies on Part (Examples: Aluminum, Steel, PVC)
Thickness	Varies on Part
Radiation	Surface Condition
Incoming Total Solar	Calculated
Mean Radiant Temperature	Calculated
Initial Temperature	Bypass Steady State (20 °C)
Imposed Heat	Varies By Part (Commonly 0 °C)
Convection	H and T Fluid
H Coefficient	Varies by Material
Fluid Temperature	Fluid (attached to associated fluid)
Relative Humidity	From Weather (Only used on parts exposed to atmosphere)

The temperature of each part is set to calculated, as all heat sources interact within the simulation. The parts must be fully defined in the simulation for the assessment to begin.

### Fluids

Fluids are the basis of the thermal network within TAItherm. A fluid node may be generated independently of a geometrical part, such as air in front of the vehicle. A fluid reservoir may also be represented within a geometry to classify a fluid volume.

Another usage is a point in space used to record temperatures via convection to the fluid from surrounding objects. Fluid nodes may be connected to other types of fluids by use of advection links. Advection links connect various nodes together to form a stream. They may connect one fluid to another fluid or a fluid streams to another fluid stream. Both fluids and fluid streams are shown graphically in the model as a small green box. Fluid streams will be discussed in the next section. An example of a fluid node setup is shown in Figure 39.

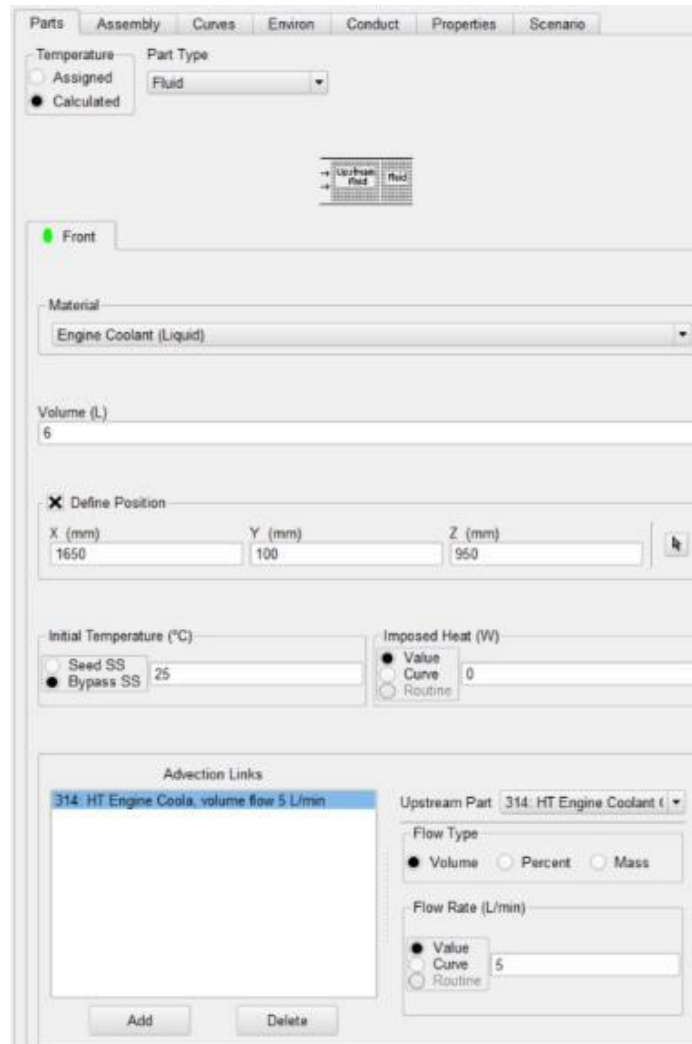


**Figure 39: Fluid Editor**

## Fluid Streams

Fluid streams are used to create a stream of fluid nodes that are connected in a manner that is similar to fluids and advection links. Fluid streams automatically create the fluid nodes of a system that is contained within the boundary of a part, and are particularly useful for quickly replicating fluids within an enclosed space. The editor tab is shown in Figure 40.

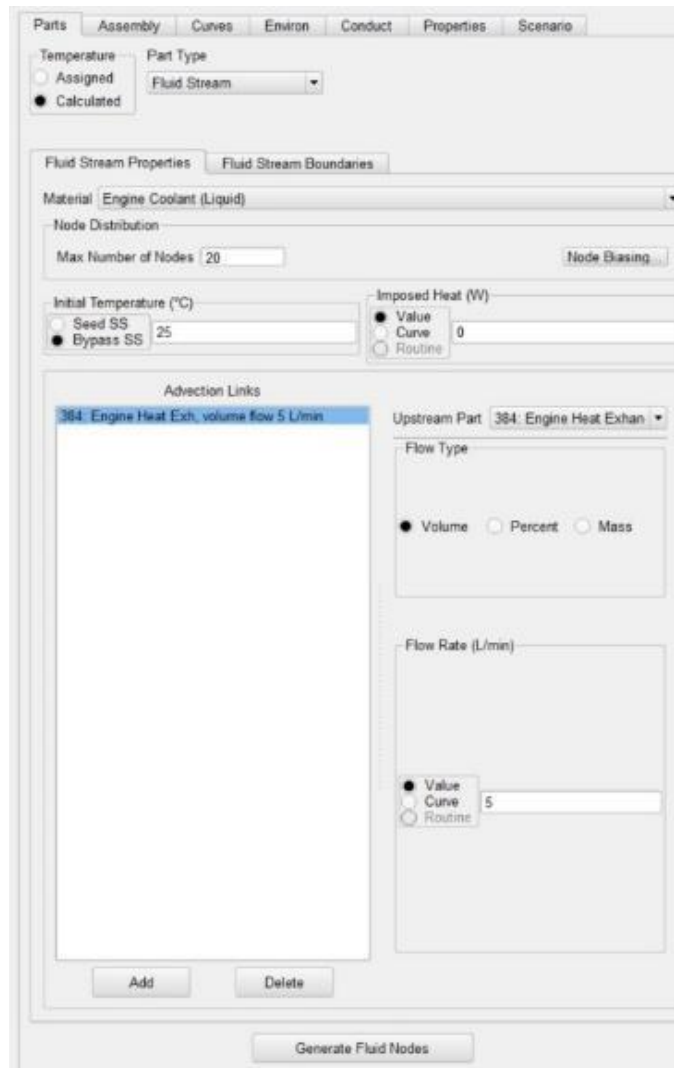


**Figure 40: Fluid Stream Editor**

In the editor tab, the temperature may be assigned or calculated as in the parts editor tab. The part type must be defined as a fluid stream as this is the part being created. A more detailed description of the options available in the fluid stream is listed in Appendix C.

Node biasing dictates to the solver how to prioritize the nodal points. This allows the node distribution to be prioritized from the set point. Node biasing allows the user to control the fidelity of the fluid stream where geometry may have many twisted pathways. The node biasing menu is shown in Figure 41. A detailed description of node biasing is given in Table 4.



**Figure 41: Fluid Stream Node Biasing**

**Table 4: Fluid Stream Node Biasing Editor**

Fluid Stream Node Biasing Editor		
Category	Selections	Purpose
Node Biasing	None	No node bias.
	Inlet	Prioritizes the inlet for creating the fluid node generation.
	Outlet	Prioritizes the outlet for creating the fluid node generation.
	Both Ends	Prioritizes the ends of both inlet and outlet for fluid node generation.
	Center	Creation of the fluid nodes is prioritized from the middle of the bounded part and extends to the inlet and outlet. This is used as the recommended option.

The fluid stream boundary conditions must be set for the fluid stream. The fluid stream boundary points are selectable from the mesh or, if the positions are known, may be set up manually. The menu is shown in Figure 42. A detailed explanation of the selections is shown in

Table 5.



**Figure 42: Fluid Stream Boundaries Editor**



**Table 5: Fluid Stream Boundaries Editor**

Fluid Stream Boundaries Editor		
Category	Selections	Purpose
Inlet Position	X, Y, Z	Select or Manually set the input of the fluid boundary.
Outlet Position	X, Y, Z	Select or Manually set the output of the fluid boundary.
Bounding Parts	N/A	Select the part in which the fluid stream will be bounded.
Specify Face	Both Sides	Sets both faces of the mesh to the boundary.
	Front Only	Sets only the outer face as the fluid boundary.
	Back Only	Sets only the back face as the fluid boundary.
Automatically Set Convection Type for	Selected Parts	Sets the convection faces to the bounded parts that are selected.
	All Parts	Sets the convection faces to all parts selected.
Generate Fluid Nodes	N/A	Utilizes TAItherm to automatically generate the set number of fluid nodes to the stream. The higher the fluid nodes, the higher the fidelity.

### Curves

The heat rate curves of each imposed heat source are unique to this methodology. Typically, these numbers may be derived by physical testing of the components. In this method, the numerical calculations are used to estimate the anticipated heat curve. The numerical analysis used to generate the curves in Figure 43 through Figure 47. The heat generation is placed upon the part using the imposed heat curve. This allows the heat conduction, convection, and radiation to be distributed within the simulation. The data collected for this section are in Appendix A.

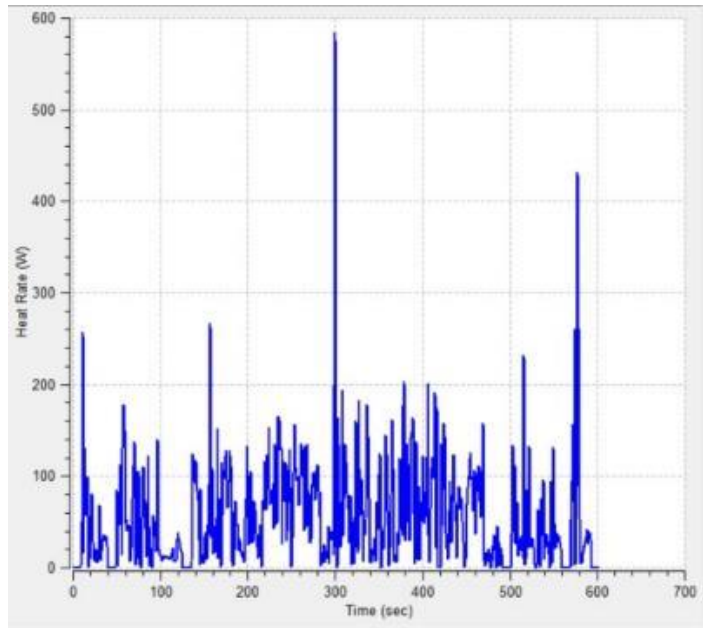


**Figure 43: Battery Heat Rate Curve**

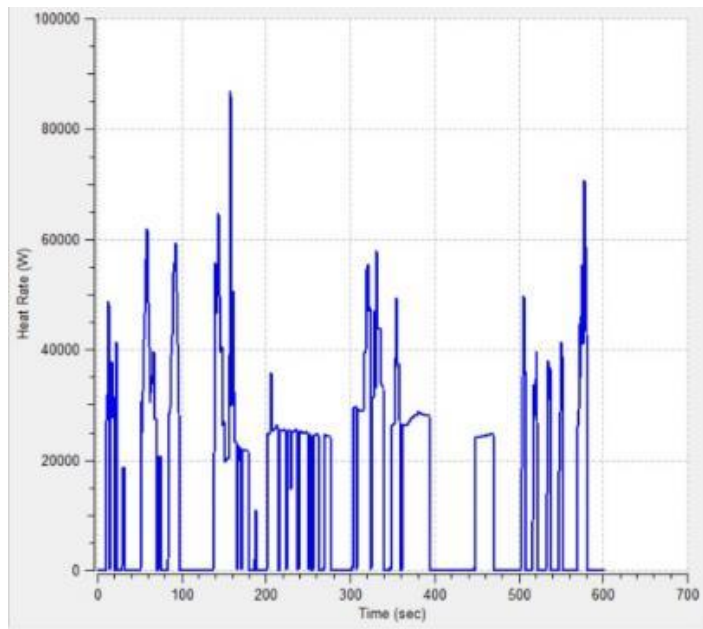


**Figure 44: Engine Heat Rate Curve**

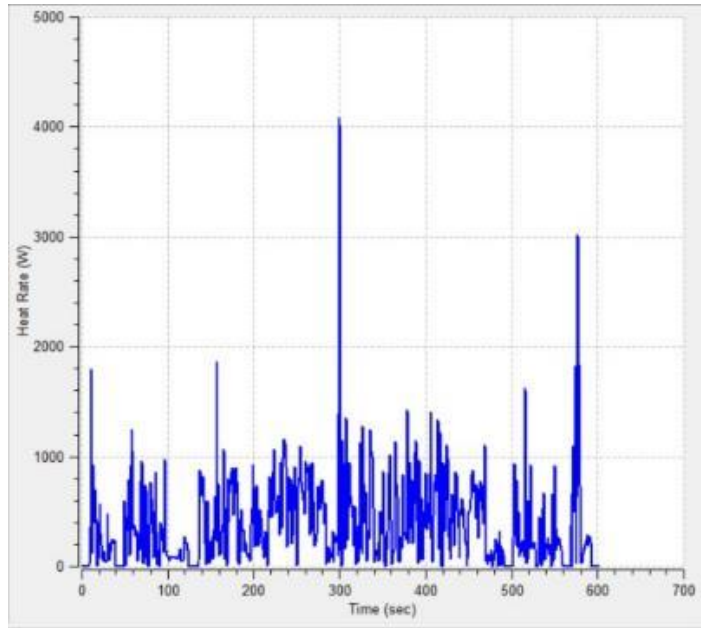


**Figure 45: Inverter Heat Rate Curve**

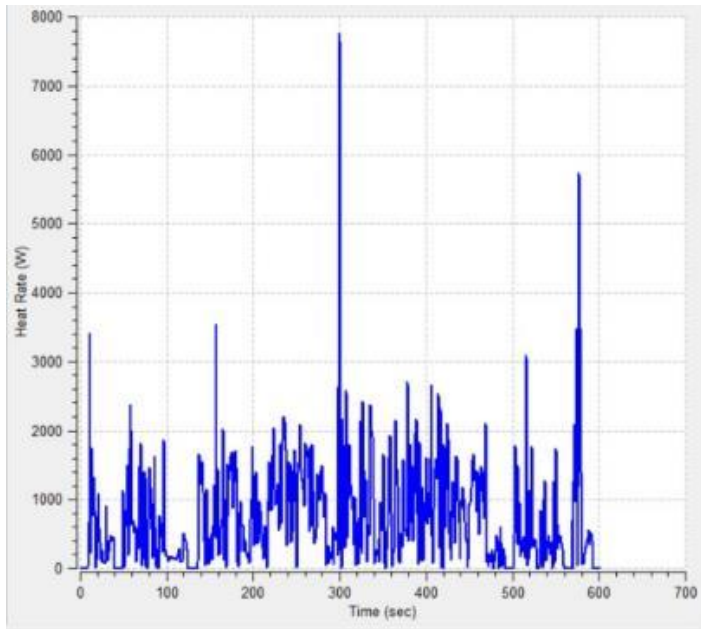


**Figure 46: EM Heat Rate Curve**

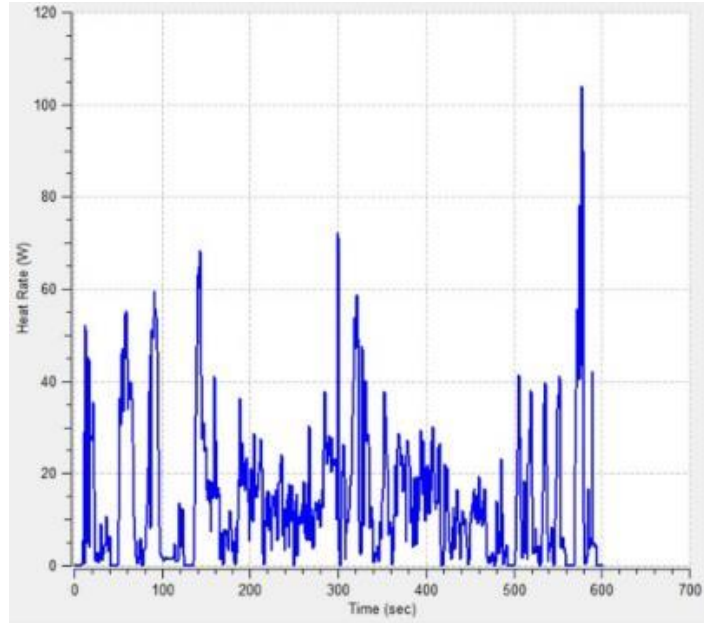


**Figure 47: Transmission Heat Rate Curve**

The calculations performed in Section 0 dictate the intake air flow based upon the displacement of the ICE. The total intake air was based upon the need of the GM 2.4-liter LEA Ecotec ICE. The required total required air intake at various points in time during the US06 drive cycle is shown in Figure 48.

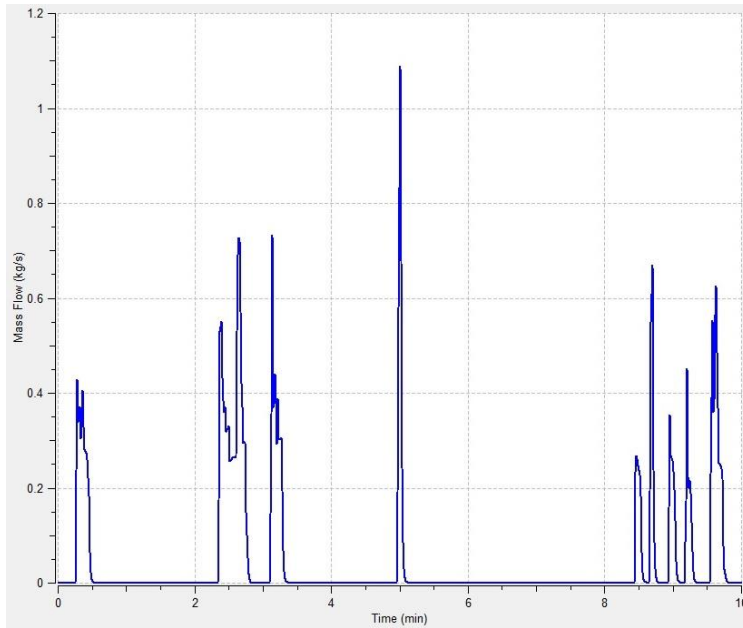


**Figure 48: Total Intake Air**

To reduce the computational time, the air intake was assumed to be split evenly into each of the four cylinders. The air intake for a single cylinder is shown in Figure 49.

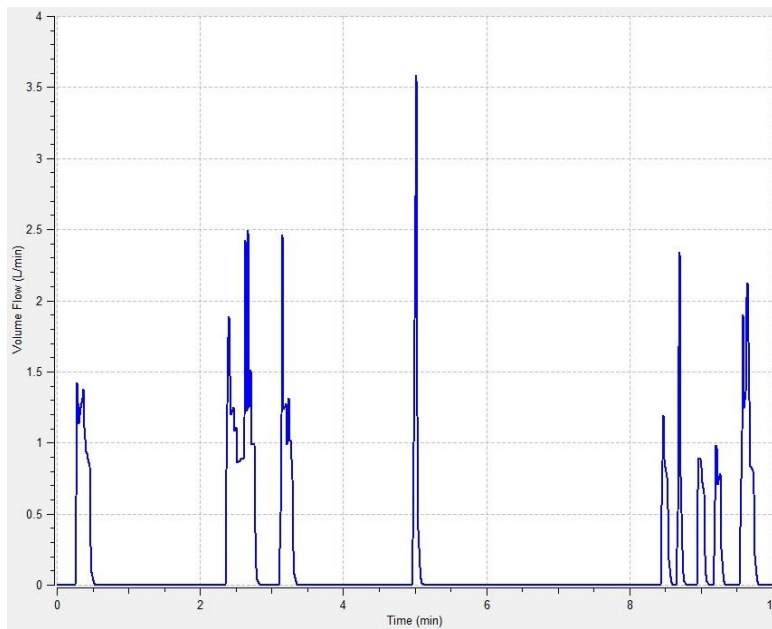


**Figure 49: One Cylinder Intake Flow**

Upon combustion within the cylinder chamber, air expands, moving the cylinder head. The resultant air flow was computed and is shown in Figure 50. Computation of the flow rate is discussed in Section 0.

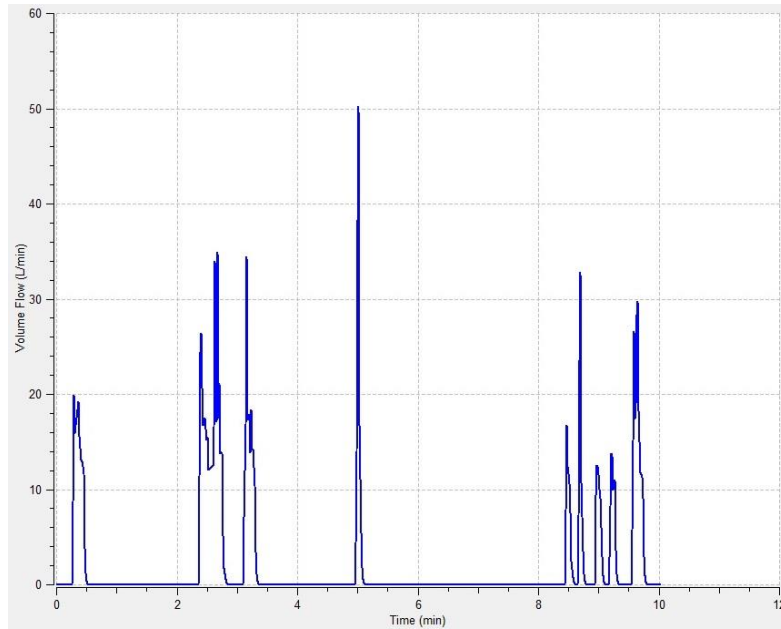


**Figure 50: One Cylinder Manifold Exhaust Flow**

The total exhaust flow recombines upon departure from the cylinder to the exhaust manifold. The air is combined with the exhaust before the catalytic converter. This combined exhaust flow is shown in Figure 51.

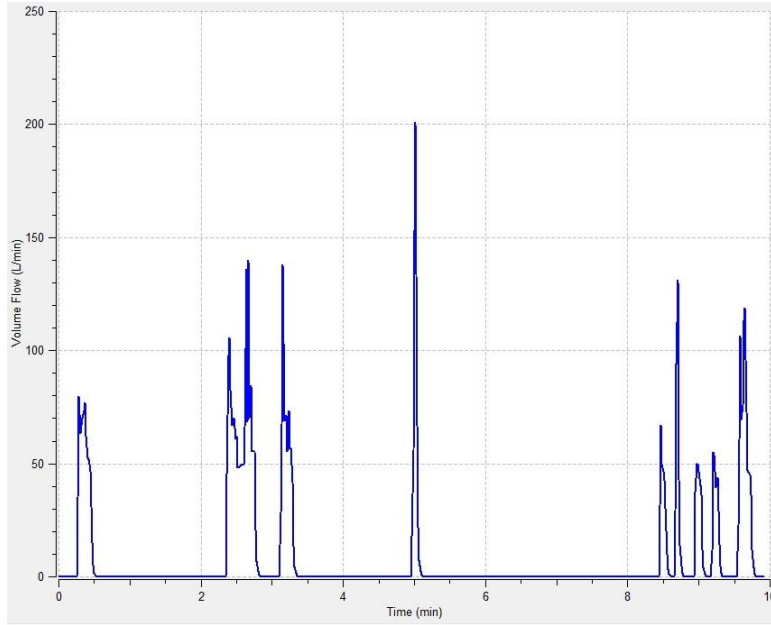


**Figure 51: Total Exhaust Flow**

## Weather

The program allows for outside weather conditions to be added to the simulation for accurate analysis of the geometry mesh in relation to the local weather. The data are provided by a website called “Weather Underground” [44]. The website utilizes a simple Perl script to extract the weather for a specified day which is then imported into TAITherm for analysis.

The website tracks and stores weather data from various parts of the world. The environment selected for this simulation is Phoenix, Arizona on July 15<sup>th</sup>, 2016. The sample of the data extracted from the website is shown in

Table 6.

**Table 6: Historic Weather Data Excerpt 07/15/2016**

Time (MST)	Temperature (°F)	Dew Point (°F)	Humidity (%)	Pressure (in)	Visibility (mi)	Wind Dir	Wind Speed (mph)	Gust Speed (mph)	Precipitation	Events	Conditions
12:51 AM	98.1	48.9	19	29.74	10.0	NNW	5.8	-	N/A		Clear
1:51 AM	93.9	50.0	22	29.74	10.0	WSW	3.5	-	N/A		Clear
2:51 AM	93.0	50.0	23	29.74	10.0	West	3.5	-	N/A		Clear
3:51 AM	91.0	51.1	25	29.75	10.0	Calm	Calm	-	N/A		Clear
4:51 AM	91.0	52.0	26	29.77	10.0	East	6.9	-	N/A		Clear
5:51 AM	90.0	52.0	27	29.79	10.0	ENE	4.6	-	N/A		Partly Cloudy
6:51 AM	91.0	48.9	23	29.81	10.0	Variabl e	6.9	-	N/A		Clear
7:51 AM	93.9	50.0	22	29.83	10.0	NNW	9.2	-	N/A		Clear
8:51 AM	97.0	48.0	19	29.83	10.0	WNW	11.5	-	N/A		Clear
9:51 AM	100.0	48.9	18	29.84	10.0	West	10.4	-	N/A		Clear
10:51 AM	100.9	48.9	17	29.83	10.0	Variabl e	5.8	-	N/A		Clear
11:51 AM	105.1	48.9	15	29.81	10.0	Calm	Calm	-	N/A		Clear
12:51 PM	108.0	48.0	13	29.78	10.0	WSW	10.4	16.1	N/A		Clear

The data are then extracted into a TAItherm-provided Perl script. The Perl script translates the data into a weather file which is then read by the program. The data that must be provided contain the year, month, day, longitude, latitude, and the elevation of the route. These data are then shown in the Environment tab, as seen in Figure 52**Error! Reference source not found.**, with the Natural weather option selected.



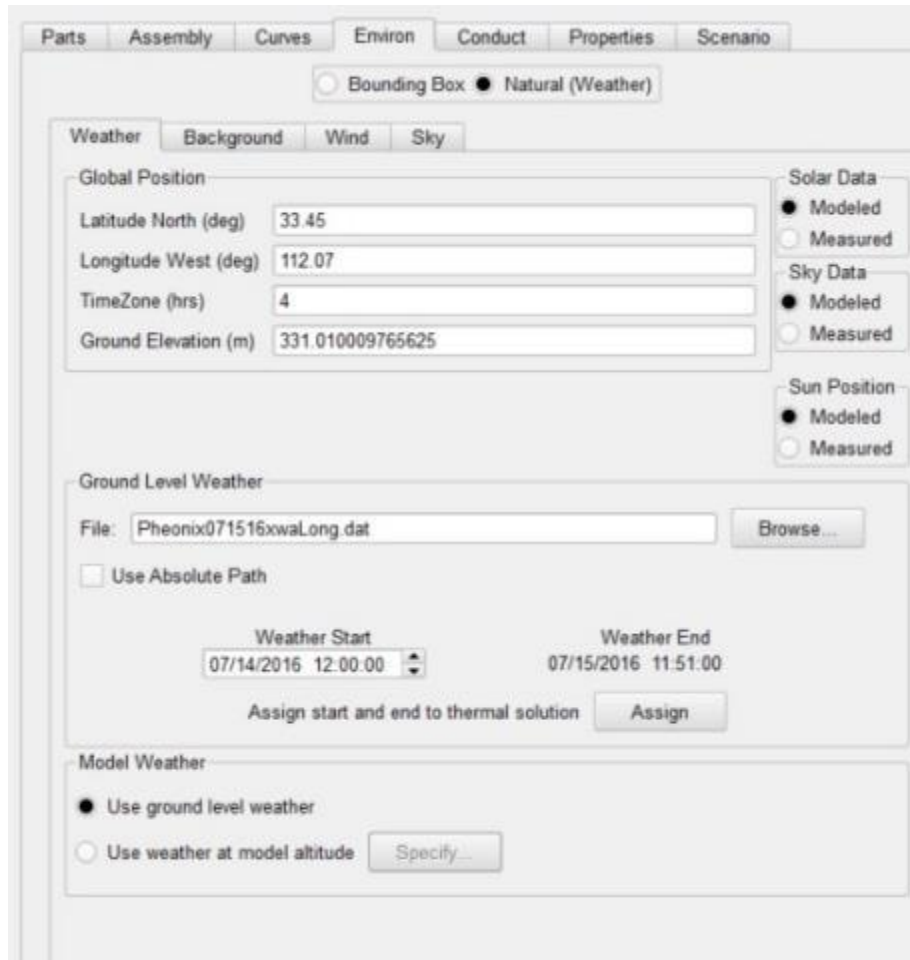


**Figure 52: Environment**

TAItherm also allows for control of the background, wind, and sky conditions. These conditions include the type of road, surface condition, wetness, and core temperature of the selected terrain to be given. The selected background conditions are shown in Figure 53. The background term refers to the type of road terrain the surrounding the meshed object. The type of road selected is an Interstate Road that has an aged condition and that is exposed to weather. The core temperature is selected as 41 °C. This was selected as the average ambient temperature during the timeframe for the simulation. The solar, sky, and sun position are used to model the geographical data in

relation to the global position to calculate the solar radiation angles. This allows for the algorithm routines to calculate the solar azimuth and zenith.



**Figure 53: Background Conditions**

The wind conditions, shown in Figure 54, are determined by using a McAdam’s Linear Convection model [4]. This equation is commonly used between two plates. In this case, the lower plate is the asphalt of the terrain and the upper plate is the vehicle underbody. This method is best suited for modeling air flows around objects smaller than a building [4].

The other options include Low Turbulent Intensity and Power Law models. The Low Turbulent Intensity model is used to better model laminar to low-turbulent wind conditions. The model is based on actual data collected in wind tunnels. The underlying principle of this method is using a standard boundary layer and then calculating convection coefficients. Other effects included are temperature-dependent air properties,

characteristic length, and the angle between the wind vector and the direction normal to the geometry surface [4]. The power law convection is particularly useful for large-scale modeling of buildings or highly turbulent air flows. As this simulation is utilizing a small vehicle model, the appropriate method of wind calculations that should be used is the Linear Convection model.

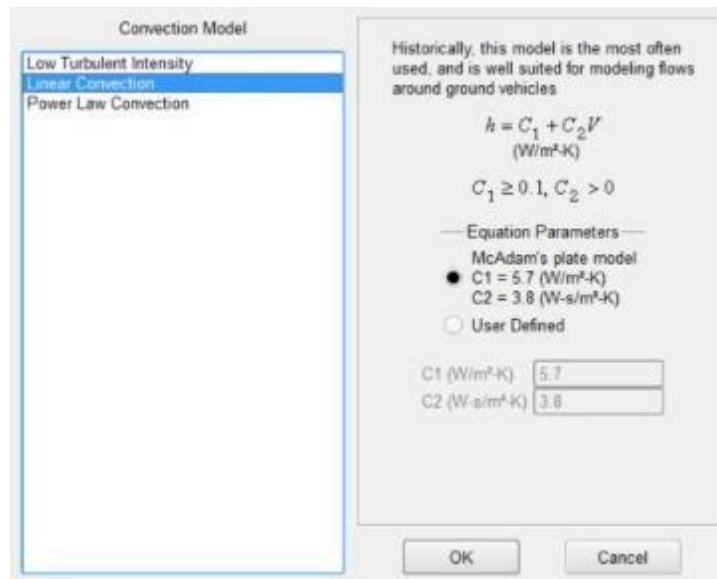


**Figure 54: Wind Conditions**

The basis of the Sky tab, as seen in Figure 55, is to determine the Sky Radiance model equations that will be used. The Brunt-Gubler model will be used for each loading scenario. This is utilized as the Centeno model requires humidity to be more than 40 percent. Since analysis is being conducted in multiple places with various levels of humidity, including the Phoenix, AZ area where humidity rarely exceeds 40%, the Brunt-Gubler model provides a superior option for all loading conditions for the vehicle.

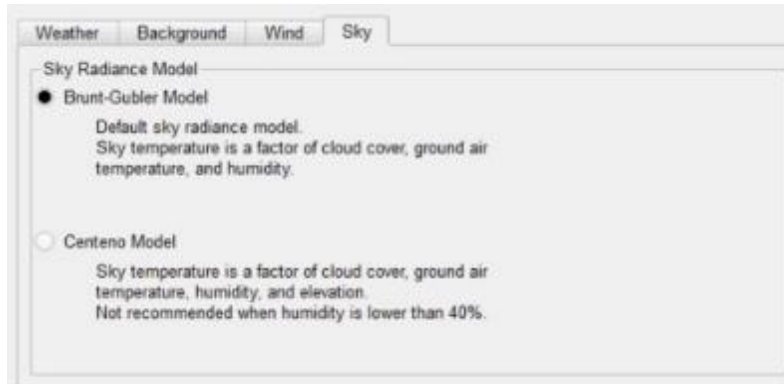


**Figure 55: Sky Conditions**

## Scenario

The scenario tab sets up what kind of simulation is to be conducted. The scenario tab is shown in Figure 56. A “Vehicle with Engine” was selected as it identifies to the TAItherm algorithm that it is a vehicle with an ICE. The heading is set to 10° and is used in the solar azimuth and solar zenith calculation from the weather file to determine at what angle the vehicle is in relation to the sun. The vehicle speed is extracted from the US06 drive cycle. The US06 drive cycle was utilized as it is considered a harsh acceleration and braking conditions. The modified Chevrolet Camaro PHEV vehicle mass is reflective of the actual mass as it is built.

The rolling resistance is used to determine the friction that is given from the vehicle tires to the road terrain determined in Section 0. The road grade is used as a static incline or decline to the road terrain. This value is set to match the road grade of the numerical simulations. The ICE state can be set to a constant value and can be dynamic similarly to a curve. The vehicle state is set to the calculated vehicle velocity of the given US06 drive cycle.

The frontal area consists of the total area of the front of the Camaro, as built since the modifications did not include changes to the exterior of the vehicle. The drag coefficient is related to the aerodynamics of the vehicle. The wheel diameter, in conjunction with the rolling resistance, is set the stock Chevrolet Camaro 2LT wheel diameter, as built.

The image shows a software interface with a 'Scenario' tab selected. The interface is divided into several sections for configuring vehicle parameters. At the top, there are tabs for 'Parts', 'Assembly', 'Curves', 'Environ', 'Conduct', 'Properties', and 'Scenario'. Below these, the 'Model Type' section has three radio buttons: 'Other', 'Vehicle', and 'Vehicle with Engine', with 'Vehicle with Engine' selected. The 'Vehicle Heading (deg)' section has radio buttons for 'Value', 'Curve', and 'Routine', with 'Value' selected and a text input field containing '10'. The 'Vehicle Speed (km/hr)' section has radio buttons for 'Value', 'Curve', and 'Routine', with 'Curve' selected and a dropdown menu showing 'US06 Drive Cycle'. The 'Vehicle Mass (kg)' section has radio buttons for 'Value', 'Curve', and 'Routine', with 'Value' selected and a text input field containing '1765'. The 'Rolling Resistance' section has radio buttons for 'Value', 'Curve', and 'Routine', with 'Value' selected and a text input field containing '0.015'. The 'Road Grade (%)' section has radio buttons for 'Value', 'Curve', and 'Routine', with 'Value' selected and a text input field containing '0.5'. The 'Engine State' section has radio buttons for 'Value', 'Curve', and 'Routine', with 'Value' selected and a dropdown menu showing 'Vehicle Speed'. At the bottom, there are three text input fields: 'Frontal Area (m²)' with '0.716416', 'Drag Coefficient' with '0.37', and 'Wheel Diameter (mm)' with '678.18'.

Parameter	Value
Model Type	Vehicle with Engine
Vehicle Heading (deg)	10
Vehicle Speed (km/hr)	US06 Drive Cycle
Vehicle Mass (kg)	1765
Rolling Resistance	0.015
Road Grade (%)	0.5
Engine State	Vehicle Speed
Frontal Area (m²)	0.716416
Drag Coefficient	0.37
Wheel Diameter (mm)	678.18

**Figure 56: Scenario Tab**

**Table 7: Scenario Editor Tab**

Scenario Editor		
Category	Selections	Purpose
Model Type	Other	
	Vehicle	Sets the algorithm to a vehicle.
	Vehicle with Engine	Sets the algorithm to a vehicle with the additional settings of an ICE.
Vehicle Heading	Value	Utilized in conjunction with the weather file or solar lamp fluid to determine the solar position in relation to the vehicle.
	Curve	Not Used.
	Routine	Not Used.
Vehicle Mass	Value	Sets the value of the vehicle weight to a constant.
	Curve	Not Used.
	Routine	Not Used.
Road Grade	Value	Sets the road grade percentage to a constant.
	Curve	Not Used.
	Routine	Not Used.
Vehicle Speed	Value	Sets the vehicle speed to a constant. Used for steady-state analysis.
	Curve	Sets the vehicle speed to a curve. In this case, the US06 drive cycle.
	Routine	Not Used.
Rolling Resistances	Value	Sets the coefficient drag of the tires.
	Curve	Not Used.
	Routine	Not Used.
Engine State	Value	Utilized to accept a dynamic changing curve as the other options have been removed.
	Curve	Not Used.
	Routine	Not Used.

Scenario Editor		
Category	Selections	Purpose
Frontal Area	N/A	This number represents the total area of the vehicle in contact with the wind.
Drag Coefficient	N/A	Related to the aerodynamics of the vehicle.
Wheel Diameter	N/A	Sets the diameter of the given wheel. The stock 2LT Camaro is built with a 20-inch diameter wheel.

## RESULTS

Originally, numerical analysis was performed on an electric vehicle system to simulate the total vehicle thermal management. Following the methodology discussed in Section 4.1, the ESS thermal management design and optimization is explored. The comparison of series to parallel controlled coolant loops is compared for battery modules using electronically actuated valves. However, the full interaction between the components in a conductive, convective, and radiative method was shown to be arduous for research. Adequately accounting for the convective and radiative heat transfers become difficult as surface area spacing and interaction between all components must be known before the modeling can be done. Various cooling patterns for more efficient and adequate cooling and heating in order to keep each battery module within its optimal temperature envelop are explored.

The results reflect that significant limitations within the modeling environment exist. The results of this investigation are discussed in Section 4.2. The results of the numerical simulation show the necessity of extending research into other domains. The combined methodology and results for the total vehicle thermal management are discussed in Section 4.2.

### Numerical Simulation

The simulation utilized two consecutive US06 drive cycles, and was utilized for all three cases that are outlined below. Two simulations were run to verify the E-NTU heat exchanger in each case. Case 1 (in red) set the baseline for the battery system with no cooling. This baseline case is used to determine the maximum heat that was generated by



the battery system. Case 2 (in green) was utilized a serial coolant flow. Case 3 (in blue) utilized the electronically actuated valves to control coolant flow and is presented as the parallel case. The results of the simulation are presented in Figure 57.

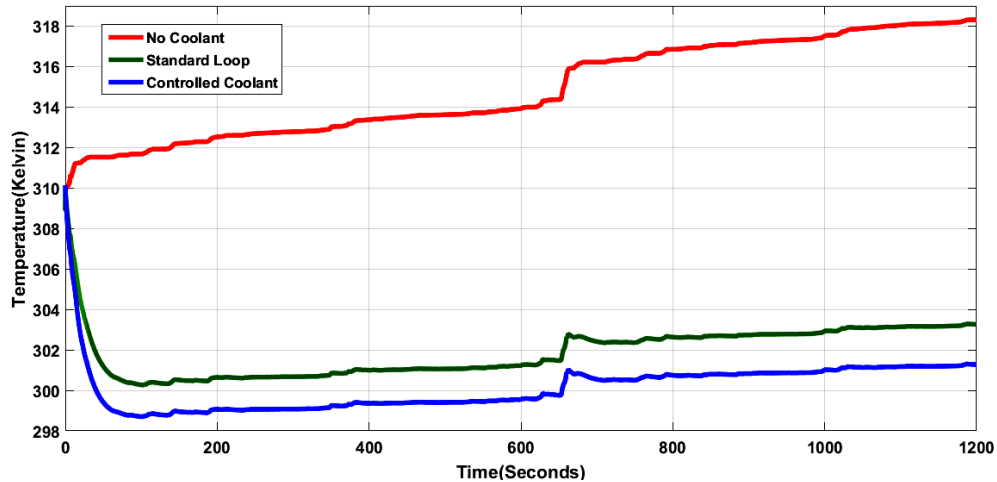


**Figure 57: Average Heat Generation vs. Time**

The figure shows that at the beginning of the simulation, each of the systems are at the same temperature. In both Case 2 and Case 3, the heat generation begins at the start of the drive cycle. Additionally, the coolant temperature is set to 310.0 Kelvin triggering the response of the TMS. This results in an increase in temperature in Case 1. For Case 2 and Case 3, the heat generated triggered the initial response of the TMS. In Case 1, the study of no coolant, the temperature rise is significantly higher than Case 2 or 3. The optimal operating temperature range for the battery cells is between 25 and 35 °C, as provided by the manufacturer's datasheet [44].

As seen in Figure 57, at approximately 600 seconds into the simulation, which is at the beginning of the second US06 cycle, there is a marked increase in temperature related to the hard accelerations at the beginning of the drive cycle. The delay of the

coolant system absorbing the heat generated is consistent with the heat generation and transfer coefficients of the coolant plate and liquid coolant.

The standard control of the TMS shown in Case 2 lowers the temperature of the entire system by approximately 10-14 °K. Case 3 of the controlled coolant flow algorithm is able to lower the entire systems temperature further than the capability of Case 2. The temperature difference between Case 1 and Case 3 is 13-16.5 °K. The differences between Case 1 for both Case 2 and Case 3 are seen in Figure 58. When compared to Case 1, the ESS can maintain the power demand and stay within its operating range. This indicates that the TMS is working properly, but also that its operation can be improved.

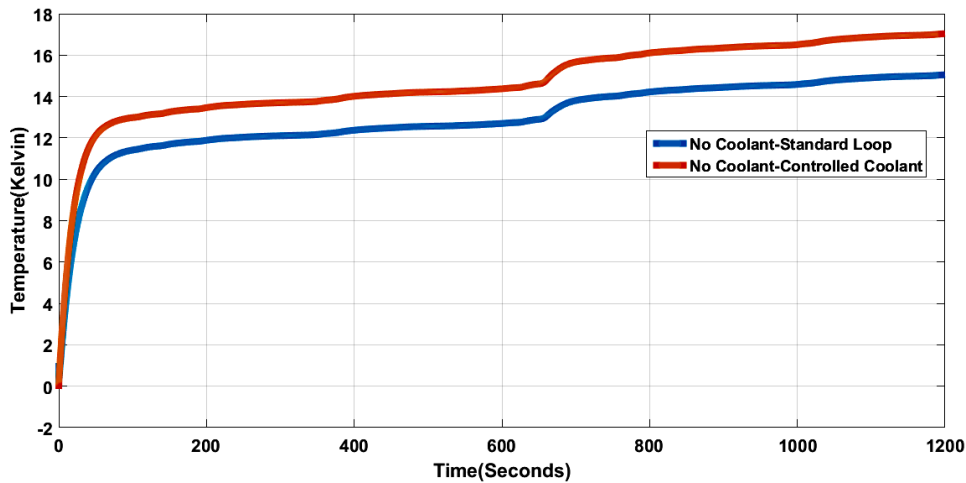


**Figure 58: No Coolant minus Standard Coolant Loop**

Figure 59 shows the increase of the temperature differential between Case 2 and Case 3. The difference results from increased heat absorption by the coolant in Case 3. By applying specific cooling to each module, rather than a serial connection, the overall temperature of the system is reduced further. By utilization of parallel coolant loops, the

coolant is able absorb the heat and leave the system without continuing to the next module. Compared to Case 2, where there is only a serial loop, the fluid is sent from one module to the next, thereby reducing the heat absorption capability of the fluid. This is in relation to the change in temperature of the fluid when entering the system. This change is determined by the final temperature minus the initial temperature. The disparity causes the coolant temperature to rise from module to module and reduces the capability of the system to absorb and reject the heat.

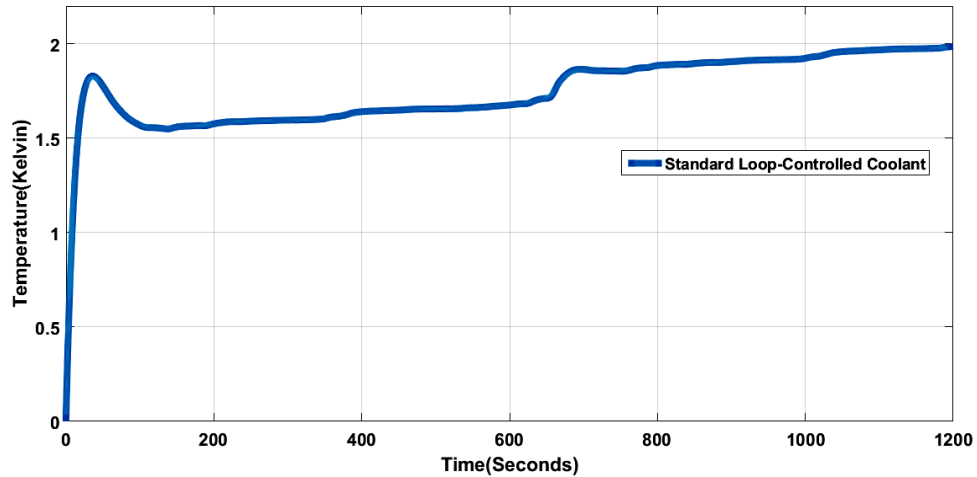


**Figure 59. Standard Coolant Loop minus Controlled Coolant**

Case 3 lowers the coolant temperature by a difference of 1.8 °K for the first US06 drive cycle. During the second US06 drive cycle, the temperature is lowered by 1.9° K. As mentioned previously, both Case 2 and Case 3 can keep the ESS within the optimum temperature range between 25 and 35 °C. However, Case 3 can maintain a better temperature differential. This indicates that use of the electronically actuated valves in a parallel loop allows for better temperature control of the ESS.

During both Case 2 and Case 3, the initial spike because of the aggressive drive cycle is minimized. The steepness of the temperature climb is also reduced. However, when comparing both systems, the overall system can maintain the system within the optimal temperature range in Case 3. The data extracted from the graphs at the end of each of the two drive cycles are shown in Table 8.

**Table 8. Tabulated Results**

	Initialization Temp.	Temp. Cycle 1 End	Temp. Cycle 2 End
No Cooling	310.0 K	314.4 K	318.3 K
Unregulated Cooling	310.0 K	301.6 K	303.4 K
Controlled Cooling	310.0 K	299.8 K	301.3 K

Combined Methodology

The overall system stability relies upon the ability to effectively mitigate the thermally conductive, convective, and radiative behavior exhibited by the components. The primary concerns for this analysis are the temperature-sensitive components and coolant system components: ICE, exhaust manifold, EM, inverter, ICE heat exchanger, inverter and EM heat exchangers, ESS heat exchanger, and ESS. The initial TAITherm mesh is shown in Figure 60.

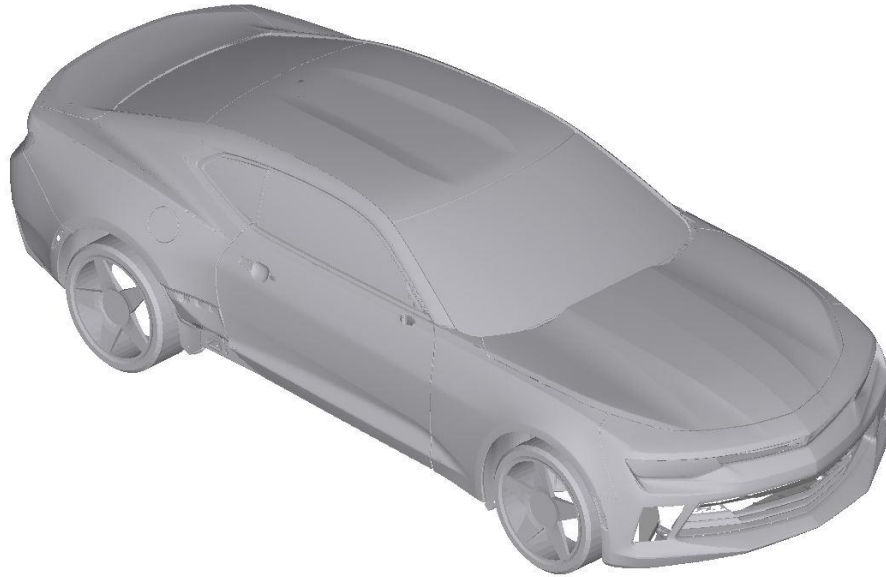


**Figure 60: Initial TAITherm Mesh**

To conduct thermal analysis with high accuracy, TAITherm required a 3D mesh representation of the targeted system. The quality of the mesh, as described in the previous section, requires a meticulous attention to hasten the calculation process, as shown in Section 3.1.2. To illustrate the temperature curve, net heat rates for conduction, convection, and radiation, as well as 2D spatial boundaries, are shown in each section. The following parts have been coupled in the same thermal management loop as the temperatures are similar. This is done as temperature is an indicator for heat flux.

1. Inverter and EM
2. ESS
3. Heat Exchangers
4. ICE and Exhaust Manifold

Additionally, results show that at 400 s into the simulation, the temperature within the engine bay is at its peak. The ICE and exhaust manifold produce high temperatures, thus creating high heat flux, as compared to the electric drive components. During this time, the inverter becomes the primary concern for heat soak. A mesh plot of each system is shown in each of the respective sections. A summary of the temperature profiles for each section is presented in Table 9.

### Inverter & EM

The inverter and electric motor temperature curve are shown in Figure 61. The curve indicates that the TMS solution for the inverter and EM is lacking, particularly for the inverter. A temperature of 90 °C is operating within the de-rated zone of operation for the inverter. The net heat rates for conduction, convection, and radiation of the inverter and electric motor are shown in Figure 62, Figure 63, and Figure 64, respectively. For the inverter and electric motor the dominate mode of heat generation is conduction. However, convection is the most significant mode of external heat transfer.

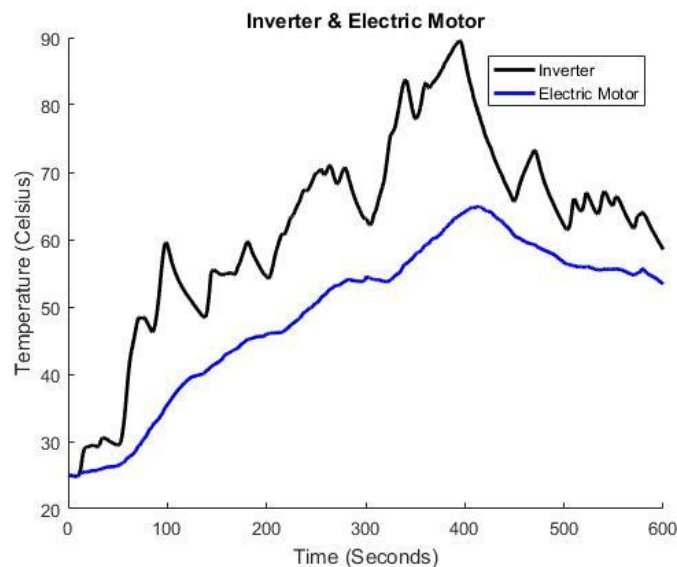


**Figure 61: Inverter & EM Temperature Curve**

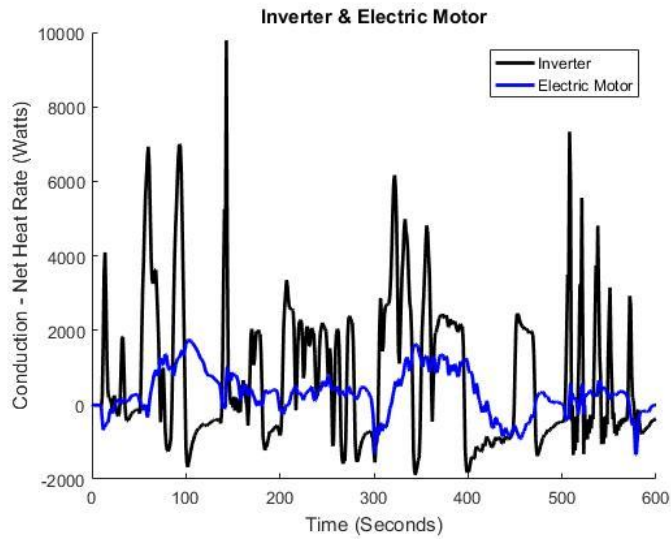


**Figure 62: Inverter & EM Conduction Net Heat Rate**

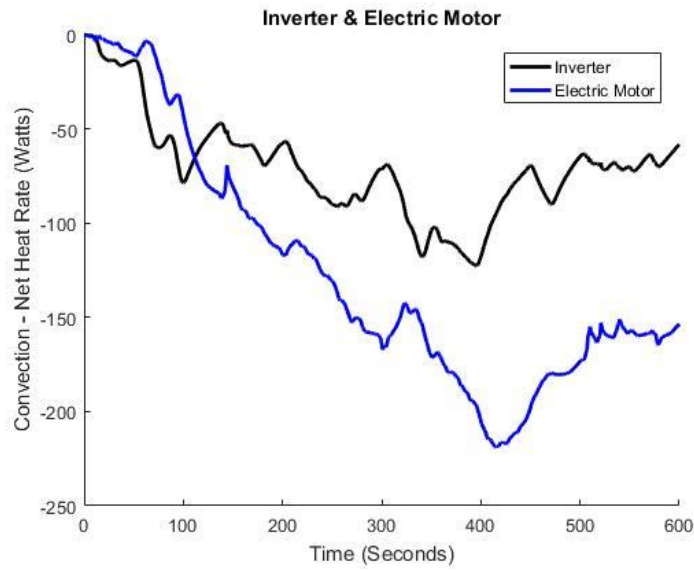


**Figure 63: Inverter & EM Convection Net Heat Rate**

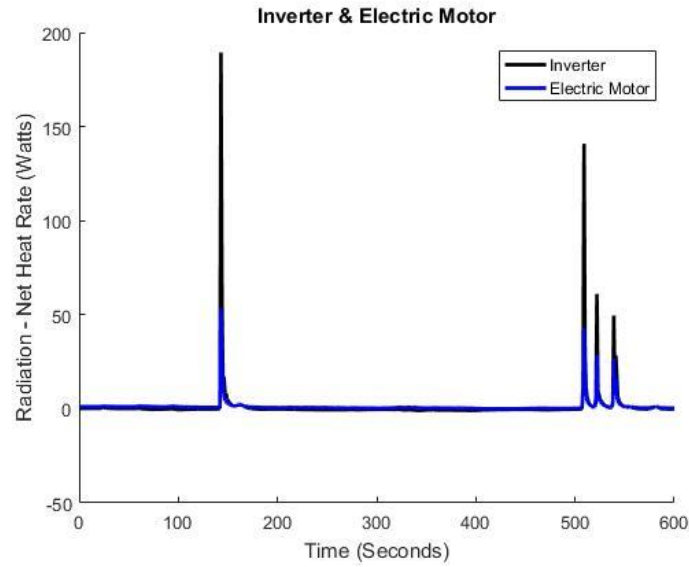


**Figure 64: Inverter & EM Radiation Net Heat Rate**

ESS

The ESS temperature curve is shown in Figure 65. The curve indicates that the TMS solution for the ESS is adequate. The net heat rates for conduction, convection, and radiation of the ESS are shown in Figure 66, Figure 67, and Figure 68, respectively.



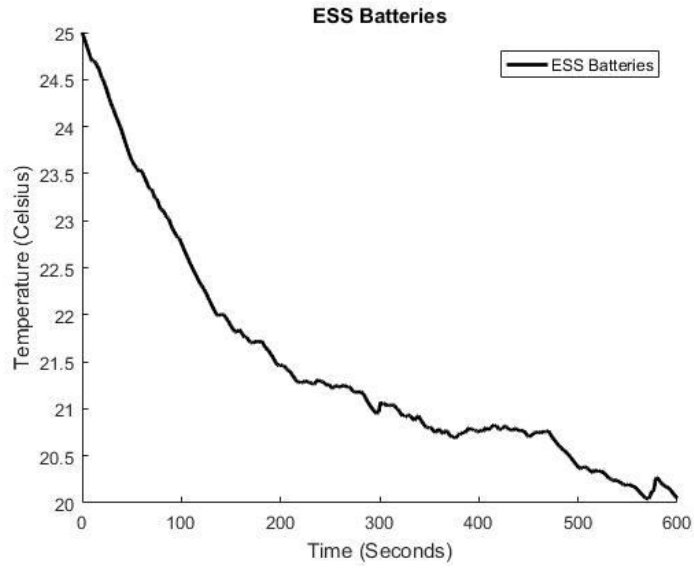


**Figure 65: ESS Temperature Curve**

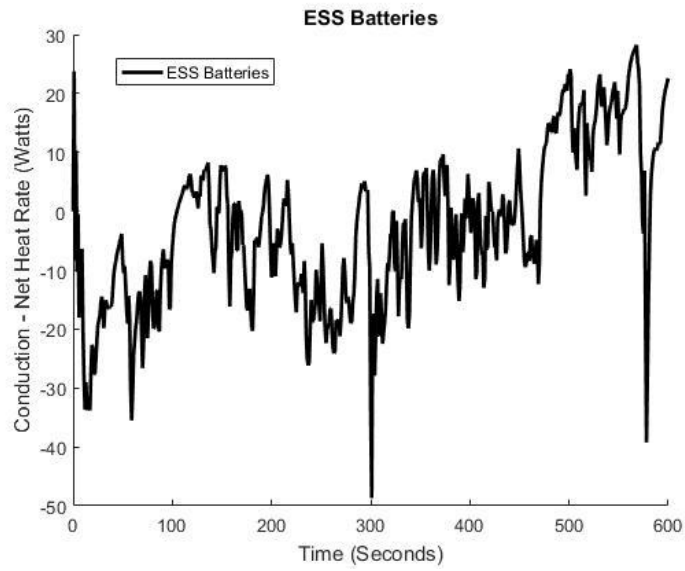


**Figure 66: ESS Conduction Net Heat Rate**

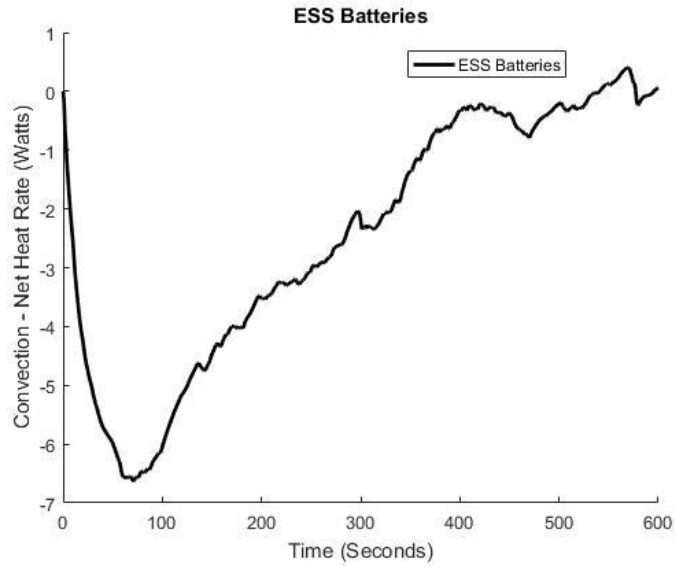


**Figure 67: ESS Convection Net Heat Rate**

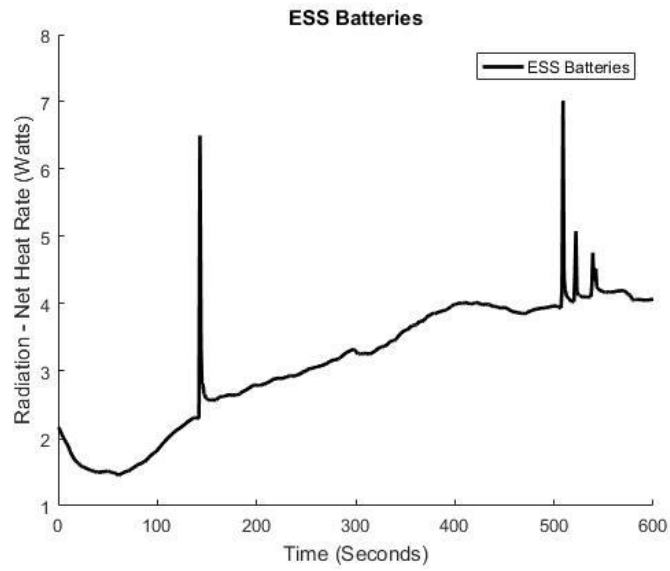


**Figure 68: ESS Radiation Net Heat Rate**

Heat Exchangers – Inverter & EM 1 & 2, ICE, and ESS

The heat exchanger temperature curves are shown in Figure 69. The heat exchanger temperature curves include the ICE, inverter and EM, and ESS coolant loops. The curve indicates that the TMS solution for the heat exchangers is adequate. The net heat rates for conduction, convection, and radiation of the heat exchangers are shown in Figure 70, Figure 71, and Figure 72, respectively.

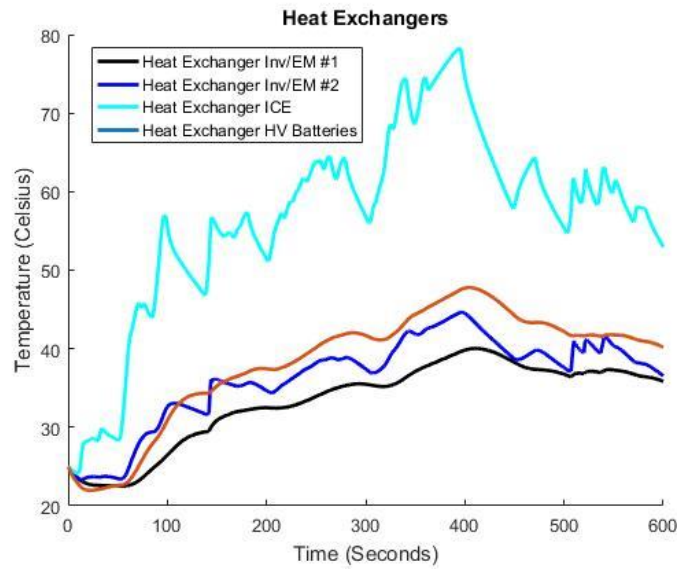


**Figure 69: Heat Exchangers Temperature Curve**

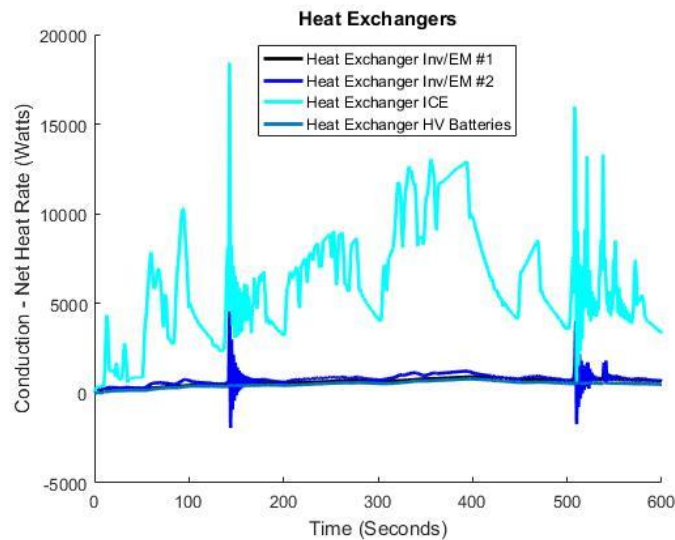


**Figure 70: Heat Exchangers Conduction Net Heat Rate**

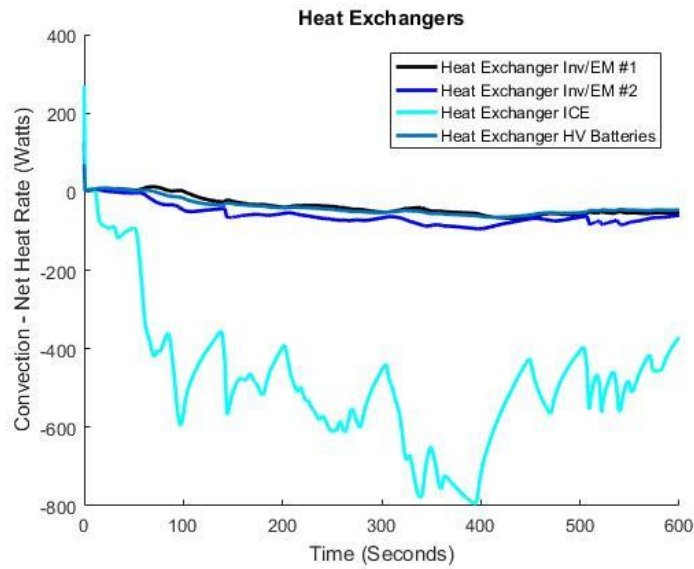


**Figure 71: Heat Exchangers Convection Net Heat Rate**

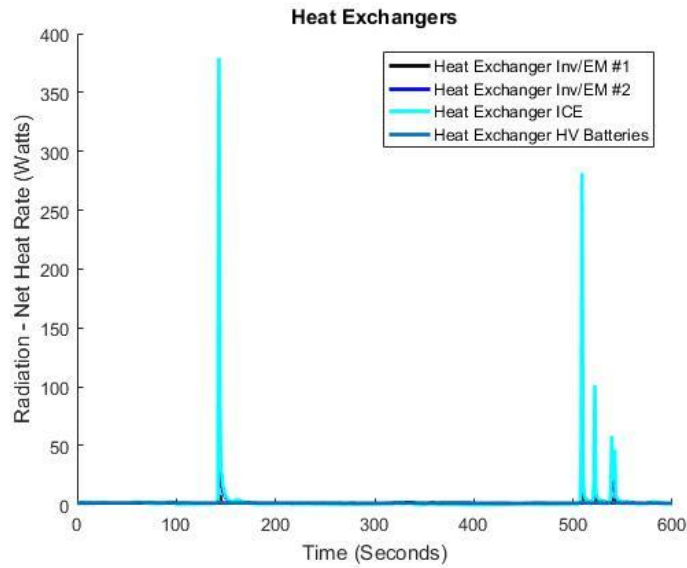


**Figure 72: Heat Exchangers Radiation Net Heat Rate**

## ICE & Exhaust Manifold

The ICE and exhaust manifold curves are shown in Figure 73. The curve indicates that the TMS solution for the ICE and exhaust manifold is adequate. The net heat rates for conduction, convection, and radiation of the ICE and exhaust manifold are shown in Figure 74, Figure 75, and Figure 76, respectively.

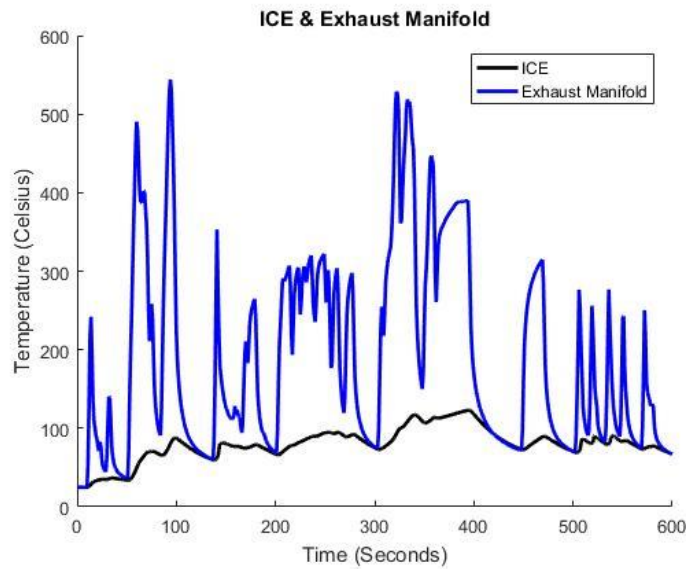


**Figure 73: ICE & Exhaust Manifold Temperature Curve**

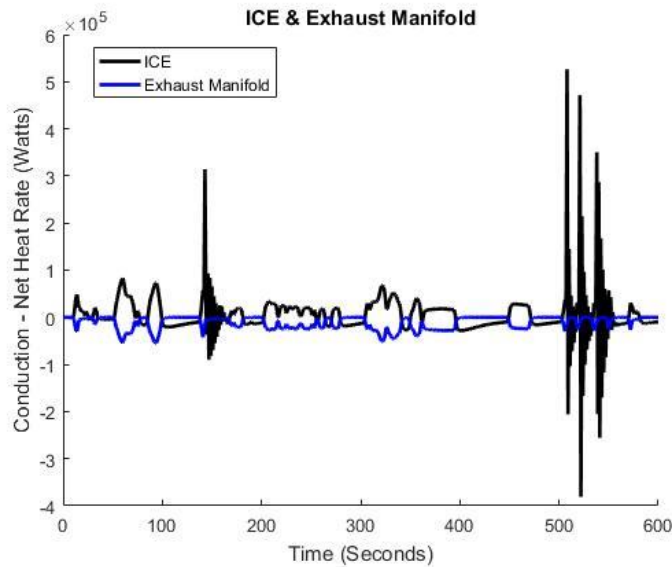


**Figure 74: ICE & Exhaust Manifold Conduction Net Heat Rate**

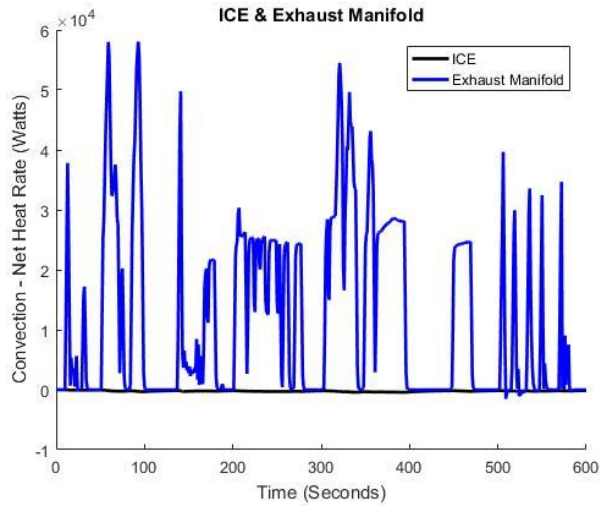


**Figure 75: ICE & Exhaust Convection Net Heat Rate**

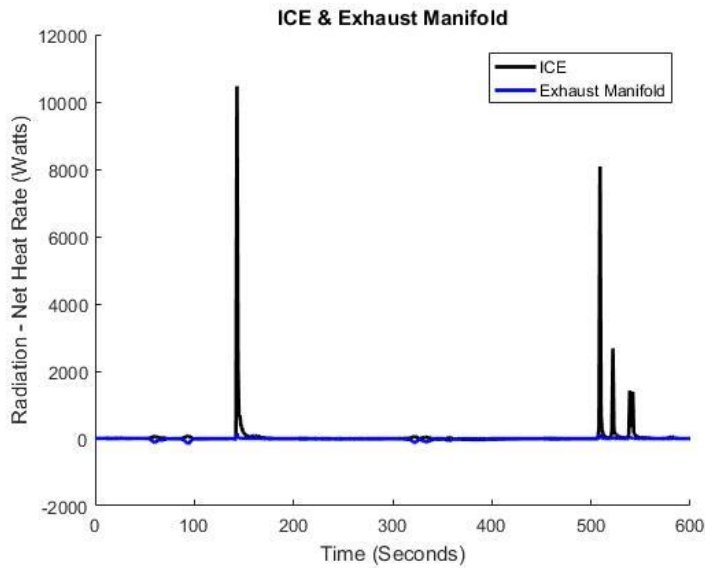


**Figure 76: ICE & Exhaust Radiation Net Heat Rate**

## Temperature Curve Results

Final and max average temperatures from the US06 run are shown in Table 9. With one exception, the maximum average temperature of any given major powertrain component has been found to be within the specified limits of the associated datasheets [35, 36, 37, 38, 42]. However, the inverter extends past 80 °C in the de-rated area of operation.

**Table 9: Final, Average, & Maximum Temperatures**

Component	Final Temperature (°C)	Max Average Temperature Time (Seconds)	Max Average Temperature (°C)
Inverter	58.5	395	89.5
EM	53.4	414	64.9
ESS	20.0	0	25.0
Heat Exchanger – Inverter/EM #1	35.9	397	44.7
Heat Exchanger – Inverter/EM #2	36.6	411	40.0
Heat Exchanger – ESS	40.2	404	47.8
Heat Exchanger – ICE	53.0	394	78.3
ICE	67.1	161	123.1
Exhaust Manifold	67.0	94	544.1

The maximum average temperatures indicated that the highest under the hood temperatures are seen at approximately 400 seconds into the US06 drive cycle. To properly identify potential problem areas arising due to the temperature rise, the mesh of

each component was manually checked in the mesh for thermal hot spots. The results of this analysis are listed below in Table 10.

**Table 10: Component Hot Spot Max Thermal Temperature**

Component	Hot Spot Temperature (°C)
Inverter	146.5
EM	82.1
ESS	21.6
Heat Exchanger – Inverter/EM #1	50.3
Heat Exchanger – Inverter/EM #2	47.3
Heat Exchanger – ESS	68.7
Heat Exchanger - ICE	118.6
ICE	223.8
Exhaust Manifold	225.7

To provide further analysis Figure 77 through Figure 80 illustrate the mesh of each component thermal hot spot identified at the 400-second mark. The hot spot on the passenger side of the inverter was created by its proximity to the exhaust manifold. The hot spot created by the heat flux is shown in Figure 77.



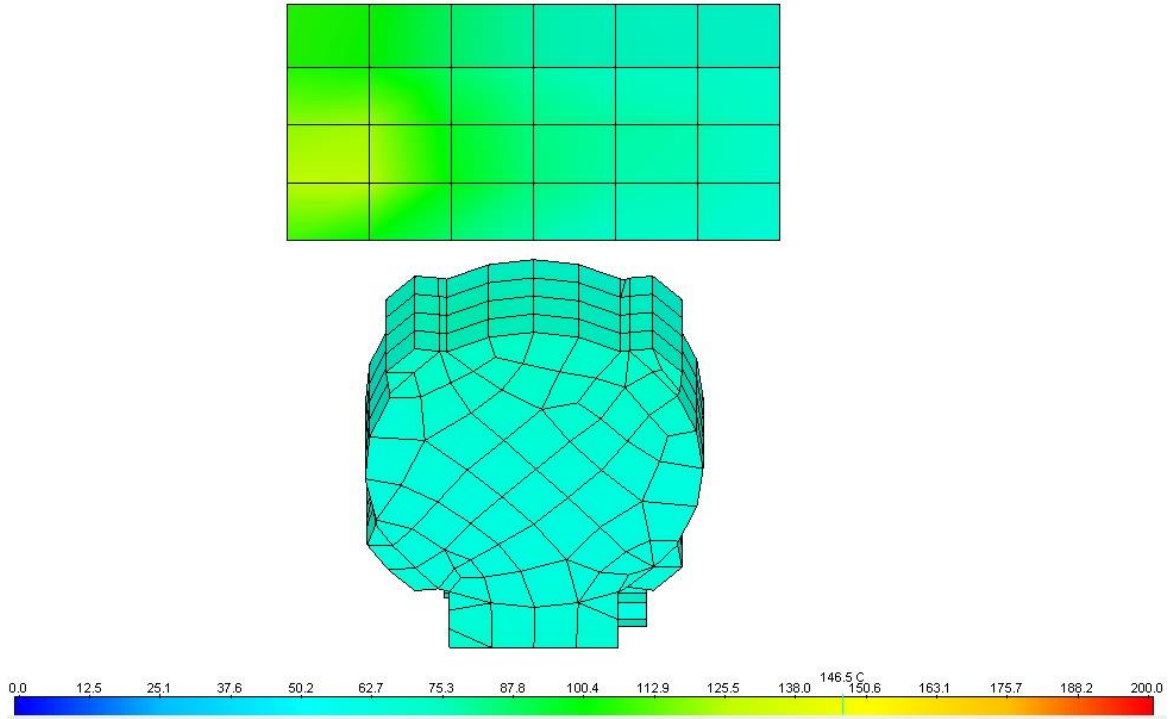


**Figure 77: Inverter & EM TAITherm Mesh at 400 s**

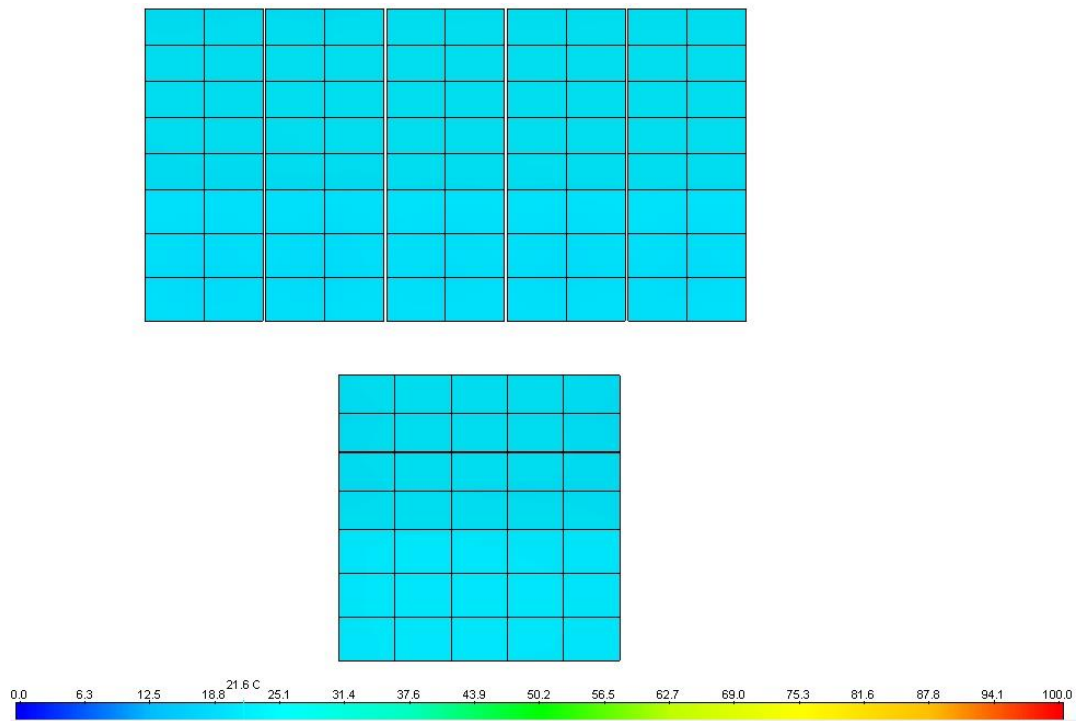


**Figure 78: ESS TAITherm Mesh at 400 s**

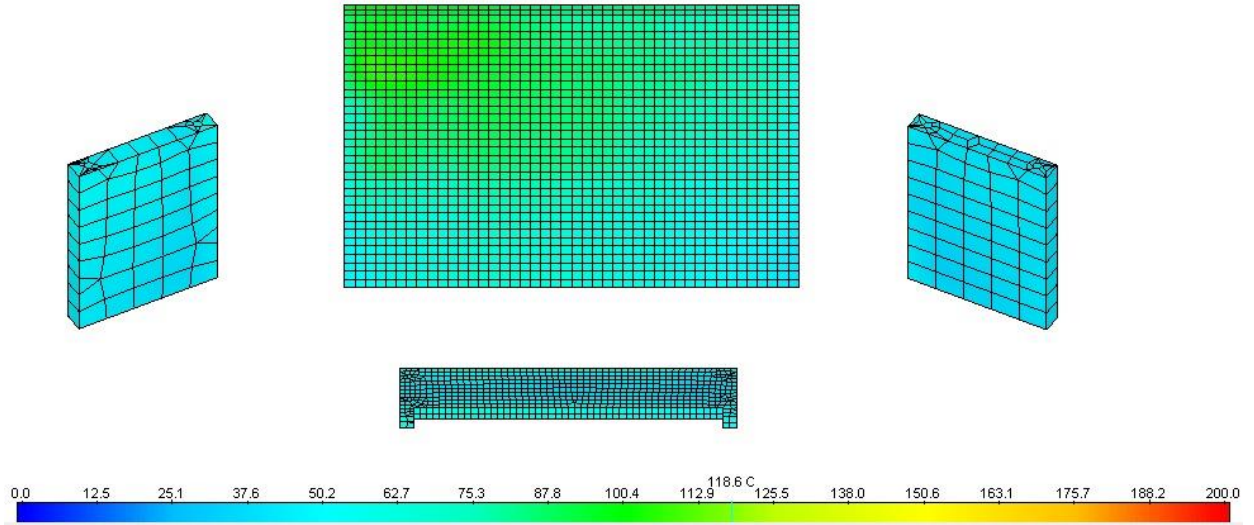


**Figure 79: Heat Exchangers TAITherm Mesh at 400 s**

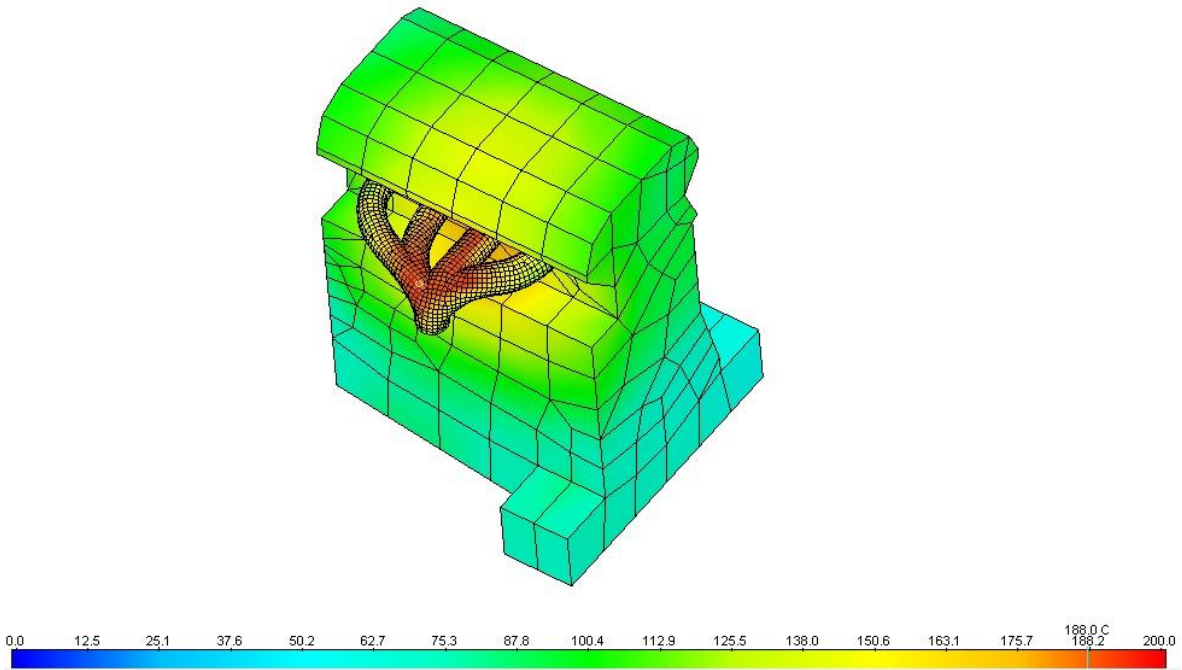


**Figure 80: ICE & Exhaust TAITherm Mesh at 400 s**

The three major heat-producing components are the ICE, exhaust manifold, and the ICE heat exchanger. The original stock Camaro SS transmission cooler was

repurposed to be the ESS heat exchanger. The proximity to the ICE heat exchanger may potentially cause issues in the future due to heat flux. However, there is currently no significant issue with cooling of the ESS as seen above in Figure 78.

The Rinehart PM150DX inverter datasheet lists the operational temperature to be 80° C [37]. The inverter will be de-rated, meaning that it will operate in a limited mode, at 105 °C. It is the findings of this research that additional heat shielding, to protect from the heat flux, must be done to properly isolate these potential hot spots that may occur at high ambient temperatures, for example during the summer in the Phoenix metropolitan area. Heat shielding will properly isolate the high-temperature regions of the ICE from the electric drive portion of the vehicle. Additionally, it may be beneficial to increase the flow rate of the coolant pump of the inverter and electric motor loop. Increased flow rate with the addition of heat shields could mitigate inverter hot spots. The heat exchangers are well sized as the heat dissipation is proper for the system fluid temperature.

## CONCLUSION & FUTURE WORK

The MBD approach was shown to be useful in TMS design and analysis. The temperatures seen are in within the operating limits of all the components except for the inverter. The results from the model dictate potential issues with the Rinehart inverter and GKN EM. The issues may be encountered during repetitive hard accelerations and decelerations. As noted in the Results section, internal CAD data were not received for these components. Obtaining the high-fidelity fluid pathways for these components may resolve these issues. The rudimentary fluid paths used in the model may not be consistent with actual internal component characteristics.

For future work, it is recommended that the heat exchangers be further analyzed. During Charge Depleting (CD) performance operation that the PHEV ESS may become overheated. Also, in extremely hot ambient temperatures, temperatures of the outer body of the vehicle may cause limited operation of the vehicle. The model should be further verified in various cold, hot, and humid weather conditions.

The model is ready for Human Thermal Comfort (HTC) to be performed. Analysis of these data will determine if the HVAC system will operate as intended or if additional modifications may become necessary.

The analysis in this work was conducted during Charge Sustaining (CS) mode rather than CD mode. The focus behind this research was under-hood power electronics, ICE, exhaust, and heat exchangers to identify and mitigate potential thermal issues. CD mode operates with limited ICE use and with an SOC of the ESS that is above 32 percent. This increases thermal stress on the ESS while lowering engine bay temperatures. CD

mode limits or even eliminates GHG emissions, dependent on the driver, and the ESS is placed under different loading conditions and thermal stress on the ESS is increased.

## REFERENCES

- [1] "MathWorks - Makers of MATLAB and Simulink", *Mathworks.com*, 2017. [Online]. Available: <https://www.mathworks.com/>. [Accessed: 11- Mar- 2017].
- [2] "Siemens Global Website", *Siemens.com*, 2017. [Online]. Available: <http://www.siemens.com/us/en/home.html>. [Accessed: 11- Mar- 2017].
- [3] "ThermoAnalytics", *Thermoanalytics.com*, 2017. [Online]. Available: <http://www.thermoanalytics.com/>. [Accessed: 11- Mar- 2017].
- [4] TAITherm Manual, ThermoAnalytics, Inc, 04/2016
- [5] L. Glicksman and L. Glicksman, *Modeling and approximation in heat transfer*, 1st ed.
- [6] Lane, Robert C., Hae-won Choi, Jeff Weintraub, Carlos Mario Aguirre, Mark Riegel, Orion A. King, Nathan Chidiac et al. "Energy storage system with heat pipe thermal management." *U.S. Patent Application 14/189,219*, filed February 25, 2014.
- [7] Claypole, George M., and Mark D. Nemesh. "Integrated vehicle cooling system." *U.S. Patent 7,669,558*, issued March 2, 2010.
- [8] Chen, S.C., C.C. Wan, and Y.Y. Wang. 2005. "Thermal Analysis Of Lithium-Ion Batteries". *Journal Of Power Sources 140* (1): 111-124. doi:10.1016/j.jpowsour.2004.05.064.
- [9] Doughty, Daniel H, Paul C Butler, Rudolph G Jungst, and E.Peter Roth. 2002. "Lithium Battery Thermal Models". *Journal Of Power Sources 110* (2): 357-363. doi:10.1016/s0378-7753(02)00198-2.
- [10] Pesaran, Ahmad A. 2002. "Battery Thermal Models For Hybrid Vehicle Simulations". *Journal Of Power Sources 110* (2): 377-382. doi:10.1016/s0378-7753(02)00200-8.
- [11] National Renewable Energy Laboratory, 1999. An Approach For Designing Thermal Management Systems For Electric And Hybrid Vehicle Battery Packs. Golden, Colorado: National Renewable Energy Laboratory.
- [12] F. Zhao, M. Lai and D. Harrington, "Automotive spark-ignited direct-injection gasoline engines", *Progress in Energy and Combustion Science*, vol. 25, no. 5, pp. 437-562, 1999.
- [13] N. Javani, I. Dincer, G. Naterer and G. Rohrauer, "Modeling of passive thermal management for electric vehicle battery packs with PCM between cells", 2017.
- [14] Z. Rao and S. Wang, "A review of power battery thermal energy management", *Renewable and Sustainable Energy Reviews*, vol. 15, no. 9, pp. 4554-4571, 2011.

- [15] R. Kizilel, R. Sabbah, J. Selman and S. Al-Hallaj, "An alternative cooling system to enhance the safety of Li-ion battery packs", *Journal of Power Sources*, vol. 194, no. 2, pp. 1105-1112, 2009.
- [16] National Renewable Energy Laboratory,. 2001. Battery Thermal Management In Evs And Hevs: Issues And Solutions. Golden, Colorado: National Renewable Energy Laboratory.
- [17] Sato, Noboru. 2001. "Thermal Behavior Analysis Of Lithium-Ion Batteries For Electric And Hybrid Vehicles". *Journal Of Power Sources* 99 (1-2): 70-77. doi:10.1016/s0378-7753(01)00478-5.
- [18] Smith, Kandler and Chao-Yang Wang. 2006. "Power And Thermal Characterization Of A Lithium-Ion Battery Pack For Hybrid-Electric Vehicles". *Journal Of Power Sources* 160 (1): 662-673. doi:10.1016/j.jpowsour.2006.01.038.
- [19] N. Javani, I. Dincer and G. Naterer, "Numerical Modeling of Submodule Heat Transfer With Phase Change Material for Thermal Management of Electric Vehicle Battery Packs", *Journal of Thermal Science and Engineering Applications*, vol. 7, no. 3, p. 031005, 2015.
- [20] A. Emadi, Young Joo Lee and K. Rajashekara, "Power Electronics and Motor Drives in Electric, Hybrid Electric, and Plug-In Hybrid Electric Vehicles", *IEEE Transactions on Industrial Electronics*, vol. 55, no. 6, pp. 2237-2245, 2008.
- [21] M.A. Lambert, B.J. Jones, Automotive adsorption air conditioner powered by exhaust heat. Part 1: conceptual and embodiment design, Proc. IMechE Part D: J. Automobile Eng. 220 (2006) 959–97
- [22] Y. Farzaneh and A. Tootoonchi, "Controlling automobile thermal comfort using optimized fuzzy controller", *Applied Thermal Engineering*, vol. 28, no. 14-15, pp. 1906-1917, 2008.
- [23] G. Hundy, A. Trott and T. Welch, *Refrigeration, air conditioning and heat pumps*.
- [24] M. Cerdoun, C. Carcasci and A. Ghenaiet, "An approach for the thermal analysis of internal combustion engines' exhaust valves", 2017.
- [25] S. Sharma, P. Saini and N. Samria, "Experimental Thermal Analysis of Diesel Engine Piston and Cylinder Wall", 2017.
- [26] C. Wu, R. Chen, J. Pu and T. Lin, "The influence of air–fuel ratio on engine performance and pollutant emission of an SI engine using ethanol–gasoline-blended fuels", 2017.
- [27] S. Yu and L. Li "Effect of Fuel Metering on Combustion and Emissions of a PFI Gasoline Engine During Fast Startup Under an HEV-like Mode", *International Journal of Automotive Technology*, vol. 15, no. 5, pp. 699-708, 2014.

- [28] Yu, G. Dong and L. LI, "Transient characteristics of emissions during engine start/stop operation employing a conventional gasoline engine for HEV application", *International Journal of Automotive Technology*, vol. 9, no. 5, pp. 543-549, 2008.
- [29] A. Oakley, H. Zhao, N. Ladommatos and T. Ma, "Experimental Studies on Controlled Auto-ignition (CAI) Combustion of Gasoline in a 4-Stroke Engine", *SAE Technical Paper Series*, 2001.
- [30] T. Chan, E. Meloche, J. Kubsh, R. Brezny, D. Rosenblatt and G. Rideout, "Impact of Ambient Temperature on Gaseous and Particle Emissions from a Direct Injection Gasoline Vehicle and its Implications on Particle Filtration", *SAE International Journal of Fuels and Lubricants*, vol. 6, no. 2, pp. 350-371, 2013.
- [31] S. Kim, "Thermal Performance of Motor and Inverter in an Integrated Starter Generator System for a Hybrid Electric Vehicle", *Energies*, vol. 6, no. 11, pp. 6102-6119, 2013.
- [32] Kimotho, J.K. and Hwang, P., 2011. *Thermal management of electric vehicle BLDC motor* (No. 2011-28-0134). SAE Technical Paper.
- [33] Wu, Mao-Sung, K.H. Liu, Yung-Yun Wang, and Chi-Chao Wan. 2002. "Heat Dissipation Design For Lithium-Ion Batteries". *Journal Of Power Sources* 109 (1): 160-166. doi:10.1016/s0378-7753(02)00048-4.
- [34] S. Jung, S. Park and B. Choi, "Power control strategy for preventing thermal failure of passively cooled automotive battery packs", *International Journal of Automotive Technology*, vol. 18, no. 1, pp. 117-124, 2016.
- [35] "CPx-Unit -", *Fte-automotive.com.cn*, 2017. [Online]. Available: <http://www.fte-automotive.com.cn/en/products/clutch-systems/cpx-unit.html>. [Accessed: 11- Mar- 2017].
- [36] "Standard", *Rinehart Motion Systems, LLC*, 2017. [Online]. Available: <http://www.rinehartmotion.com/standard.html>. [Accessed: 11- Mar- 2017].
- [37] "A123 Systems", *A123systems.com*, 2017. [Online]. Available: <http://www.a123systems.com/>. [Accessed: 11- Mar- 2017].
- [38] "Electric Pump Remote, High Flow Inline, Single out, 55GPM", *Kentico E-commerce site*, 2017. [Online]. Available: <https://www.meziere.com/Products/Cooling-System-Products/Pumps-Electric/Remote-Mount/Electric-Pump-Remote-High-Flow-Inline-Single-out-55GPM.aspx>. [Accessed: 11- Mar- 2017].
- [39] J. Contes, "Powertrain Losses", Arizona State University, 2016.



[40] K. Oshiro, "Powertrain Losses", Arizona State University, 2016.

[41] C. Stubbs, "Powertrain Losses", Arizona State University, 2016.

[42] "Cylindrical type | Industrial Devices & Solutions | Panasonic", *Industrial.panasonic.com*, 2017. [Online]. Available: <https://industrial.panasonic.com/ww/products/batteries/secondary-batteries/lithium-ion/cylindrical-type?reset=1>. [Accessed: 11- Mar- 2017].

## APPENDIX A

### PARTS TAB FUNCTION, EXPLANATION, AND VALUES

Part Editor		
Category	Selections	Purpose
Temperature	Assigned	Allows the selected mesh elements (part) to be set to a designated temperature, and is set to either a constant or variable value. Parts may be linked through convection. However, only convection from fluid part to the Assigned part is considered. The part type may be Assigned with Geometry, Interpolated, or Solar Lamp.
	Calculated	Temperature is a calculated function of all heat sources applied to the part. The part may have various Part Types explained in more detail below.
Part Type	Standard	This is a standard, one-layer part.
	Highly Conductive	This is a highly conductive part. For example, a thermal gel inserted between parts.
	Multi-Layer	A standard multi-layer part where definitions for each part may be utilized similar to a standard part. For example, the floor of a vehicle utilizes multiple layers for structural integrity as well as for the inner insulator and carpet.
	Multi-Layer Soil	Similar to multi-layer, this allows ground terrain to be meshed for conduction between the wheels and roadway.
	Engine	An experimental collaboration between TAItherm and a university for experimental diesel engine use only.
	Terrain	Allows definition of a mesh for a single layer of terrain or roadway.
Material	Selection	Allows for a selection of various defined materials for selection. This information includes the material type, density, conductivity and specific heat values. Materials may be added if these values are known in the Properties Tab.
Thickness	Selection	Defines the thickness of the mesh.
Radiation	Surface Condition	Sets the surface emissivity value for the thermal calculations, which informs the algorithm how much heat may be reflected, absorbed and emitted by the part. This varies on the material selected
	Texture Map	The texture map is no longer utilized.

Part Editor		
Category	Selections	Purpose
Incoming Total Solar	Calculated	Calculates the incoming total solar loading on the part. When utilized with a weather file, the value changes with regards to the solar azimuth and solar zenith.
	Value	The defined set value in the for the incoming total solar loading.
	Curve	Sets a defined curve for simulations that do not utilize a weather file.
	Routine	Utilized in a co-simulation environment when coupled to other simulation packages.
Mean Radiant Temperature	Calculated	Calculates the radiant temperature of the part. Allows for the interaction of changing radiant temperatures between parts.
	Value	Sets a constant value for the radiant temperature of the part.
	Curve	Sets a defined variable curve for the simulation.
	Routine	Utilized in a co-simulation environment when coupled to other simulation packages.
Initial Temperature	Seed SS	Sets the steady-state initial temperature to find convergence during the calculation. Not used for discrete analysis.
	Bypass SS	Sets the initial temperature for discrete analysis of the part. The part will react at an assigned temperature and thermal interaction is calculated for the duration of the simulation for a transient solution.
Imposed Heat	Value	Sets a constant value for heat that is continuously introduced to the part.
	Curve	Sets a curve for variable heat that is introduced into the part.
	Routine	Utilized in a co-simulation environment when coupled to other simulation packages.
Convection	None	No convection occurs with the part.
	H and T Fluid	Allows for the defining of interactions more defined below.

Part Editor		
Category	Selections	Purpose
	Library	Utilizes a library fluid for interaction.
	Fluid Stream	Allows for interaction with a fluid stream. For example, the interaction may occur if the part is defined as a coolant line and the fluid boundary is the part. Therefore, an interaction between the materials will occur.
	Wind	Utilized for stationary convection. For example, a building where the air is moving around a point.
	Co-Simulation	Utilized in a co-simulation environment when coupled to other simulation packages.
H Coefficient	Value	A set value for the interaction between the part and fluid.
	Curve	Not utilized. A variable interaction between the part and fluid. For example, phase change material.
	Routine	Utilized in a co-simulation environment when coupled to other simulation packages.
Fluid Temperature	Value	A set value for the incoming fluid temperature.
	Curve	A variable value that is sent through the part.
	Routine	Utilized in a co-simulation environment when coupled to other simulation packages.
	Fluid	A calculated value that interactions with a pre-defined fluid path. This is utilized when the fluid is variable and dependent on multiple variables.
Relative Humidity	Value	A set value for the humidity around the part.
	Curve	A variable value for the humidity around the part as set by the curve.
	Routine	Utilized in a co-simulation environment when coupled to other simulation packages.
	From Weather	Utilizes a weather file to create a humidity curve.

## APPENDIX B

### FLUID EDITOR FUNCTION, EXPLANATION, AND VALUES

Fluid Editor		
Category	Selections	Purpose
Temperature	Assigned	Allows the selected mesh elements (part) to be set to a designated temperature set to a constant or variable value. Parts may be linked through convection. However, only convection from fluid part to the Assigned part is considered. The part type may be Assigned with Geometry, Interpolated, or Solar Lamp.
	Calculated	Temperature is a calculated function of all heat sources applied to the part. The part may have various Part Types explained in more detail below.
Material	N/A	Select from various material types or use an added type from the properties menu.
Volume	N/A	
Position	X, Y, Z	Set the position of the fluid node based on the geometry of the mesh.
Initial Temperature	Seed SS	Sets the steady-state initial temperature to find convergence during the calculation. Not used for discrete analysis.
	Bypass SS	Sets the initial temperature for discrete analysis of the part. The part will react at an assigned temperature and calculated for the duration of the simulation for a transient solution.
Imposed Heat	Value	Sets a constant value for heat that is continuously introduced to the part.
	Curve	Sets a curve for variable heat that is introduced into the part.
	Routine	Utilized in a co-simulation environment when coupled to other simulation packages.
Advection Links	N/A	Advection links tell TAItherm where the fluid is moving to and from a position. They may not be used for general fluid use such as ambient air.
Upstream Part	N/A	If connected to a fluid stream this links the fluid node to the fluid stream.
Flow Type	Volume	Allows for a manual selection of a specific volume of fluid to exist at the node.

Fluid Editor		
Category	Selections	Purpose
	Percent	Utilized when multiple advection links are used from one central point
	Mass	Sets a mass flow rate.
Volume (Flow Rate)	Value	Sets a controlled volumetric flow rate.
	Curve	Sets a curve for a variable volumetric flow rate.
	Routine	No longer utilized.
Percent (Flow Rate)	Percent Value	May be used for fluids to determine the percentage that is transferred via an advection link.
Mass (Flow Rate)	Value	Sets a constant mass flow rate.
	Curve	Sets the curve for variable mass flow rate.



## APPENDIX C

### FLUID STREAMS FUNCTION, EXPLANATION, AND VALUES

Fluid Stream Editor		
Category	Selections	Purpose
Temperature	Assigned	Allows the selected mesh elements (part) to be set to a designated temperature set to a constant or variable value. Parts may be linked through convection. However, only convection from fluid part to the Assigned part is considered. The part type may be Assigned with Geometry, Interpolated, or Solar Lamp.
	Calculated	Temperature is a calculated function of all heat sources applied to the part. The part may have various Part Types explained in more detail below.
Material	N/A	Select from various material types or use an added type from the properties menu.
Node Distribution	Max Number of Nodes	Tells the solver the maximum number of nodes that will be contained within the boundary conditions. The higher this max number is, the more fidelity is received within the bounded part.
	Node Biasing	Explain Below.
Volume	N/A	
Position	X, Y, Z	Set the position of the fluid node based on the geometry of the mesh.
Initial Temperature	Seed SS	Sets the steady-state initial temperature to find convergence during the calculation. Not used for discrete analysis.
	Bypass SS	Sets the initial temperature for discrete analysis of the part. The part will react at an assigned temperature and calculated for the duration of the simulation for a transient solution.
Imposed Heat	Value	Sets a constant value for heat that is continuously introduced to the part.
	Curve	Sets a curve for variable heat that is introduced into the part.
	Routine	Utilized in a co-simulation environment when coupled to other simulation packages.

Fluid Stream Editor		
Category	Selections	Purpose
Advection Links	N/A	Advection links tell TAItherm where the fluid is moving to and from a position. They may not be used for general fluid use such as ambient air.
Upstream Part	N/A	If connected to a fluid stream this links the fluid node to the fluid stream.
Flow Type	Volume	Allows for a manual selection of a specific volume of fluid to exist at the node.
	Percent	Utilized when multiple advection links are used from one central point
	Mass	Sets a mass flow rate.
Flow Type	Volume	Allows for a manual selection of a specific volume of fluid to exist at the node.
	Percent	Utilized when multiple advection links are used from one central point
	Mass	Sets a mass flow rate.
Volume (Flow Rate)	Value	Sets a controlled volumetric flow rate.
	Curve	Sets a curve for a variable volumetric flow rate.

APPENDIX D

DATA COLLECTED JANUARY-MARCH 2017

	Battery Heat Rate	Engine Heat Rate	Inverter Heat Rate	EM Heat Rate	Transmission Heat Rate
Time (s)	Heat (W)	Heat (W)	Heat (W)	Heat (W)	Heat (W)
1	0.00	0.00	0.00	0.00	0.00
2	0.00	0.00	0.00	0.00	0.00
3	0.00	0.00	0.00	0.00	0.00
4	0.00	0.00	0.00	0.00	0.00
5	0.00	0.00	0.00	0.00	0.00
6	0.05	0.00	0.00	0.66	0.01
7	0.62	0.00	0.00	8.23	0.08
8	1.07	0.00	0.00	14.23	0.13
9	2.48	0.00	0.00	33.02	0.31
10	50.70	0.00	0.00	674.26	5.57
11	256.81	27050.80	27050.80	3415.60	28.82
12	15.94	31813.60	31813.60	211.98	0.27
13	131.92	48714.60	48714.60	1754.50	52.18
14	76.30	0.00	0.00	1014.83	4.47
15	57.34	19097.60	19097.60	762.63	25.45
16	99.42	32650.30	32650.30	1322.30	45.30
17	63.22	37769.80	37769.80	840.81	3.78
18	0.83	27779.70	27779.70	11.06	27.84
19	9.89	29677.70	29677.70	131.54	28.19

	Battery Heat Rate	Engine Heat Rate	Inverter Heat Rate	EM Heat Rate	Transmission Heat Rate
Time (s)	Heat (W)	Heat (W)	Heat (W)	Heat (W)	Heat (W)
20	56.73	31451.10	31451.10	754.57	27.29
21	79.74	0.00	0.00	1060.57	35.31
22	44.64	41369.70	41369.70	593.69	32.21
23	29.07	36626.60	36626.60	386.64	16.80
24	10.02	0.01	0.00	133.30	1.29
25	6.90	0.00	0.00	91.78	0.93
26	20.53	0.00	0.00	272.99	2.78
27	8.67	0.00	0.00	115.29	1.17
28	5.72	0.00	0.00	76.05	0.77
29	8.86	638.53	638.53	117.78	1.20
30	68.01	18644.40	18644.40	904.50	9.16
31	31.50	17096.90	17096.90	419.01	4.25
32	8.88	18786.50	18786.50	118.14	1.20
33	18.33	0.00	0.00	243.79	2.49
34	31.55	0.00	0.00	419.67	4.29
35	35.94	0.00	0.00	478.06	4.89
36	30.89	0.00	0.00	410.84	9.48
37	29.76	0.00	0.00	395.84	10.74
38	34.30	0.00	0.00	456.16	4.57

	Battery Heat Rate	Engine Heat Rate	Inverter Heat Rate	EM Heat Rate	Transmission Heat Rate
Time (s)	Heat (W)	Heat (W)	Heat (W)	Heat (W)	Heat (W)
39	24.14	0.00	0.00	321.11	3.15
40	0.01	0.00	0.00	0.11	6.46
41	0.00	0.00	0.00	0.00	0.02
42	0.00	0.00	0.00	0.00	0.00
43	0.00	0.00	0.00	0.00	0.00
44	0.00	0.00	0.00	0.00	0.00
45	0.00	0.00	0.00	0.00	0.00
46	0.00	0.00	0.00	0.00	0.00
47	0.00	0.00	0.00	0.00	0.00
48	0.00	0.00	0.00	0.00	0.00
49	0.13	0.00	0.00	1.67	0.02
50	85.24	0.00	0.00	1133.73	9.76
51	1.33	0.00	0.00	17.74	20.92
52	63.58	30743.60	30743.60	845.60	36.36
53	47.04	25156.30	25156.30	625.70	30.38
54	112.17	32496.60	32496.60	1491.79	46.01
55	50.00	41760.50	41760.50	665.01	47.20
56	14.44	46566.30	46566.30	192.07	33.58
57	130.82	51176.00	51176.00	1739.86	44.75

	Battery Heat Rate	Engine Heat Rate	Inverter Heat Rate	EM Heat Rate	Transmission Heat Rate
Time (s)	Heat (W)	Heat (W)	Heat (W)	Heat (W)	Heat (W)
58	178.11	56406.00	56406.00	2368.89	54.50
59	152.05	61990.80	61990.80	2022.31	55.18
60	48.43	48687.70	48687.70	644.12	44.96
61	51.96	40552.40	40552.40	691.02	33.94
62	40.08	30546.20	30546.20	533.10	35.96
63	41.32	32083.30	32083.30	549.60	37.66
64	46.56	33666.50	33666.50	619.25	39.92
65	7.49	35196.60	35196.60	99.67	36.20
66	43.00	36447.10	36447.10	571.85	34.41
67	21.06	39673.90	39673.90	280.12	26.76
68	75.72	27479.00	27479.00	1007.07	10.84
69	111.37	27392.60	27392.60	1481.16	5.68
70	137.18	27342.30	27342.30	1824.52	1.87
71	4.01	0.00	0.00	53.35	0.52
72	3.77	0.00	0.00	50.16	0.52
73	8.53	20649.60	20649.60	113.38	1.14
74	105.60	20604.10	20604.10	1404.48	5.37
75	101.03	20635.40	20635.40	1343.70	6.02
76	2.42	0.00	0.00	32.21	0.30



	Battery Heat	Engine Heat	Inverter Heat	EM Heat	Transmission
	Rate	Rate	Rate	Rate	Heat Rate
Time					
(s)	Heat (W)	Heat (W)	Heat (W)	Heat (W)	Heat (W)
77	8.11	0.00	0.00	107.86	1.11
78	0.20	0.00	0.00	2.69	0.02
79	53.98	0.00	0.00	717.92	3.52
80	109.69	0.00	0.00	1458.86	3.54
81	88.27	0.00	0.00	1174.01	6.59
82	75.31	0.00	0.00	1001.59	8.49
83	43.54	0.00	0.00	579.07	13.16
84	11.75	2040.13	2040.13	156.25	21.23
85	71.00	28445.60	28445.60	944.32	37.71
86	122.16	29536.30	29536.30	1624.73	45.70
87	46.00	39024.50	39024.50	611.84	7.93
88	2.75	40953.40	40953.40	36.60	51.13
89	21.81	42728.50	42728.50	290.10	49.19
90	0.49	54031.90	54031.90	6.49	53.83
91	28.70	55808.20	55808.20	381.70	59.43
92	57.42	57692.90	57692.90	763.71	55.60
93	34.37	59345.60	59345.60	457.15	54.01
94	49.62	50571.20	50571.20	659.92	46.82
95	17.98	41059.70	41059.70	239.16	25.39

	Battery Heat Rate	Engine Heat Rate	Inverter Heat Rate	EM Heat Rate	Transmission Heat Rate
Time (s)	Heat (W)	Heat (W)	Heat (W)	Heat (W)	Heat (W)
96	72.62	28630.90	28630.90	965.83	18.33
97	140.06	28602.50	28602.50	1862.76	8.61
98	20.25	0.00	0.00	269.32	2.62
99	14.73	0.00	0.00	195.97	1.98
100	13.12	0.00	0.00	174.48	1.77
101	8.27	0.00	0.00	109.93	1.11
102	8.13	0.00	0.00	108.15	1.10
103	11.30	0.00	0.00	150.35	1.53
104	13.26	0.00	0.00	176.40	1.80
105	12.01	0.00	0.00	159.73	1.63
106	12.83	0.00	0.00	170.65	1.74
107	10.67	0.00	0.00	141.95	1.45
108	12.41	0.00	0.00	165.09	1.69
109	11.27	0.00	0.00	149.86	1.54
110	11.95	0.00	0.00	158.91	1.63
111	9.99	0.00	0.00	132.83	1.37
112	11.46	0.00	0.00	152.37	1.57
113	15.88	0.00	0.00	211.26	2.17
114	22.09	0.00	0.00	293.77	4.68

	Battery Heat Rate	Engine Heat Rate	Inverter Heat Rate	EM Heat Rate	Transmission Heat Rate
Time (s)	Heat (W)	Heat (W)	Heat (W)	Heat (W)	Heat (W)
115	18.37	0.00	0.00	244.36	2.52
116	7.39	0.00	0.00	98.27	1.03
117	7.29	0.00	0.00	96.90	1.01
118	8.77	0.00	0.00	116.59	1.21
119	31.06	0.00	0.00	413.13	13.67
120	38.64	0.00	0.00	513.92	5.28
121	31.78	0.00	0.00	422.61	4.30
122	30.43	0.00	0.00	404.78	4.10
123	20.89	0.00	0.00	277.79	12.42
124	18.45	0.00	0.00	245.37	2.43
125	0.34	0.00	0.00	4.58	0.02
126	0.20	0.00	0.00	2.69	0.09
127	0.20	0.00	0.00	2.69	0.04
128	0.20	0.00	0.00	2.69	0.02
129	0.20	0.00	0.00	2.69	0.00
130	0.20	0.00	0.00	2.69	0.00
131	0.20	0.00	0.00	2.69	0.00
132	0.20	0.00	0.00	2.69	0.00
133	0.20	0.00	0.00	2.69	0.00

	Battery Heat Rate	Engine Heat Rate	Inverter Heat Rate	EM Heat Rate	Transmission Heat Rate
Time (s)	Heat (W)	Heat (W)	Heat (W)	Heat (W)	Heat (W)
134	0.20	0.00	0.00	2.69	0.00
135	0.20	0.00	0.00	2.69	0.00
136	7.55	0.00	0.00	100.38	0.91
137	124.52	0.00	0.00	1656.13	12.91
138	94.38	21392.40	21392.40	1255.32	32.43
139	101.85	38105.80	38105.80	1354.60	47.64
140	91.84	55806.30	55806.30	1221.53	63.22
141	116.07	46581.60	46581.60	1543.78	60.11
142	84.17	55460.50	55460.50	1119.49	64.77
143	73.57	59625.00	59625.00	978.53	68.33
144	30.50	64707.80	64707.80	405.63	41.37
145	3.06	49881.60	49881.60	40.66	34.63
146	85.68	39637.30	39637.30	1139.57	27.38
147	14.09	40686.10	40686.10	187.43	31.10
148	6.20	31794.10	31794.10	82.50	24.87
149	4.72	26361.60	26361.60	62.83	25.70
150	33.14	27026.50	27026.50	440.72	22.30
151	21.82	19626.30	19626.30	290.15	16.53
152	38.57	19836.70	19836.70	512.98	14.34

	Battery Heat	Engine Heat	Inverter Heat	EM Heat	Transmission
	Rate	Rate	Rate	Rate	Heat Rate
Time					
(s)	Heat (W)	Heat (W)	Heat (W)	Heat (W)	Heat (W)
153	9.83	20092.40	20092.40	130.68	18.67
154	46.33	20363.60	20363.60	616.14	13.72
155	91.08	20380.50	20380.50	1211.41	7.36
156	36.22	20498.30	20498.30	481.71	15.29
157	266.34	39131.10	39131.10	3542.33	18.13
158	32.14	86858.20	86858.20	427.45	14.52
159	108.82	29735.00	29735.00	1447.34	41.22
160	13.78	44289.40	44289.40	183.31	17.17
161	32.98	50336.20	50336.20	438.67	27.24
162	17.05	32381.50	32381.50	226.78	14.63
163	45.21	23402.50	23402.50	601.23	16.96
164	53.69	23549.80	23549.80	714.05	15.87
165	151.71	0.29	0.00	2017.76	1.77
166	11.27	0.00	0.00	149.93	1.47
167	10.17	22588.70	22588.70	135.29	1.37
168	74.90	22473.20	22473.20	996.23	7.26
169	1.31	19918.90	19918.90	17.43	0.16
170	114.33	22169.80	22169.80	1520.55	5.66
171	57.74	0.00	0.00	767.95	7.93

	Battery Heat Rate	Engine Heat Rate	Inverter Heat Rate	EM Heat Rate	Transmission Heat Rate
Time (s)	Heat (W)	Heat (W)	Heat (W)	Heat (W)	Heat (W)
172	97.44	21860.20	21860.20	1295.94	7.76
173	105.85	21921.50	21921.50	1407.73	6.57
174	121.92	21779.40	21779.40	1621.55	4.16
175	127.48	21691.50	21691.50	1695.54	3.27
176	96.88	21619.00	21619.00	1288.44	7.60
177	66.20	21709.60	21709.60	880.41	12.06
178	93.57	21749.30	21749.30	1244.44	8.20
179	127.93	21640.30	21640.30	1701.48	3.18
180	123.38	0.00	0.00	1640.98	3.72
181	111.94	0.00	0.00	1488.84	5.29
182	6.86	0.00	0.00	91.21	0.89
183	2.38	0.00	0.00	31.65	0.33
184	61.31	0.00	0.00	815.48	8.26
185	19.53	0.00	0.00	259.79	2.57
186	73.45	0.00	0.00	976.87	9.88
187	46.22	1978.01	1978.01	614.70	18.61
188	48.24	10963.10	10963.10	641.66	36.24
189	19.26	0.12	0.00	256.15	33.19
190	32.34	0.00	0.00	430.08	17.22

	Battery Heat Rate	Engine Heat Rate	Inverter Heat Rate	EM Heat Rate	Transmission Heat Rate
Time (s)	Heat (W)	Heat (W)	Heat (W)	Heat (W)	Heat (W)
191	30.43	0.00	0.00	404.77	26.73
192	17.65	0.00	0.00	234.70	22.68
193	12.76	0.00	0.00	169.75	17.35
194	11.05	0.00	0.00	146.96	16.31
195	17.14	0.00	0.00	227.97	21.69
196	6.41	0.00	0.00	85.31	23.46
197	53.42	0.00	0.00	710.55	16.95
198	75.77	0.00	0.00	1007.77	13.81
199	132.86	0.00	0.00	1766.98	5.58
200	103.14	0.00	0.00	1371.74	9.73
201	25.27	0.00	0.00	336.10	20.97
202	85.51	24835.90	24835.90	1137.27	12.50
203	105.54	24734.80	24734.80	1403.65	9.57
204	72.51	24789.70	24789.70	964.40	14.32
205	27.58	25021.60	25021.60	366.88	28.57
206	28.76	35833.60	35833.60	382.48	17.68
207	73.39	25327.20	25327.20	976.06	14.78
208	62.49	25421.50	25421.50	831.15	16.41
209	59.19	25519.10	25519.10	787.27	16.97

	Battery Heat	Engine Heat	Inverter Heat	EM Heat	Transmission
	Rate	Rate	Rate	Rate	Heat Rate
Time					
(s)	Heat (W)	Heat (W)	Heat (W)	Heat (W)	Heat (W)
210	38.59	25647.90	25647.90	513.27	20.04
211	22.74	25841.00	25841.00	302.39	22.48
212	10.73	26084.90	26084.90	142.72	27.40
213	35.91	26316.10	26316.10	477.59	21.09
214	46.15	26390.80	26390.80	613.76	19.75
215	20.77	0.00	0.00	276.25	2.68
216	1.00	0.00	0.00	13.28	0.12
217	72.65	25204.90	25204.90	966.24	9.82
218	72.91	25320.30	25320.30	969.73	14.75
219	116.48	25326.30	25326.30	1549.16	8.52
220	63.38	25294.70	25294.70	842.93	16.11
221	64.28	25463.00	25463.00	854.98	16.11
222	122.88	25394.30	25394.30	1634.27	7.70
223	88.87	25343.40	25343.40	1181.92	12.53
224	152.93	0.00	0.00	2033.97	3.26
225	86.55	25149.20	25149.20	1151.05	12.67
226	69.08	25313.60	25313.60	918.76	15.27
227	85.24	25306.70	25306.70	1133.68	12.99
228	79.56	25305.80	25305.80	1058.21	10.75



	Battery Heat Rate	Engine Heat Rate	Inverter Heat Rate	EM Heat Rate	Transmission Heat Rate
Time (s)	Heat (W)	Heat (W)	Heat (W)	Heat (W)	Heat (W)
229	92.35	25274.30	25274.30	1228.29	12.47
230	41.39	14791.10	14791.10	550.43	16.51
231	135.60	25020.90	25020.90	1803.44	5.50
232	50.02	25120.00	25120.00	665.32	17.81
233	47.99	25295.30	25295.30	638.31	18.27
234	139.08	25381.70	25381.70	1849.80	18.71
235	164.91	25556.20	25556.20	2193.30	22.17
236	160.95	25767.30	25767.30	2140.63	24.08
237	128.81	0.00	0.00	1713.17	6.65
238	131.52	25379.50	25379.50	1749.24	6.50
239	25.43	0.00	0.00	338.26	3.41
240	86.94	25001.20	25001.20	1156.36	12.46
241	114.93	25088.30	25088.30	1528.58	8.48
242	72.86	24996.80	24996.80	969.02	14.46
243	114.51	25147.80	25147.80	1522.95	15.44
244	29.21	25017.10	25017.10	388.50	3.95
245	39.72	24871.90	24871.90	528.23	17.62
246	106.27	24879.70	24879.70	1413.43	9.54
247	72.09	24894.90	24894.90	958.81	14.44

	Battery Heat Rate	Engine Heat Rate	Inverter Heat Rate	EM Heat Rate	Transmission Heat Rate
Time (s)	Heat (W)	Heat (W)	Heat (W)	Heat (W)	Heat (W)
248	129.26	25003.20	25003.20	1719.11	17.40
249	89.80	25024.40	25024.40	1194.28	12.12
250	0.81	0.00	0.00	10.77	0.08
251	32.64	24613.70	24613.70	434.12	4.42
252	103.67	24663.90	24663.90	1378.85	13.99
253	115.20	24774.60	24774.60	1532.17	15.53
254	157.15	0.02	0.00	2090.03	2.03
255	110.37	0.00	0.00	1467.97	8.60
256	96.12	0.00	0.00	1278.40	10.65
257	99.72	24505.00	24505.00	1326.22	10.11
258	86.16	24517.00	24517.00	1145.89	12.07
259	67.96	24502.70	24502.70	903.91	9.19
260	99.81	24470.10	24470.10	1327.46	13.47
261	135.00	24636.50	24636.50	1795.55	18.17
262	121.85	24661.90	24661.90	1620.54	7.11
263	128.68	0.00	0.00	1711.37	6.00
264	99.09	0.00	0.00	1317.88	13.36
265	40.68	0.00	0.00	541.09	5.50
266	132.36	0.00	0.00	1760.40	17.81

	Battery Heat Rate	Engine Heat Rate	Inverter Heat Rate	EM Heat Rate	Transmission Heat Rate
Time (s)	Heat (W)	Heat (W)	Heat (W)	Heat (W)	Heat (W)
267	43.94	0.00	0.00	584.40	30.47
268	135.46	508.15	508.15	1801.55	5.17
269	83.79	0.00	0.00	1114.37	12.52
270	81.37	24674.30	24674.30	1082.21	10.99
271	27.46	24510.30	24510.30	365.26	3.72
272	31.63	24378.60	24378.60	420.62	4.28
273	42.62	24294.80	24294.80	566.82	5.77
274	90.92	24304.50	24304.50	1209.30	12.27
275	103.56	24397.00	24397.00	1377.32	13.97
276	88.79	24402.00	24402.00	1180.95	11.98
277	74.41	24386.90	24386.90	989.59	10.05
278	106.08	0.00	0.00	1410.86	14.31
279	101.20	0.00	0.00	1345.89	13.65
280	112.50	0.00	0.00	1496.28	8.30
281	83.15	0.00	0.00	1105.89	12.50
282	56.05	0.00	0.00	745.45	16.47
283	82.38	0.00	0.00	1095.69	12.79
284	2.97	0.00	0.00	39.45	25.07
285	16.83	0.00	0.00	223.81	37.66

	Battery Heat	Engine Heat	Inverter Heat	EM Heat	Transmission
	Rate	Rate	Rate	Rate	Heat Rate
Time					
(s)	Heat (W)	Heat (W)	Heat (W)	Heat (W)	Heat (W)
286	5.50	0.00	0.00	73.19	26.18
287	25.61	0.00	0.00	340.66	22.04
288	5.96	0.00	0.00	79.29	26.72
289	18.41	0.00	0.00	244.92	23.58
290	13.30	0.00	0.00	176.93	28.23
291	10.68	0.00	0.00	142.02	25.23
292	45.85	0.00	0.00	609.80	20.39
293	5.26	0.00	0.00	70.00	27.83
294	36.51	0.00	0.00	485.55	22.18
295	39.98	0.00	0.00	531.68	21.81
296	30.79	0.00	0.00	409.53	23.30
297	39.66	0.00	0.00	527.47	22.20
298	197.82	0.00	0.00	2631.06	22.89
299	13.07	0.00	0.00	173.80	9.69
300	583.93	0.00	0.00	7766.33	72.20
301	34.93	0.00	0.00	464.50	3.32
302	0.20	766.60	766.60	2.69	0.09
303	163.32	0.00	0.00	2172.17	6.13
304	135.36	29443.80	29443.80	1800.28	10.02

	Battery Heat	Engine Heat	Inverter Heat	EM Heat	Transmission
	Rate	Rate	Rate	Rate	Heat Rate
Time					
(s)	Heat (W)	Heat (W)	Heat (W)	Heat (W)	Heat (W)
305	61.75	29460.10	29460.10	821.25	20.53
306	23.13	29671.10	29671.10	307.62	26.20
307	71.80	29760.30	29760.30	954.97	19.38
308	193.79	0.00	0.00	2577.34	1.28
309	34.08	29210.00	29210.00	453.25	7.04
310	75.31	29016.40	29016.40	1001.61	10.15
311	134.95	28910.40	28910.40	1794.84	9.44
312	115.47	28871.20	28871.20	1535.72	12.16
313	92.01	28821.30	28821.30	1223.76	15.48
314	80.80	28849.90	28849.90	1074.60	17.11
315	64.45	28883.80	28883.80	857.18	19.50
316	26.90	29098.10	29098.10	357.79	32.51
317	44.93	39402.50	39402.50	597.63	35.35
318	78.45	39752.80	39752.80	1043.33	40.25
319	3.16	53759.60	53759.60	42.06	53.85
320	50.58	54543.90	54543.90	672.68	47.10
321	24.46	55459.90	55459.90	325.35	58.46
322	5.36	46990.90	46990.90	71.34	57.15
323	54.69	47830.60	47830.60	727.44	49.62

	Battery Heat Rate	Engine Heat Rate	Inverter Heat Rate	EM Heat Rate	Transmission Heat Rate
Time (s)	Heat (W)	Heat (W)	Heat (W)	Heat (W)	Heat (W)
324	160.63	33119.80	33119.80	2136.35	9.85
325	22.49	0.00	0.00	299.17	2.88
326	17.10	31376.10	31376.10	227.45	2.35
327	182.49	31367.40	31367.40	2427.09	24.60
328	108.35	37232.00	37232.00	1441.10	47.68
329	56.90	47034.10	47034.10	756.77	8.33
330	96.78	32805.40	32805.40	1287.17	39.86
331	63.12	57997.20	57997.20	839.56	40.27
332	7.26	43652.60	43652.60	96.50	34.50
333	47.58	43826.80	43826.80	632.77	26.92
334	36.05	43920.50	43920.50	479.42	28.64
335	52.71	44083.00	44083.00	700.99	26.40
336	178.54	33796.90	33796.90	2374.55	8.23
337	149.30	33498.40	33498.40	1985.65	12.13
338	143.30	33404.80	33404.80	1905.89	12.83
339	76.26	33173.30	33173.30	1014.32	10.40
340	5.72	0.00	0.00	76.04	0.73
341	5.99	0.00	0.00	79.73	0.77
342	20.64	0.00	0.00	274.48	2.76

	Battery Heat Rate	Engine Heat Rate	Inverter Heat Rate	EM Heat Rate	Transmission Heat Rate
Time (s)	Heat (W)	Heat (W)	Heat (W)	Heat (W)	Heat (W)
343	13.79	0.00	0.00	183.43	1.84
344	14.94	0.00	0.00	198.70	2.00
345	31.88	0.00	0.00	423.98	4.30
346	7.50	0.00	0.00	99.70	1.00
347	71.49	671.75	671.75	950.77	9.67
348	66.31	0.00	0.00	881.87	8.97
349	42.40	26363.00	26363.00	563.92	5.75
350	101.94	26335.70	26335.70	1355.85	13.77
351	124.47	26411.70	26411.70	1655.41	16.79
352	5.68	26541.90	26541.90	75.54	27.09
353	0.34	38386.70	38386.70	4.47	37.82
354	40.55	36778.40	36778.40	539.31	32.48
355	20.73	49484.00	49484.00	275.73	24.38
356	45.95	37414.50	37414.50	611.11	20.93
357	120.44	37467.80	37467.80	1601.85	10.31
358	144.83	37230.80	37230.80	1926.22	6.64
359	123.90	27340.90	27340.90	1647.88	9.55
360	61.63	0.00	0.00	819.70	8.53
361	2.53	0.00	0.00	33.70	0.33

	Battery Heat	Engine Heat	Inverter Heat	EM Heat	Transmission
	Rate	Rate	Rate	Rate	Heat Rate
Time					
(s)	Heat (W)	Heat (W)	Heat (W)	Heat (W)	Heat (W)
362	18.30	26490.10	26490.10	243.42	2.49
363	22.04	26319.80	26319.80	293.12	2.99
364	80.66	26233.10	26233.10	1072.71	10.91
365	161.58	26384.90	26384.90	2148.97	21.74
366	108.52	26454.20	26454.20	1443.34	10.78
367	90.64	26379.80	26379.80	1205.46	13.31
368	6.73	26579.90	26579.90	89.48	25.44
369	14.16	26889.60	26889.60	188.37	28.62
370	6.17	27126.60	27126.60	82.05	26.11
371	38.40	27296.40	27296.40	510.75	21.72
372	36.68	27432.20	27432.20	487.86	22.12
373	24.19	27629.70	27629.70	321.67	24.08
374	119.19	27716.80	27716.80	1585.21	16.10
375	43.62	27755.70	27755.70	580.08	21.48
376	41.48	28010.80	28010.80	551.64	21.98
377	36.07	28023.20	28023.20	479.79	5.05
378	177.25	28121.30	28121.30	2357.39	23.85
379	203.35	28382.30	28382.30	2704.60	27.32
380	29.78	28555.30	28555.30	396.12	24.12



	Battery Heat Rate	Engine Heat Rate	Inverter Heat Rate	EM Heat Rate	Transmission Heat Rate
Time (s)	Heat (W)	Heat (W)	Heat (W)	Heat (W)	Heat (W)
381	47.86	28676.60	28676.60	636.52	21.78
382	135.01	28678.20	28678.20	1795.63	9.30
383	109.86	28537.10	28537.10	1461.07	12.79
384	112.08	28575.80	28575.80	1490.62	12.45
385	29.52	28382.80	28382.80	392.59	4.04
386	81.33	28214.80	28214.80	1081.72	11.01
387	142.06	28303.20	28303.20	1889.34	19.16
388	147.70	28288.50	28288.50	1964.45	7.02
389	163.54	28079.50	28079.50	2175.14	4.55
390	59.37	28071.70	28071.70	789.65	19.44
391	4.67	28228.90	28228.90	62.07	9.87
392	86.29	28140.00	28140.00	1147.61	11.68
393	137.46	28137.20	28137.20	1828.21	18.55
394	9.54	28313.10	28313.10	126.93	29.40
395	67.01	0.00	0.00	891.29	18.72
396	88.86	0.00	0.00	1181.89	15.63
397	8.34	0.00	0.00	110.97	27.23
398	50.19	0.00	0.00	667.51	21.49
399	71.69	0.00	0.00	953.42	9.72

	Battery Heat	Engine Heat	Inverter Heat	EM Heat	Transmission
	Rate	Rate	Rate	Rate	Heat Rate
Time					
(s)	Heat (W)	Heat (W)	Heat (W)	Heat (W)	Heat (W)
400	121.56	0.00	0.00	1616.77	11.30
401	91.31	0.00	0.00	1214.42	15.58
402	48.86	0.00	0.00	649.84	21.73
403	55.34	0.00	0.00	735.98	20.92
404	82.66	0.00	0.00	1099.39	11.21
405	120.29	0.00	0.00	1599.91	16.26
406	200.60	0.00	0.00	2668.01	26.96
407	36.33	0.00	0.00	483.19	23.91
408	6.02	0.00	0.00	80.04	30.08
409	64.81	0.00	0.00	861.96	20.24
410	109.04	0.00	0.00	1450.28	13.87
411	120.17	0.00	0.00	1598.22	12.22
412	103.47	0.00	0.00	1376.11	14.01
413	98.05	0.00	0.00	1304.05	13.27
414	190.79	0.00	0.00	2537.54	25.66
415	23.11	0.00	0.00	307.40	26.22
416	21.88	0.00	0.00	291.04	26.57
417	174.98	0.00	0.00	2327.28	4.62
418	0.90	0.00	0.00	11.99	0.06

	Battery Heat	Engine Heat	Inverter Heat	EM Heat	Transmission
	Rate	Rate	Rate	Rate	Heat Rate
Time					
(s)	Heat (W)	Heat (W)	Heat (W)	Heat (W)	Heat (W)
419	0.66	0.00	0.00	8.81	0.06
420	0.20	0.00	0.00	2.69	3.15
421	133.69	0.00	0.00	1778.10	9.27
422	44.85	0.00	0.00	596.44	22.03
423	88.01	0.00	0.00	1170.47	11.92
424	158.04	0.00	0.00	2101.97	21.29
425	86.16	0.00	0.00	1145.98	11.66
426	142.74	0.00	0.00	1898.46	7.94
427	38.82	0.00	0.00	516.25	5.28
428	21.64	0.00	0.00	287.87	2.95
429	9.77	0.00	0.00	129.95	1.33
430	62.38	0.00	0.00	829.63	8.46
431	94.53	0.00	0.00	1257.27	12.78
432	56.67	0.00	0.00	753.78	7.68
433	27.06	0.00	0.00	359.96	3.67
434	78.30	0.00	0.00	1041.35	10.60
435	122.54	0.00	0.00	1629.81	16.54
436	119.53	0.00	0.00	1589.68	16.14
437	73.26	0.00	0.00	974.31	9.91

	Battery Heat	Engine Heat	Inverter Heat	EM Heat	Transmission
	Rate	Rate	Rate	Rate	Heat Rate
Time					
(s)	Heat (W)	Heat (W)	Heat (W)	Heat (W)	Heat (W)
438	50.81	0.00	0.00	675.74	6.89
439	10.82	0.00	0.00	143.86	1.47
440	67.89	0.00	0.00	902.95	9.19
441	75.51	0.00	0.00	1004.29	10.21
442	88.24	0.00	0.00	1173.60	11.93
443	64.90	0.00	0.00	863.16	8.78
444	76.80	0.00	0.00	1021.47	10.39
445	51.04	0.00	0.00	678.82	6.91
446	32.29	0.00	0.00	429.40	4.37
447	29.15	589.43	589.43	387.65	3.95
448	0.82	0.00	0.00	10.93	0.14
449	9.48	24100.20	24100.20	126.09	1.28
450	69.88	24040.10	24040.10	929.45	9.44
451	72.40	24082.10	24082.10	962.92	9.77
452	87.41	24036.30	24036.30	1162.50	11.79
453	99.85	24123.90	24123.90	1327.96	13.46
454	118.98	24187.60	24187.60	1582.37	16.03
455	124.97	24312.30	24312.30	1662.09	16.83
456	96.25	24318.00	24318.00	1280.13	10.42

	Battery Heat	Engine Heat	Inverter Heat	EM Heat	Transmission
	Rate	Rate	Rate	Rate	Heat Rate
Time					
(s)	Heat (W)	Heat (W)	Heat (W)	Heat (W)	Heat (W)
457	99.42	24316.80	24316.80	1322.34	9.95
458	62.46	24375.70	24375.70	830.70	15.29
459	106.78	24440.10	24440.10	1420.23	9.00
460	84.85	24380.10	24380.10	1128.46	12.11
461	36.98	24558.70	24558.70	491.85	19.09
462	101.48	24630.00	24630.00	1349.71	9.95
463	84.13	24570.30	24570.30	1118.99	12.41
464	111.42	24628.00	24628.00	1481.94	8.53
465	85.09	24567.90	24567.90	1131.67	12.26
466	73.41	24686.40	24686.40	976.31	14.02
467	55.21	24752.80	24752.80	734.31	16.70
468	105.27	24817.50	24817.50	1400.04	9.60
469	158.28	24636.00	24636.00	2105.07	1.83
470	7.47	0.00	0.00	99.38	0.96
471	12.62	0.00	0.00	167.89	1.71
472	2.98	0.00	0.00	39.68	0.40
473	16.24	0.00	0.00	215.99	2.20
474	6.96	0.00	0.00	92.50	0.95
475	11.73	0.00	0.00	156.02	1.60

	Battery Heat	Engine Heat	Inverter Heat	EM Heat	Transmission
	Rate	Rate	Rate	Rate	Heat Rate
Time					
(s)	Heat (W)	Heat (W)	Heat (W)	Heat (W)	Heat (W)
476	20.76	0.00	0.00	276.09	2.83
477	17.30	0.00	0.00	230.10	2.36
478	0.56	0.00	0.00	7.48	0.09
479	7.42	0.00	0.00	98.68	1.02
480	19.49	0.00	0.00	259.22	2.66
481	23.17	0.00	0.00	308.19	13.77
482	35.82	0.00	0.00	476.46	4.89
483	19.10	0.00	0.00	253.99	2.62
484	0.01	0.00	0.00	0.14	7.52
485	29.38	0.00	0.00	390.74	4.02
486	45.04	0.00	0.00	598.99	23.27
487	28.29	0.00	0.00	376.30	11.45
488	1.91	0.00	0.00	25.44	0.28
489	20.66	0.00	0.00	274.73	2.78
490	20.99	0.00	0.00	279.14	3.32
491	15.35	0.00	0.00	204.21	2.03
492	0.20	0.00	0.00	2.68	4.46
493	0.20	0.00	0.00	2.69	0.06
494	0.20	0.00	0.00	2.69	0.00

	Battery Heat	Engine Heat	Inverter Heat	EM Heat	Transmission
	Rate	Rate	Rate	Rate	Heat Rate
Time					
(s)	Heat (W)	Heat (W)	Heat (W)	Heat (W)	Heat (W)
495	0.20	0.00	0.00	2.69	0.00
496	0.20	0.00	0.00	2.69	0.00
497	0.20	0.00	0.00	2.69	0.00
498	0.20	0.00	0.00	2.69	0.00
499	0.20	0.00	0.00	2.69	0.00
500	0.20	0.00	0.00	2.69	0.00
501	0.20	0.00	0.00	2.69	0.00
502	37.64	0.00	0.00	500.62	3.01
503	134.05	18328.90	18328.90	1782.85	14.95
504	48.86	22201.00	22201.00	649.88	25.09
505	27.97	35025.80	35025.80	371.96	35.57
506	112.76	49837.40	49837.40	1499.71	41.47
507	25.83	36194.30	36194.30	343.56	28.10
508	71.37	29772.00	29772.00	949.21	9.94
509	12.76	0.00	0.00	169.64	1.63
510	16.83	0.00	0.00	223.80	2.29
511	18.26	0.00	0.00	242.86	2.48
512	31.21	0.00	0.00	415.15	18.38
513	34.37	0.00	0.00	457.18	4.61

	Battery Heat	Engine Heat	Inverter Heat	EM Heat	Transmission
	Rate	Rate	Rate	Rate	Heat Rate
Time					
(s)	Heat (W)	Heat (W)	Heat (W)	Heat (W)	Heat (W)
514	19.68	0.00	0.00	261.79	2.59
515	11.27	0.00	0.00	149.91	1.46
516	232.36	8948.46	8948.46	3090.44	22.00
517	4.14	23235.90	23235.90	55.00	22.28
518	8.40	33612.50	33612.50	111.67	29.61
519	85.19	28152.30	28152.30	1133.05	37.95
520	41.30	34693.20	34693.20	549.35	20.49
521	22.13	39396.80	39396.80	294.27	14.95
522	132.45	27357.80	27357.80	1761.59	2.73
523	23.19	0.00	0.00	308.45	2.95
524	30.10	0.00	0.00	400.40	4.07
525	23.80	0.00	0.00	316.56	8.14
526	31.88	0.00	0.00	424.02	4.27
527	22.22	0.00	0.00	295.49	2.93
528	5.25	0.00	0.00	69.88	0.71
529	0.20	0.00	0.00	2.68	4.23
530	0.20	0.00	0.00	2.69	0.07
531	3.28	0.00	0.00	43.67	0.38
532	63.37	0.00	0.00	842.86	6.76



	Battery Heat	Engine Heat	Inverter Heat	EM Heat	Transmission
	Rate	Rate	Rate	Rate	Heat Rate
Time					
(s)	Heat (W)	Heat (W)	Heat (W)	Heat (W)	Heat (W)
533	23.12	13939.10	13939.10	307.51	15.93
534	22.58	25463.80	25463.80	300.34	25.98
535	1.73	38019.60	38019.60	22.99	35.20
536	75.05	31039.00	31039.00	998.19	39.63
537	35.81	36782.00	36782.00	476.30	22.01
538	95.81	20615.10	20615.10	1274.25	7.05
539	8.17	0.00	0.00	108.66	1.05
540	22.70	0.00	0.00	301.85	3.07
541	30.46	0.00	0.00	405.08	4.12
542	36.49	0.00	0.00	485.33	5.02
543	23.32	0.00	0.00	310.19	8.37
544	15.09	0.00	0.00	200.71	1.99
545	28.50	0.00	0.00	379.08	0.84
546	0.20	0.00	0.00	2.69	0.04
547	94.26	0.00	0.00	1253.66	10.06
548	23.56	17860.10	17860.10	313.30	18.94
549	6.51	28633.20	28633.20	86.54	25.37
550	131.00	41396.60	41396.60	1742.32	33.94
551	49.23	31780.70	31780.70	654.76	37.16

	Battery Heat	Engine Heat	Inverter Heat	EM Heat	Transmission
	Rate	Rate	Rate	Rate	Heat Rate
Time					
(s)	Heat (W)	Heat (W)	Heat (W)	Heat (W)	Heat (W)
552	21.28	39432.30	39432.30	283.03	41.04
553	37.82	0.00	0.00	503.04	4.12
554	28.55	0.00	0.00	379.68	3.72
555	34.97	0.00	0.00	465.15	5.33
556	35.06	0.00	0.00	466.27	6.32
557	27.68	0.00	0.00	368.15	3.71
558	21.46	0.00	0.00	285.36	2.82
559	3.26	0.00	0.00	43.37	0.35
560	0.20	0.00	0.00	2.69	0.11
561	0.20	0.00	0.00	2.69	0.00
562	0.20	0.00	0.00	2.69	0.00
563	0.20	0.00	0.00	2.69	0.00
564	0.20	0.00	0.00	2.69	0.00
565	0.20	0.00	0.00	2.69	0.00
566	0.20	0.00	0.00	2.69	0.00
567	0.20	0.00	0.00	2.69	0.00
568	0.20	0.00	0.00	2.69	0.00
569	52.50	0.00	0.00	698.26	4.71
570	0.02	26168.10	26168.10	0.28	21.77

	Battery Heat	Engine Heat	Inverter Heat	EM Heat	Transmission
	Rate	Rate	Rate	Rate	Heat Rate
Time					
(s)	Heat (W)	Heat (W)	Heat (W)	Heat (W)	Heat (W)
571	94.55	29031.30	29031.30	1257.47	38.13
572	156.53	44553.30	44553.30	2081.81	55.61
573	71.75	35141.10	35141.10	954.32	43.40
574	260.74	46010.60	46010.60	3467.82	78.25
575	2.57	55307.70	55307.70	34.16	40.42
576	85.04	41044.40	41044.40	1131.01	42.28
577	431.59	45434.90	45434.90	5740.09	104.03
578	264.47	70727.20	70727.20	3517.47	90.83
579	105.34	58910.30	58910.30	1401.05	44.32
580	54.23	43371.90	43371.90	721.29	9.30
581	4.24	6.66	6.66	56.43	0.56
582	4.69	0.00	0.00	62.36	0.65
583	16.44	0.00	0.00	218.65	2.24
584	24.44	0.00	0.00	325.05	3.33
585	22.81	0.00	0.00	303.34	16.71
586	28.51	0.00	0.00	379.17	3.89
587	33.78	0.00	0.00	449.23	4.62
588	41.66	0.00	0.00	554.02	5.87
589	26.77	0.00	0.00	356.10	42.13

	Battery Heat Rate	Engine Heat Rate	Inverter Heat Rate	EM Heat Rate	Transmission Heat Rate
Time (s)	Heat (W)	Heat (W)	Heat (W)	Heat (W)	Heat (W)
590	32.75	0.00	0.00	435.60	4.43
591	38.09	0.00	0.00	506.64	5.10
592	31.01	0.00	0.00	412.43	4.12
593	0.20	0.00	0.00	2.63	4.65
594	0.20	0.00	0.00	2.69	0.07
595	0.20	0.00	0.00	2.69	0.00
596	0.20	0.00	0.00	2.69	0.00
597	0.20	0.00	0.00	2.69	0.00
598	0.20	0.00	0.00	2.69	0.00
599	0.20	0.00	0.00	2.69	0.00
600	0.20	0.00	0.00	2.69	0.00
601	0.20	0.00	0.00	2.69	0.00

APPENDIX E

DATA COLLECTED JANUARY-MARCH 2017

Volumetric Flow Rate				
Time (s)	Flow Rate (L)	1 Cylinder Flow Rate (L)	1 Cylinder Exhaust Flow (L)	Full Exhaust Flow (L)
1	0	0	0	0
2	0	0	0	0
3	0	0	0	0
4	0	0	0	0
5	0	0	0	0
6	0	0	0	0
7	0	0	0	0
8	0	0	0	0
9	0	0	0	0
10	0	0	0	0
11	0	0	0	0
12	0	0	0	0
13	0	0	0	0
14	0	0	0	0
15	0	0	0	0
16	2.495021	0.623755	8.732572	34.93029
17	5.693284	1.423321	19.92649	79.70597
18	4.533428	1.133357	15.867	63.46799
19	4.782141	1.195535	16.7375	66.94998
20	5.006506	1.251626	17.52277	70.09108
21	5.249054	1.312263	18.37169	73.48676

Volumetric Flow Rate				
Time (s)	Flow Rate (L)	1 Cylinder Flow Rate (L)	1 Cylinder Exhaust Flow (L)	Full Exhaust Flow (L)
22	5.50184	1.37546	19.25644	77.02576
23	4.447211	1.111803	15.56524	62.26095
24	3.756845	0.939211	13.14896	52.59582
25	3.688327	0.922082	12.90914	51.63657
26	3.553789	0.888447	12.43826	49.75305
27	3.339172	0.834793	11.6871	46.74841
28	1.093112	0.273278	3.825892	15.30357
29	0.357841	0.08946	1.252445	5.00978
30	0.117143	0.029286	0.410001	1.640003
31	0.038348	0.009587	0.134218	0.536872
32	0.012554	0.003138	0.043938	0.17575
33	0.00411	0.001027	0.014383	0.057534
34	0.001345	0.000336	0.004709	0.018834
35	0.00044	0.00011	0.001541	0.006166
36	0.000144	3.6E-05	0.000505	0.002018
37	4.72E-05	1.18E-05	0.000165	0.000661
38	1.54E-05	3.86E-06	5.41E-05	0.000216
39	5.06E-06	1.26E-06	1.77E-05	7.08E-05
40	1.66E-06	4.14E-07	5.79E-06	2.32E-05
41	5.42E-07	1.36E-07	1.9E-06	7.59E-06
42	1.77E-07	4.44E-08	6.21E-07	2.48E-06

Volumetric Flow Rate				
Time (s)	Flow Rate (L)	1 Cylinder Flow Rate (L)	1 Cylinder Exhaust Flow (L)	Full Exhaust Flow (L)
43	5.81E-08	1.45E-08	2.03E-07	8.13E-07
44	1.90E-08	4.75E-09	6.65E-08	2.66E-07
45	6.22E-09	1.56E-09	2.18E-08	8.71E-08
46	2.04E-09	5.09E-10	7.13E-09	2.85E-08
47	6.67E-10	1.67E-10	2.33E-09	9.34E-09
48	2.18E-10	5.46E-11	7.64E-10	3.06E-09
49	7.15E-11	1.79E-11	2.5E-10	1E-09
50	2.34E-11	5.85E-12	8.19E-11	3.28E-10
51	7.66E-12	1.92E-12	2.68E-11	1.07E-10
52	2.51E-12	6.27E-13	8.78E-12	3.51E-11
53	8.21E-13	2.05E-13	2.87E-12	1.15E-11
54	2.69E-13	6.72E-14	9.41E-13	3.76E-12
55	8.80E-14	2.2E-14	3.08E-13	1.23E-12
56	2.88E-14	7.2E-15	1.01E-13	4.03E-13
57	9.43E-15	2.36E-15	3.3E-14	1.32E-13
58	3.09E-15	7.72E-16	1.08E-14	4.32E-14
59	1.01E-15	2.53E-16	3.54E-15	1.41E-14
60	3.31E-16	8.27E-17	1.16E-15	4.63E-15
61	1.08E-16	2.71E-17	3.79E-16	1.52E-15
62	3.54E-17	8.86E-18	1.24E-16	4.96E-16
63	1.16E-17	2.9E-18	4.06E-17	1.62E-16



Volumetric Flow Rate				
Time (s)	Flow Rate (L)	1 Cylinder Flow Rate (L)	1 Cylinder Exhaust Flow (L)	Full Exhaust Flow (L)
64	3.80E-18	9.5E-19	1.33E-17	5.32E-17
65	1.24E-18	3.11E-19	4.35E-18	1.74E-17
66	4.07E-19	1.02E-19	1.42E-18	5.7E-18
67	1.33E-19	3.33E-20	4.66E-19	1.87E-18
68	4.36E-20	1.09E-20	1.53E-19	6.11E-19
69	1.43E-20	3.57E-21	5E-20	2E-19
70	4.67E-21	1.17E-21	1.64E-20	6.54E-20
71	1.53E-21	3.83E-22	5.36E-21	2.14E-20
72	5.01E-22	1.25E-22	1.75E-21	7.01E-21
73	1.64E-22	4.1E-23	5.74E-22	2.3E-21
74	5.37E-23	1.34E-23	1.88E-22	7.52E-22
75	1.76E-23	4.39E-24	6.15E-23	2.46E-22
76	5.75E-24	1.44E-24	2.01E-23	8.05E-23
77	1.88E-24	4.71E-25	6.59E-24	2.64E-23
78	6.17E-25	1.54E-25	2.16E-24	8.63E-24
79	2.02E-25	5.05E-26	7.06E-25	2.83E-24
80	6.61E-26	1.65E-26	2.31E-25	9.25E-25
81	2.16E-26	5.41E-27	7.57E-26	3.03E-25
82	7.08E-27	1.77E-27	2.48E-26	9.91E-26
83	2.32E-27	5.79E-28	8.11E-27	3.25E-26
84	7.59E-28	1.9E-28	2.66E-27	1.06E-26

Volumetric Flow Rate				
Time (s)	Flow Rate (L)	1 Cylinder Flow Rate (L)	1 Cylinder Exhaust Flow (L)	Full Exhaust Flow (L)
85	2.48E-28	6.21E-29	8.69E-28	3.48E-27
86	8.13E-29	2.03E-29	2.85E-28	1.14E-27
87	2.66E-29	6.65E-30	9.32E-29	3.73E-28
88	8.71E-30	2.18E-30	3.05E-29	1.22E-28
89	2.85E-30	7.13E-31	9.98E-30	3.99E-29
90	9.34E-31	2.33E-31	3.27E-30	1.31E-29
91	3.06E-31	7.64E-32	1.07E-30	4.28E-30
92	1.00E-31	2.5E-32	3.5E-31	1.4E-30
93	3.28E-32	8.19E-33	1.15E-31	4.59E-31
94	1.07E-32	2.68E-33	3.75E-32	1.5E-31
95	3.51E-33	8.78E-34	1.23E-32	4.92E-32
96	1.15E-33	2.87E-34	4.02E-33	1.61E-32
97	3.76E-34	9.41E-35	1.32E-33	5.27E-33
98	1.23E-34	3.08E-35	4.31E-34	1.72E-33
99	4.03E-35	1.01E-35	1.41E-34	5.64E-34
100	1.32E-35	3.3E-36	4.62E-35	1.85E-34
101	4.32E-36	1.08E-36	1.51E-35	6.05E-35
102	1.41E-36	3.54E-37	4.95E-36	1.98E-35
103	4.63E-37	1.16E-37	1.62E-36	6.48E-36
104	1.52E-37	3.79E-38	5.31E-37	2.12E-36
105	4.96E-38	1.24E-38	1.74E-37	6.95E-37

Volumetric Flow Rate				
Time (s)	Flow Rate (L)	1 Cylinder Flow Rate (L)	1 Cylinder Exhaust Flow (L)	Full Exhaust Flow (L)
106	1.62E-38	4.06E-39	5.69E-38	2.27E-37
107	5.32E-39	1.33E-39	1.86E-38	7.44E-38
108	1.74E-39	4.35E-40	6.09E-39	2.44E-38
109	5.70E-40	1.42E-40	1.99E-39	7.98E-39
110	1.87E-40	4.66E-41	6.53E-40	2.61E-39
111	6.11E-41	1.53E-41	2.14E-40	8.55E-40
112	2.00E-41	5E-42	7E-41	2.8E-40
113	6.54E-42	1.64E-42	2.29E-41	9.16E-41
114	2.14E-42	5.36E-43	7.5E-42	3E-41
115	7.01E-43	1.75E-43	2.45E-42	9.82E-42
116	2.30E-43	5.74E-44	8.04E-43	3.21E-42
117	7.52E-44	1.88E-44	2.63E-43	1.05E-42
118	2.46E-44	6.15E-45	8.61E-44	3.44E-43
119	8.05E-45	2.01E-45	2.82E-44	1.13E-43
120	2.64E-45	6.59E-46	9.23E-45	3.69E-44
121	8.63E-46	2.16E-46	3.02E-45	1.21E-44
122	2.83E-46	7.06E-47	9.89E-46	3.96E-45
123	9.25E-47	2.31E-47	3.24E-46	1.29E-45
124	3.03E-47	7.57E-48	1.06E-46	4.24E-46
125	9.91E-48	2.48E-48	3.47E-47	1.39E-46
126	3.24E-48	8.11E-49	1.14E-47	4.54E-47

Volumetric Flow Rate				
Time (s)	Flow Rate (L)	1 Cylinder Flow Rate (L)	1 Cylinder Exhaust Flow (L)	Full Exhaust Flow (L)
127	1.06E-48	2.66E-49	3.72E-48	1.49E-47
128	3.48E-49	8.69E-50	1.22E-48	4.87E-48
129	1.14E-49	2.85E-50	3.98E-49	1.59E-48
130	3.73E-50	9.32E-51	1.3E-49	5.22E-49
131	1.22E-50	3.05E-51	4.27E-50	1.71E-49
132	3.99E-51	9.98E-52	1.4E-50	5.59E-50
133	1.31E-51	3.27E-52	4.58E-51	1.83E-50
134	4.28E-52	1.07E-52	1.5E-51	5.99E-51
135	1.40E-52	3.5E-53	4.9E-52	1.96E-51
136	4.59E-53	1.15E-53	1.61E-52	6.42E-52
137	1.50E-53	3.75E-54	5.25E-53	2.1E-52
138	4.91E-54	1.23E-54	1.72E-53	6.88E-53
139	1.61E-54	4.02E-55	5.63E-54	2.25E-53
140	5.27E-55	1.32E-55	1.84E-54	7.37E-54
141	1.72E-55	4.31E-56	6.03E-55	2.41E-54
142	3.250278	0.812569	11.37597	45.50389
143	6.96942	1.742355	24.39297	97.57189
144	7.548997	1.887249	26.42149	105.686
145	5.902807	1.475702	20.65982	82.63929
146	4.787609	1.196902	16.75663	67.02653
147	4.921187	1.230297	17.22415	68.89662

Volumetric Flow Rate				
Time (s)	Flow Rate (L)	1 Cylinder Flow Rate (L)	1 Cylinder Exhaust Flow (L)	Full Exhaust Flow (L)
148	5.00841	1.252102	17.52943	70.11773
149	4.350237	1.087559	15.22583	60.90331
150	4.438112	1.109528	15.53339	62.13357
151	3.441154	0.860289	12.04404	48.17616
152	3.469022	0.867256	12.14158	48.56631
153	3.503235	0.875809	12.26132	49.04528
154	3.53921	0.884803	12.38724	49.54894
155	3.541412	0.885353	12.39494	49.57976
156	3.557106	0.889277	12.44987	49.79949
157	4.723221	1.180805	16.53127	66.1251
158	9.703757	2.425939	33.96315	135.8526
159	4.872102	1.218026	17.05236	68.20943
160	9.987093	2.496773	34.95482	139.8193
161	5.013698	1.253425	17.54794	70.19178
162	6.045698	1.511424	21.15994	84.63977
163	3.948767	0.987192	13.82069	55.28274
164	3.968998	0.992249	13.89149	55.56597
165	3.961899	0.990475	13.86665	55.46659
166	1.484584	0.371146	5.196044	20.78418
167	0.485994	0.121498	1.700978	6.803912
168	0.159095	0.039774	0.556833	2.22733

Volumetric Flow Rate				
Time (s)	Flow Rate (L)	1 Cylinder Flow Rate (L)	1 Cylinder Exhaust Flow (L)	Full Exhaust Flow (L)
169	0.052081	0.01302	0.182285	0.729139
170	0.017049	0.004262	0.059673	0.238691
171	0.005581	0.001395	0.019534	0.078138
172	0.001827	0.000457	0.006395	0.025579
173	0.000598	0.00015	0.002093	0.008374
174	0.000196	4.89E-05	0.000685	0.002741
175	6.41E-05	1.6E-05	0.000224	0.000897
176	2.10E-05	5.25E-06	7.34E-05	0.000294
177	6.87E-06	1.72E-06	2.4E-05	9.62E-05
178	2.25E-06	5.62E-07	7.87E-06	3.15E-05
179	7.36E-07	1.84E-07	2.58E-06	1.03E-05
180	2.41E-07	6.02E-08	8.43E-07	3.37E-06
181	7.89E-08	1.97E-08	2.76E-07	1.1E-06
182	2.58E-08	6.46E-09	9.04E-08	3.62E-07
183	8.45E-09	2.11E-09	2.96E-08	1.18E-07
184	2.77E-09	6.92E-10	9.69E-09	3.87E-08
185	9.06E-10	2.26E-10	3.17E-09	1.27E-08
186	2.97E-10	7.41E-11	1.04E-09	4.15E-09
187	2.031022	0.507756	7.108577	28.43431
188	4.799479	1.19987	16.79818	67.19271
189	9.85426	2.463565	34.48991	137.9596

Volumetric Flow Rate				
Time (s)	Flow Rate (L)	1 Cylinder Flow Rate (L)	1 Cylinder Exhaust Flow (L)	Full Exhaust Flow (L)
190	4.940437	1.235109	17.29153	69.16611
191	5.01982	1.254955	17.56937	70.27748
192	5.110295	1.277574	17.88603	71.54413
193	3.963549	0.990887	13.87242	55.48968
194	5.24444	1.31111	18.35554	73.42215
195	4.050521	1.01263	14.17682	56.7073
196	4.08564	1.02141	14.29974	57.19897
197	2.976266	0.744067	10.41693	41.66773
198	0.974311	0.243578	3.410089	13.64036
199	0.318951	0.079738	1.116328	4.46531
200	0.104412	0.026103	0.365441	1.461765
201	0.03418	0.008545	0.119631	0.478524
202	0.011189	0.002797	0.039162	0.15665
203	0.003663	0.000916	0.01282	0.051281
204	0.001199	0.0003	0.004197	0.016787
205	0.000393	9.81E-05	0.001374	0.005495
206	0.000129	3.21E-05	0.00045	0.001799
207	4.21E-05	1.05E-05	0.000147	0.000589
208	1.38E-05	3.44E-06	4.82E-05	0.000193
209	4.51E-06	1.13E-06	1.58E-05	6.31E-05
210	1.48E-06	3.69E-07	5.17E-06	2.07E-05

Volumetric Flow Rate				
Time (s)	Flow Rate (L)	1 Cylinder Flow Rate (L)	1 Cylinder Exhaust Flow (L)	Full Exhaust Flow (L)
211	4.83E-07	1.21E-07	1.69E-06	6.76E-06
212	1.58E-07	3.95E-08	5.54E-07	2.21E-06
213	5.18E-08	1.29E-08	1.81E-07	7.25E-07
214	1.69E-08	4.24E-09	5.93E-08	2.37E-07
215	5.55E-09	1.39E-09	1.94E-08	7.77E-08
216	1.82E-09	4.54E-10	6.36E-09	2.54E-08
217	5.95E-10	1.49E-10	2.08E-09	8.32E-09
218	1.95E-10	4.87E-11	6.81E-10	2.72E-09
219	6.37E-11	1.59E-11	2.23E-10	8.92E-10
220	2.09E-11	5.21E-12	7.3E-11	2.92E-10
221	6.83E-12	1.71E-12	2.39E-11	9.56E-11
222	2.24E-12	5.59E-13	7.82E-12	3.13E-11
223	7.32E-13	1.83E-13	2.56E-12	1.02E-11
224	2.40E-13	5.99E-14	8.38E-13	3.35E-12
225	7.84E-14	1.96E-14	2.74E-13	1.1E-12
226	2.57E-14	6.42E-15	8.98E-14	3.59E-13
227	8.40E-15	2.1E-15	2.94E-14	1.18E-13
228	2.75E-15	6.88E-16	9.63E-15	3.85E-14
229	9.01E-16	2.25E-16	3.15E-15	1.26E-14
230	2.95E-16	7.37E-17	1.03E-15	4.13E-15
231	9.65E-17	2.41E-17	3.38E-16	1.35E-15



Volumetric Flow Rate				
Time (s)	Flow Rate (L)	1 Cylinder Flow Rate (L)	1 Cylinder Exhaust Flow (L)	Full Exhaust Flow (L)
232	3.16E-17	7.9E-18	1.11E-16	4.42E-16
233	1.03E-17	2.59E-18	3.62E-17	1.45E-16
234	3.39E-18	8.46E-19	1.18E-17	4.74E-17
235	1.11E-18	2.77E-19	3.88E-18	1.55E-17
236	3.63E-19	9.07E-20	1.27E-18	5.08E-18
237	1.19E-19	2.97E-20	4.16E-19	1.66E-18
238	3.89E-20	9.72E-21	1.36E-19	5.44E-19
239	1.27E-20	3.18E-21	4.45E-20	1.78E-19
240	4.17E-21	1.04E-21	1.46E-20	5.83E-20
241	1.36E-21	3.41E-22	4.77E-21	1.91E-20
242	4.47E-22	1.12E-22	1.56E-21	6.25E-21
243	1.46E-22	3.65E-23	5.12E-22	2.05E-21
244	4.79E-23	1.2E-23	1.67E-22	6.7E-22
245	1.57E-23	3.92E-24	5.48E-23	2.19E-22
246	5.13E-24	1.28E-24	1.79E-23	7.18E-23
247	1.68E-24	4.2E-25	5.88E-24	2.35E-23
248	5.50E-25	1.37E-25	1.92E-24	7.69E-24
249	1.80E-25	4.5E-26	6.3E-25	2.52E-24
250	5.89E-26	1.47E-26	2.06E-25	8.24E-25
251	1.93E-26	4.82E-27	6.75E-26	2.7E-25
252	6.31E-27	1.58E-27	2.21E-26	8.84E-26

Volumetric Flow Rate				
Time (s)	Flow Rate (L)	1 Cylinder Flow Rate (L)	1 Cylinder Exhaust Flow (L)	Full Exhaust Flow (L)
253	2.07E-27	5.16E-28	7.23E-27	2.89E-26
254	6.76E-28	1.69E-28	2.37E-27	9.47E-27
255	2.21E-28	5.53E-29	7.75E-28	3.1E-27
256	7.25E-29	1.81E-29	2.54E-28	1.01E-27
257	2.37E-29	5.93E-30	8.3E-29	3.32E-28
258	7.77E-30	1.94E-30	2.72E-29	1.09E-28
259	2.54E-30	6.36E-31	8.9E-30	3.56E-29
260	8.32E-31	2.08E-31	2.91E-30	1.17E-29
261	2.72E-31	6.81E-32	9.54E-31	3.81E-30
262	8.92E-32	2.23E-32	3.12E-31	1.25E-30
263	2.92E-32	7.3E-33	1.02E-31	4.09E-31
264	9.56E-33	2.39E-33	3.35E-32	1.34E-31
265	3.13E-33	7.82E-34	1.1E-32	4.38E-32
266	1.02E-33	2.56E-34	3.59E-33	1.43E-32
267	3.35E-34	8.38E-35	1.17E-33	4.69E-33
268	1.10E-34	2.74E-35	3.84E-34	1.54E-33
269	3.59E-35	8.98E-36	1.26E-34	5.03E-34
270	1.18E-35	2.94E-36	4.12E-35	1.65E-34
271	3.85E-36	9.63E-37	1.35E-35	5.39E-35
272	1.26E-36	3.15E-37	4.41E-36	1.76E-35
273	4.13E-37	1.03E-37	1.44E-36	5.78E-36

Volumetric Flow Rate				
Time (s)	Flow Rate (L)	1 Cylinder Flow Rate (L)	1 Cylinder Exhaust Flow (L)	Full Exhaust Flow (L)
274	1.35E-37	3.38E-38	4.73E-37	1.89E-36
275	4.42E-38	1.11E-38	1.55E-37	6.19E-37
276	1.45E-38	3.62E-39	5.07E-38	2.03E-37
277	4.74E-39	1.18E-39	1.66E-38	6.64E-38
278	1.55E-39	3.88E-40	5.43E-39	2.17E-38
279	5.08E-40	1.27E-40	1.78E-39	7.11E-39
280	1.66E-40	4.16E-41	5.82E-40	2.33E-39
281	5.44E-41	1.36E-41	1.91E-40	7.62E-40
282	1.78E-41	4.45E-42	6.24E-41	2.49E-40
283	5.83E-42	1.46E-42	2.04E-41	8.17E-41
284	1.91E-42	4.77E-43	6.68E-42	2.67E-41
285	6.25E-43	1.56E-43	2.19E-42	8.75E-42
286	2.05E-43	5.12E-44	7.16E-43	2.86E-42
287	6.70E-44	1.67E-44	2.34E-43	9.38E-43
288	2.19E-44	5.48E-45	7.68E-44	3.07E-43
289	7.18E-45	1.79E-45	2.51E-44	1.01E-43
290	2.35E-45	5.88E-46	8.23E-45	3.29E-44
291	7.69E-46	1.92E-46	2.69E-45	1.08E-44
292	2.52E-46	6.3E-47	8.81E-46	3.53E-45
293	8.24E-47	2.06E-47	2.89E-46	1.15E-45
294	2.70E-47	6.75E-48	9.45E-47	3.78E-46

Volumetric Flow Rate				
Time (s)	Flow Rate (L)	1 Cylinder Flow Rate (L)	1 Cylinder Exhaust Flow (L)	Full Exhaust Flow (L)
295	8.84E-48	2.21E-48	3.09E-47	1.24E-46
296	2.89E-48	7.23E-49	1.01E-47	4.05E-47
297	9.47E-49	2.37E-49	3.31E-48	1.33E-47
298	1.268946	0.317236	4.44131	17.76524
299	3.993843	0.998461	13.97845	55.91381
300	10.94825	2.737063	38.31889	153.2755
301	14.32793	3.581982	50.14775	200.591
302	4.773783	1.193446	16.70824	66.83296
303	1.562747	0.390687	5.469613	21.87845
304	0.511581	0.127895	1.790534	7.162135
305	0.167471	0.041868	0.586149	2.344598
306	0.054823	0.013706	0.191882	0.767528
307	0.017947	0.004487	0.062815	0.251258
308	0.005875	0.001469	0.020563	0.082252
309	0.001923	0.000481	0.006732	0.026926
310	0.00063	0.000157	0.002204	0.008815
311	0.000206	5.15E-05	0.000721	0.002886
312	6.75E-05	1.69E-05	0.000236	0.000945
313	2.21E-05	5.52E-06	7.73E-05	0.000309
314	7.23E-06	1.81E-06	2.53E-05	0.000101
315	2.37E-06	5.92E-07	8.28E-06	3.31E-05

Volumetric Flow Rate				
Time (s)	Flow Rate (L)	1 Cylinder Flow Rate (L)	1 Cylinder Exhaust Flow (L)	Full Exhaust Flow (L)
316	7.75E-07	1.94E-07	2.71E-06	1.08E-05
317	2.54E-07	6.34E-08	8.88E-07	3.55E-06
318	8.30E-08	2.08E-08	2.91E-07	1.16E-06
319	2.72E-08	6.8E-09	9.51E-08	3.81E-07
320	8.90E-09	2.22E-09	3.11E-08	1.25E-07
321	2.91E-09	7.28E-10	1.02E-08	4.08E-08
322	9.54E-10	2.38E-10	3.34E-09	1.34E-08
323	3.12E-10	7.8E-11	1.09E-09	4.37E-09
324	1.02E-10	2.55E-11	3.58E-10	1.43E-09
325	3.35E-11	8.36E-12	1.17E-10	4.68E-10
326	1.10E-11	2.74E-12	3.83E-11	1.53E-10
327	3.59E-12	8.96E-13	1.25E-11	5.02E-11
328	1.17E-12	2.93E-13	4.11E-12	1.64E-11
329	3.84E-13	9.61E-14	1.34E-12	5.38E-12
330	1.26E-13	3.14E-14	4.4E-13	1.76E-12
331	4.12E-14	1.03E-14	1.44E-13	5.76E-13
332	1.35E-14	3.37E-15	4.72E-14	1.89E-13
333	4.41E-15	1.1E-15	1.54E-14	6.18E-14
334	1.44E-15	3.61E-16	5.06E-15	2.02E-14
335	4.73E-16	1.18E-16	1.65E-15	6.62E-15
336	1.55E-16	3.87E-17	5.42E-16	2.17E-15

Volumetric Flow Rate				
Time (s)	Flow Rate (L)	1 Cylinder Flow Rate (L)	1 Cylinder Exhaust Flow (L)	Full Exhaust Flow (L)
337	5.07E-17	1.27E-17	1.77E-16	7.09E-16
338	1.66E-17	4.15E-18	5.81E-17	2.32E-16
339	5.43E-18	1.36E-18	1.9E-17	7.6E-17
340	1.78E-18	4.44E-19	6.22E-18	2.49E-17
341	5.82E-19	1.45E-19	2.04E-18	8.15E-18
342	1.91E-19	4.76E-20	6.67E-19	2.67E-18
343	6.24E-20	1.56E-20	2.18E-19	8.73E-19
344	2.04E-20	5.1E-21	7.15E-20	2.86E-19
345	6.68E-21	1.67E-21	2.34E-20	9.36E-20
346	2.19E-21	5.47E-22	7.66E-21	3.06E-20
347	7.16E-22	1.79E-22	2.51E-21	1E-20
348	2.34E-22	5.86E-23	8.21E-22	3.28E-21
349	7.68E-23	1.92E-23	2.69E-22	1.07E-21
350	2.51E-23	6.28E-24	8.79E-23	3.52E-22
351	8.22E-24	2.06E-24	2.88E-23	1.15E-22
352	2.69E-24	6.73E-25	9.42E-24	3.77E-23
353	8.81E-25	2.2E-25	3.08E-24	1.23E-23
354	2.89E-25	7.21E-26	1.01E-24	4.04E-24
355	9.45E-26	2.36E-26	3.31E-25	1.32E-24
356	3.09E-26	7.73E-27	1.08E-25	4.33E-25
357	1.01E-26	2.53E-27	3.54E-26	1.42E-25

Volumetric Flow Rate				
Time (s)	Flow Rate (L)	1 Cylinder Flow Rate (L)	1 Cylinder Exhaust Flow (L)	Full Exhaust Flow (L)
358	3.31E-27	8.28E-28	1.16E-26	4.64E-26
359	1.08E-27	2.71E-28	3.8E-27	1.52E-26
360	3.55E-28	8.88E-29	1.24E-27	4.97E-27
361	1.16E-28	2.91E-29	4.07E-28	1.63E-27
362	3.81E-29	9.51E-30	1.33E-28	5.33E-28
363	1.25E-29	3.11E-30	4.36E-29	1.74E-28
364	4.08E-30	1.02E-30	1.43E-29	5.71E-29
365	1.34E-30	3.34E-31	4.67E-30	1.87E-29
366	4.37E-31	1.09E-31	1.53E-30	6.12E-30
367	1.43E-31	3.58E-32	5.01E-31	2E-30
368	4.68E-32	1.17E-32	1.64E-31	6.56E-31
369	1.53E-32	3.83E-33	5.37E-32	2.15E-31
370	5.02E-33	1.25E-33	1.76E-32	7.03E-32
371	1.64E-33	4.11E-34	5.75E-33	2.3E-32
372	5.38E-34	1.34E-34	1.88E-33	7.53E-33
373	1.76E-34	4.4E-35	6.16E-34	2.47E-33
374	5.76E-35	1.44E-35	2.02E-34	8.07E-34
375	1.89E-35	4.72E-36	6.6E-35	2.64E-34
376	6.18E-36	1.54E-36	2.16E-35	8.65E-35
377	2.02E-36	5.06E-37	7.08E-36	2.83E-35
378	6.62E-37	1.65E-37	2.32E-36	9.27E-36

Volumetric Flow Rate				
Time (s)	Flow Rate (L)	1 Cylinder Flow Rate (L)	1 Cylinder Exhaust Flow (L)	Full Exhaust Flow (L)
379	2.17E-37	5.42E-38	7.58E-37	3.03E-36
380	7.09E-38	1.77E-38	2.48E-37	9.93E-37
381	2.32E-38	5.81E-39	8.13E-38	3.25E-37
382	7.60E-39	1.9E-39	2.66E-38	1.06E-37
383	2.49E-39	6.22E-40	8.71E-39	3.48E-38
384	8.15E-40	2.04E-40	2.85E-39	1.14E-38
385	2.67E-40	6.67E-41	9.33E-40	3.73E-39
386	8.73E-41	2.18E-41	3.06E-40	1.22E-39
387	2.86E-41	7.15E-42	1E-40	4E-40
388	9.36E-42	2.34E-42	3.27E-41	1.31E-40
389	3.06E-42	7.66E-43	1.07E-41	4.29E-41
390	1.00E-42	2.51E-43	3.51E-42	1.4E-41
391	3.28E-43	8.21E-44	1.15E-42	4.6E-42
392	1.07E-43	2.69E-44	3.76E-43	1.5E-42
393	3.52E-44	8.79E-45	1.23E-43	4.92E-43
394	1.15E-44	2.88E-45	4.03E-44	1.61E-43
395	3.77E-45	9.42E-46	1.32E-44	5.28E-44
396	1.23E-45	3.08E-46	4.32E-45	1.73E-44
397	4.04E-46	1.01E-46	1.41E-45	5.66E-45
398	1.32E-46	3.31E-47	4.63E-46	1.85E-45
399	4.33E-47	1.08E-47	1.52E-46	6.06E-46



Volumetric Flow Rate				
Time (s)	Flow Rate (L)	1 Cylinder Flow Rate (L)	1 Cylinder Exhaust Flow (L)	Full Exhaust Flow (L)
400	1.42E-47	3.54E-48	4.96E-47	1.98E-46
401	4.64E-48	1.16E-48	1.62E-47	6.49E-47
402	1.52E-48	3.8E-49	5.32E-48	2.13E-47
403	4.97E-49	1.24E-49	1.74E-48	6.96E-48
404	1.63E-49	4.07E-50	5.7E-49	2.28E-48
405	5.33E-50	1.33E-50	1.86E-49	7.46E-49
406	1.74E-50	4.36E-51	6.1E-50	2.44E-49
407	5.71E-51	1.43E-51	2E-50	7.99E-50
408	1.87E-51	4.67E-52	6.54E-51	2.62E-50
409	6.12E-52	1.53E-52	2.14E-51	8.57E-51
410	2.00E-52	5.01E-53	7.01E-52	2.8E-51
411	6.56E-53	1.64E-53	2.29E-52	9.18E-52
412	2.15E-53	5.37E-54	7.51E-53	3E-52
413	7.03E-54	1.76E-54	2.46E-53	9.84E-53
414	2.30E-54	5.75E-55	8.05E-54	3.22E-53
415	7.53E-55	1.88E-55	2.64E-54	1.05E-53
416	2.46E-55	6.16E-56	8.63E-55	3.45E-54
417	8.07E-56	2.02E-56	2.82E-55	1.13E-54
418	2.64E-56	6.6E-57	9.25E-56	3.7E-55
419	8.65E-57	2.16E-57	3.03E-56	1.21E-55
420	2.83E-57	7.08E-58	9.91E-57	3.96E-56

Volumetric Flow Rate				
Time (s)	Flow Rate (L)	1 Cylinder Flow Rate (L)	1 Cylinder Exhaust Flow (L)	Full Exhaust Flow (L)
421	9.27E-58	2.32E-58	3.24E-57	1.3E-56
422	3.03E-58	7.58E-59	1.06E-57	4.25E-57
423	9.93E-59	2.48E-59	3.48E-58	1.39E-57
424	3.25E-59	8.13E-60	1.14E-58	4.55E-58
425	1.06E-59	2.66E-60	3.72E-59	1.49E-58
426	3.48E-60	8.71E-61	1.22E-59	4.88E-59
427	1.14E-60	2.85E-61	3.99E-60	1.6E-59
428	3.73E-61	9.33E-62	1.31E-60	5.23E-60
429	1.22E-61	3.06E-62	4.28E-61	1.71E-60
430	4.00E-62	1E-62	1.4E-61	5.6E-61
431	1.31E-62	3.27E-63	4.58E-62	1.83E-61
432	4.29E-63	1.07E-63	1.5E-62	6E-62
433	1.40E-63	3.51E-64	4.91E-63	1.97E-62
434	4.59E-64	1.15E-64	1.61E-63	6.43E-63
435	1.50E-64	3.76E-65	5.26E-64	2.11E-63
436	4.92E-65	1.23E-65	1.72E-64	6.89E-64
437	1.61E-65	4.03E-66	5.64E-65	2.26E-64
438	5.28E-66	1.32E-66	1.85E-65	7.39E-65
439	1.73E-66	4.32E-67	6.05E-66	2.42E-65
440	5.66E-67	1.41E-67	1.98E-66	7.92E-66
441	1.85E-67	4.63E-68	6.48E-67	2.59E-66

Volumetric Flow Rate				
Time (s)	Flow Rate (L)	1 Cylinder Flow Rate (L)	1 Cylinder Exhaust Flow (L)	Full Exhaust Flow (L)
442	6.06E-68	1.52E-68	2.12E-67	8.48E-67
443	1.98E-68	4.96E-69	6.94E-68	2.78E-67
444	6.49E-69	1.62E-69	2.27E-68	9.09E-68
445	2.13E-69	5.32E-70	7.44E-69	2.98E-68
446	6.96E-70	1.74E-70	2.44E-69	9.74E-69
447	2.28E-70	5.7E-71	7.97E-70	3.19E-69
448	7.46E-71	1.86E-71	2.61E-70	1.04E-69
449	2.44E-71	6.1E-72	8.55E-71	3.42E-70
450	7.99E-72	2E-72	2.8E-71	1.12E-70
451	2.62E-72	6.54E-73	9.16E-72	3.66E-71
452	8.57E-73	2.14E-73	3E-72	1.2E-71
453	2.80E-73	7.01E-74	9.81E-73	3.93E-72
454	9.18E-74	2.29E-74	3.21E-73	1.29E-72
455	3.00E-74	7.51E-75	1.05E-73	4.21E-73
456	9.84E-75	2.46E-75	3.44E-74	1.38E-73
457	3.22E-75	8.05E-76	1.13E-74	4.51E-74
458	1.05E-75	2.64E-76	3.69E-75	1.48E-74
459	3.45E-76	8.63E-77	1.21E-75	4.83E-75
460	1.13E-76	2.82E-77	3.95E-76	1.58E-75
461	3.70E-77	9.25E-78	1.29E-76	5.18E-76
462	1.21E-77	3.03E-78	4.24E-77	1.69E-76

Volumetric Flow Rate				
Time (s)	Flow Rate (L)	1 Cylinder Flow Rate (L)	1 Cylinder Exhaust Flow (L)	Full Exhaust Flow (L)
463	3.96E-78	9.91E-79	1.39E-77	5.55E-77
464	1.30E-78	3.24E-79	4.54E-78	1.82E-77
465	4.25E-79	1.06E-79	1.49E-78	5.95E-78
466	1.39E-79	3.48E-80	4.87E-79	1.95E-78
467	4.55E-80	1.14E-80	1.59E-79	6.37E-79
468	1.49E-80	3.72E-81	5.21E-80	2.09E-79
469	4.88E-81	1.22E-81	1.71E-80	6.83E-80
470	1.60E-81	3.99E-82	5.59E-81	2.24E-80
471	5.23E-82	1.31E-82	1.83E-81	7.32E-81
472	1.71E-82	4.28E-83	5.99E-82	2.4E-81
473	5.60E-83	1.4E-83	1.96E-82	7.84E-82
474	1.83E-83	4.58E-84	6.42E-83	2.57E-82
475	6.00E-84	1.5E-84	2.1E-83	8.4E-83
476	1.97E-84	4.91E-85	6.88E-84	2.75E-83
477	6.43E-85	1.61E-85	2.25E-84	9.01E-84
478	2.11E-85	5.26E-86	7.37E-85	2.95E-84
479	6.89E-86	1.72E-86	2.41E-85	9.65E-85
480	2.26E-86	5.64E-87	7.9E-86	3.16E-85
481	7.39E-87	1.85E-87	2.59E-86	1.03E-85
482	2.42E-87	6.05E-88	8.46E-87	3.39E-86
483	7.92E-88	1.98E-88	2.77E-87	1.11E-86

Volumetric Flow Rate				
Time (s)	Flow Rate (L)	1 Cylinder Flow Rate (L)	1 Cylinder Exhaust Flow (L)	Full Exhaust Flow (L)
484	2.59E-88	6.48E-89	9.07E-88	3.63E-87
485	8.48E-89	2.12E-89	2.97E-88	1.19E-87
486	2.78E-89	6.94E-90	9.72E-89	3.89E-88
487	9.09E-90	2.27E-90	3.18E-89	1.27E-88
488	2.98E-90	7.44E-91	1.04E-89	4.17E-89
489	9.74E-91	2.44E-91	3.41E-90	1.36E-89
490	3.19E-91	7.97E-92	1.12E-90	4.47E-90
491	1.04E-91	2.61E-92	3.65E-91	1.46E-90
492	3.42E-92	8.55E-93	1.2E-91	4.79E-91
493	1.12E-92	2.8E-93	3.92E-92	1.57E-91
494	3.66E-93	9.16E-94	1.28E-92	5.13E-92
495	1.20E-93	3E-94	4.2E-93	1.68E-92
496	3.93E-94	9.81E-95	1.37E-93	5.5E-93
497	1.29E-94	3.21E-95	4.5E-94	1.8E-93
498	4.21E-95	1.05E-95	1.47E-94	5.89E-94
499	1.38E-95	3.44E-96	4.82E-95	1.93E-94
500	4.51E-96	1.13E-96	1.58E-95	6.31E-95
501	1.48E-96	3.69E-97	5.17E-96	2.07E-95
502	4.83E-97	1.21E-97	1.69E-96	6.76E-96
503	1.58E-97	3.95E-98	5.54E-97	2.21E-96
504	5.18E-98	1.29E-98	1.81E-97	7.25E-97

Volumetric Flow Rate				
Time (s)	Flow Rate (L)	1 Cylinder Flow Rate (L)	1 Cylinder Exhaust Flow (L)	Full Exhaust Flow (L)
505	1.69E-98	4.2E-99	5.93E-98	2.37E-97
506	5.55E-99	1.4E-99	1.94E-98	7.77E-98
507	2.248606	0.562151	7.87012	31.48048
508	4.779135	1.194784	16.72697	66.90788
509	3.540184	0.885046	12.39064	49.56257
510	3.322519	0.83063	11.62882	46.51527
511	3.040931	0.760233	10.64326	42.57304
512	2.154005	0.538501	7.539017	30.15607
513	0.705136	0.176284	2.467974	9.871897
514	0.230833	0.057708	0.807917	3.231666
515	0.075566	0.018891	0.26448	1.057919
516	0.024737	0.006184	0.08658	0.346321
517	0.008098	0.002024	0.028343	0.113372
518	0.002651	0.000663	0.009278	0.037113
519	0.000868	0.000217	0.003037	0.012149
520	2.077727	0.519432	7.272043	29.08817
521	6.693209	1.673302	23.42623	93.70492
522	9.367618	2.341904	32.78666	131.1467
523	3.066585	0.766646	10.73305	42.9322
524	1.003878	0.25097	3.513573	14.05429
525	0.32863	0.082157	1.150204	4.600816

Volumetric Flow Rate				
Time (s)	Flow Rate (L)	1 Cylinder Flow Rate (L)	1 Cylinder Exhaust Flow (L)	Full Exhaust Flow (L)
526	0.10758	0.026895	0.376531	1.506124
527	0.035218	0.008804	0.123261	0.493045
528	0.011529	0.002882	0.040351	0.161403
529	0.003774	0.000944	0.013209	0.052837
530	0.001235	0.000309	0.004324	0.017297
531	0.000404	0.000101	0.001416	0.005662
532	0.000132	3.31E-05	0.000463	0.001854
533	4.33E-05	1.08E-05	0.000152	0.000607
534	1.42E-05	3.55E-06	4.97E-05	0.000199
535	4.64E-06	1.16E-06	1.63E-05	6.5E-05
536	1.52E-06	3.8E-07	5.32E-06	2.13E-05
537	2.683404	0.670851	9.391914	37.56766
538	3.57298	0.893245	12.50543	50.02171
539	3.548098	0.887024	12.41834	49.67337
540	3.31755	0.829388	11.61143	46.44571
541	2.876747	0.719187	10.06861	40.27445
542	2.590104	0.647526	9.065365	36.26146
543	0.847897	0.211974	2.96764	11.87056
544	0.277568	0.069392	0.971487	3.885949
545	0.090865	0.022716	0.318026	1.272105
546	0.029745	0.007436	0.104109	0.416437

Volumetric Flow Rate				
Time (s)	Flow Rate (L)	1 Cylinder Flow Rate (L)	1 Cylinder Exhaust Flow (L)	Full Exhaust Flow (L)
547	0.009737	0.002434	0.034081	0.136325
548	0.003188	0.000797	0.011157	0.044627
549	0.001044	0.000261	0.003652	0.014609
550	0.000342	8.54E-05	0.001196	0.004782
551	0.816017	0.204004	2.856061	11.42424
552	3.929011	0.982253	13.75154	55.00616
553	3.841693	0.960423	13.44593	53.7837
554	2.833436	0.708359	9.917025	39.6681
555	3.049989	0.762497	10.67496	42.69985
556	3.133655	0.783414	10.96779	43.87117
557	1.025834	0.256459	3.590419	14.36168
558	0.335817	0.083954	1.17536	4.701442
559	0.109933	0.027483	0.384766	1.539065
560	0.035988	0.008997	0.125957	0.503829
561	0.011781	0.002945	0.041233	0.164933
562	0.003857	0.000964	0.013498	0.053993
563	0.001263	0.000316	0.004419	0.017675
564	0.000413	0.000103	0.001447	0.005786
565	0.000135	3.38E-05	0.000474	0.001894
566	4.43E-05	1.11E-05	0.000155	0.00062
567	1.45E-05	3.62E-06	5.07E-05	0.000203



Volumetric Flow Rate				
Time (s)	Flow Rate (L)	1 Cylinder Flow Rate (L)	1 Cylinder Exhaust Flow (L)	Full Exhaust Flow (L)
568	4.75E-06	1.19E-06	1.66E-05	6.64E-05
569	1.55E-06	3.88E-07	5.44E-06	2.18E-05
570	5.09E-07	1.27E-07	1.78E-06	7.12E-06
571	1.67E-07	4.16E-08	5.83E-07	2.33E-06
572	5.45E-08	1.36E-08	1.91E-07	7.63E-07
573	1.632169	0.408042	5.712591	22.85036
574	4.331509	1.082877	15.16028	60.64112
575	7.593925	1.898481	26.57874	106.3149
576	4.965279	1.24132	17.37848	69.51391
577	5.425227	1.356307	18.9883	75.95318
578	8.094979	2.023745	28.33243	113.3297
579	8.490841	2.12271	29.71794	118.8718
580	5.211757	1.302939	18.24115	72.9646
581	3.35547	0.838867	11.74414	46.97658
582	3.31247	0.828118	11.59365	46.37458
583	3.218435	0.804609	11.26452	45.05809
584	2.583986	0.645996	9.04395	36.1758
585	0.845894	0.211474	2.960629	11.84252
586	0.276912	0.069228	0.969192	3.876769
587	0.09065	0.022662	0.317275	1.2691
588	0.029675	0.007419	0.103863	0.415453

Volumetric Flow Rate				
Time (s)	Flow Rate (L)	1 Cylinder Flow Rate (L)	1 Cylinder Exhaust Flow (L)	Full Exhaust Flow (L)
589	0.009714	0.002429	0.034001	0.136003
590	0.00318	0.000795	0.01113	0.044522
591	0.001041	0.00026	0.003644	0.014575
592	0.000341	8.52E-05	0.001193	0.004771
593	0.000112	2.79E-05	0.00039	0.001562
594	3.65E-05	9.13E-06	0.000128	0.000511
595	1.20E-05	2.99E-06	4.18E-05	0.000167
596	3.91E-06	9.78E-07	1.37E-05	5.48E-05
597	1.28E-06	3.2E-07	4.48E-06	1.79E-05
598	4.19E-07	1.05E-07	1.47E-06	5.87E-06
599	1.37E-07	3.43E-08	4.81E-07	1.92E-06
600	4.49E-08	1.12E-08	1.57E-07	6.29E-07
601	4.49E-08	1.12E-08	1.57E-07	6.29E-07